Analysis of Numerical Methods in Stereological Unfolding Problem

By

G. J. Sunil

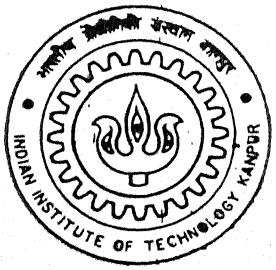

DEPARTMENT OF MATERIALS AND METALLURGICAL ENGINEERING

Indian Institute of Technology Kanpur

July, 2002

Analysis of Numerical Methods in Stereological Unfolding Problem

A Thesis submitted
in partial fulfillment of the requirements
for the degree of

Master of Technology

By
G. J. Sunil

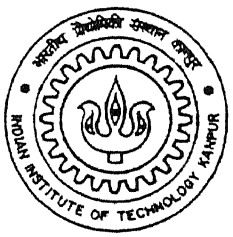

To the
Department of Materials and Metallurgical Engineering

INDIAN INSTITUTE OF TECHNOLOGY KANPUR
JULY, 2002

CERTIFICATE

This is to certify that the work contained in the thesis entitled *Analysis of Numerical Methods in Stereological Unfolding Problem*, by G. J. Sunil, has been carried out under our supervision and this work has not been submitted elsewhere for a degree.

Prof. S. Sangal
Department of Materials
and Metallurgical Engineering
I.I.T. Kanpur

Asim Tewari
Dr. Asim Tewari
Department of Materials
and Metallurgical Engineering
I.I.T. Kanpur

Date:

ACKNOWLEDGEMENTS

At the outset I praise the name of Almighty God for His abundant grace and mercy without which my graduation would have been impossibility.

I would like to express my heartfelt gratitude to my thesis supervisor Dr. Asim Tewari, who with his enthusiasm, inspiration, and great effort to explain things clearly and simply, helped me to make stereology fun for me. All through my graduation period, he provided encouragement, sound advice, good teaching, good company, and lot of good ideas. I can never forget the moral support he has given me in times of difficulty. I would have been lost without him. I shall always treasure the moments I spent with him.

I would like to express my deep sense of gratitude to my thesis supervisor Prof. S. Sangal, for his valuable suggestions, timely guidance and for teaching the basic principles of stereology with unforgettable examples.

For financial support I thank the Department of MME at IITK.

I thank my family members for their incessant prayers and moral support. I would like to convey my gratefulness to all my brethren at IITK fellowship for being a tremendous source of encouragement and for all their love and prayers.

I thank all my friends who had shared my times of joy and sorrow and extended their help selflessly in times of need.

G. J. Sunil

IIT Kanpur

CONTENTS

LIST OF FIGURES

ABSTRACT

Stereology is a collection of mathematical methods that relate the parameters that define a spatial structure to lower dimensional measurements made on sections through the structure. Applications of such methods are found in various sciences, such as materials science, medicine, biology, forestry, geology etc. Quantitative characterization of materials microstructures often require estimation of true particle/grain size distributions. In this study, numerical methods are successfully developed for de-convolution of apparent 2D profiles of spheres, variable spheroids and circular disks. It is found that use of profiles of spheroids as equivalent area circles to de-convolute 3D size distribution is not a bad approximation. Effect of sample size, width of class interval and mode of representation of mean size of a bin, on the estimates of distributions and mean particle sizes is studied. It is realized that using root mean square value (in de-convolution of spheres) to represent mean bin size provides the most bias free estimate of mean particle size.

CHAPTER 1

INTRODUCTION

Stereology (also known as quantitative microscopy or quantitative metallography) is the area of stochastics dealing with statistical inference about spatial structures from geometric samples of the structure such as two-dimensional sections and one-dimensional probes. It can be described as geometric sampling theory or a set of sampling methods for quantifying geometric parameters such as the length of dislocations, volume fraction of a particular phase, or average size of grains, in a given microstructure, or the volume of an organ. Stereology provides methods for sampling from such structures and thereby for estimating the parameter of interest. The parameter can often be estimated from simple measurements of the samples, e.g. counting. The development of stereological methods involve the use of advanced mathematical tools, especially from geometric probability theory and integral geometry [1-2]. Stereology may be applied in various sciences, such as materials science, medicine, biology, forestry and agriculture. The word 'stereology' originates from the Greek word 'stereos': solid, - here in the sense of having all the geometrical dimensions or being cubic [3]. So stereology traditionally concerns three-dimensional structures. However stereology is also applicable to structures that are subsets of a two-dimensional space.

Physically cutting a specimen of material and looking at the distribution of the particle intersections on a lower dimensional section usually obtain the raw data. The estimation of properties of the particulate phase ('particulate phase' is meant to include voids i.e. lack of material as well as true particles) using such raw data splits into two broad categories [4]. The first is the estimation of aggregate properties of the particulate phase, which are definable as average aggregate properties of particulate phase intersections on a lower dimensional section. Probably the most familiar examples of this type of analysis are area and lineal analysis volume fraction estimates.

The second category of estimation procedures depends upon first obtaining an estimate of the particle size frequency function. Moments of the estimated frequency function are then used to estimate functions of moments, such as mean particle size and surface to volume ratio. These estimation problems are not peculiar to metallurgy. Clearly, the particulate phase could be nebulae in outer space, leukocytes in blood,

aggregate in cement, nucleoli in nerve ganglion or trace mineral in rock as opposed to a metallurgy situation, such as carbon particles dispersed in steel.

In general the estimate depends upon particle shape and orientation. A system of particles is often represented simply by the mean particle diameter or by the particles per unit volume. However in order to characterize a particulate structure more completely, knowledge of the distribution of particle sizes is required. Microstructures of materials often contain particles/grains/voids/inclusions having a range of sizes and shapes. 3D size and shape distribution is an important attribute of such microstructures, since the mechanical behavior of these materials largely depend on characteristics of particle/grain size distribution. In such processes as crystallization from the melt, recrystallization and nucleation and growth of precipitate particles, it may be desired to know not only the size distribution, but also how this distribution changes with time. If the microstructure consists of population of only spherical particles having different size, then it can be characterized by a simple univariate size distribution function. But microstructures often contain a population of particles having different sizes and shapes and in such cases, more than one size parameter is required to uniquely identify any given particle in the population. Such microstructures are characterized by bivariate or multivariate size distribution functions. Global parameters such as the number density (N_v) of particles, are not sufficient for the microstructure characterization during different processes of grain formation and grain growth. It is necessary to describe the population of particles by parameters corresponding to their individual geometry, namely the size, shape factor and orientation. However, these may interact with each other and, therefore, the joint probability distribution of geometrical parameters has to be estimated.

Present study aims at developing numerical procedures for the estimation of 3D size distribution of spherical particles, bivariate size-shape distribution of variable spheroids and bivariate size-orientation distribution of circular disks from the corresponding 2D profile measurements. The appropriateness of assuming spherical shapes for non-spherical systems to de-convolute 3D distributions is studied. Effect of variables like sample size, class interval and choice of mean bin size on 3D estimations is also analyzed. In addition to this introductory chapter this thesis consists of five chapters. In second chapter a detailed review of the development of different stereological methods over the past years is given. Whereas, third chapter consists of the theoretical background of the stereological methods for unfolding the probability distribution of

geometrical parameters of spheres and spheroids. The results obtained in the present study are given in fourth chapter along with a brief discussion about the results. The fifth chapter consists of the concluding remarks, followed by a chapter on suggestions for future work.

CHAPTER 2

BACKGROUND

As mentioned in the introduction, stereological estimation methods fall into two broad categories: 1) Methods for estimation of aggregate properties of the particles, 2) Methods for estimation of distribution function of geometric parameters of the particles. A brief overview is given in this section about the development of these methods and their underlying principles.

2.1 METHODS FOR ESTIMATION OF AGGREGATE PROPERTIES

The earliest work on quantitative microscopic analysis goes back to French petrographer A. Delesse (1848) , who proved mathematically that in a fully random cross section of a uniform aggregate, the area occupied by each constituent of the aggregate is exactly proportional to its volume in the mass of the rock [5]. Delesse measured the relative areas of minerals lying in a macroscopic section by cutting out segments of thin foil to represent the areas occupied by the various minerals. He then weighed the pieces of tin corresponding to a given mineral, and divided this by the total weight of tin corresponding to the entire structure. Sorby (1856) extended the areal method of analysis to microstructures by using a camera for tracing on "an evenly thick piece of drawing paper" the outlines of minerals seen under a petrographic microscope [6]. He weighed the whole sketch, and then cut the areas representing the various minerals and weighed them as Delesse did with tin foil for much coarser structures. Sollas (1887) combined the two methods by cutting out areas of tin foil corresponding to a camera tracing [7]. Julien (1903) made similar determinations in a petrographic study, but attained greater precision by photographing the structure, and then cutting and weighing the paper segments of the micrographic print [8]. A few years later, Rosiwal (1898) showed that the volume proportions of minerals in uniform rock are equal to the lineal proportions intercepted by the minerals on a random line passed through the structure [9]. He not only demonstrated the applicability of lineal analysis to geometrically produced areas, but also found good agreement with the areal method of Delesse as applied to actual macroscopic sections. For microstudies, Rosiwal employed a micrometer ocular to measure the fraction of a line-traverse intersected by

the minerals of each type. A number of areal and lineal methods of measurement have been developed with a view to increasing precision and decreasing tedium. Joly (1903) traced the enlarged image of a microstructure (projected onto the ground glass of a camera) on graph paper, and estimated the proportions of the individual squares occupied by the various minerals [10]. He then summed up the total area of each microconstituent in the polished section. Johannsen (1919) made tracings of microconstituents with the aid of a camera, and measured the areas with a regular planimeter [11]. The earliest applications of point ratios as estimators of areal ratios appear to have been made by Thomson (1930). He used one and two-dimensional point grids in order to determine the fractional number of points falling within the boundaries of a constituent in the section plane [12]. Lightner and Herty (1932) improved upon the point-counting procedure by photographically superimposing a grid on a print of the microstructure [13]. Gardner (1943) carried out point-counting by covering the micrographic prints with translucent graph paper [14]. H. S. Rawdon proposed a photometric method for determining relative areas of dark and light constituents in a two-constituent structure but it is hardly suitable for routine work [15]. Polushkin (1925) appears to have been the first to apply lineal analysis to metallic structures (Bi-Sn eutectic) [16]. He mounted micrographs on a movable platform, and used a recording tape to sum up the lengths of a given constituent intercepted during a traverse. He was able to determine the proportion of eutectics and eutectoids in various alloys by this method of analysis. A number of critical petrographic studies have been made to compare the areal and lineal methods of quantitative analysis. Thomson (1930) has applied the Delesse, Rosiwal and grid methods to synthetic aggregates and actual structures, and has found agreement of all three techniques within a few percent. Karlsson and Drar (1980) demonstrated the volume fraction determination by the aid of computer modeling [17]. In the nomenclature of quantitative metallography developed by Underwood [18] this is expressed by

Equation 2-1

$$V_V = A_A = L_L = P_P$$

Saltykov (1945) gave another major breakthrough in stereological estimation methods, when he first derived the following basic equation for obtaining the area of surfaces in a volume, just from a simple counting on two-dimensional section [19].

Equation 2-2

$$S_V = 2P_L$$

The importance of this equation can be appreciated from the fact that it has been rederived at least eight times since 1945. This equation applies to any system of surfaces in space, whether plane or curved, continuous or interrupted, isolated or connected i.e. systems of surfaces with any configuration. It is as valid for systems of interconnected surfaces as for systems of discontinuous, separated, or bounded surfaces. Tomkeieff (1945) proposed a relationship between the surface-to-volume ratio of an isolated, convex body and the mean intercept length through the body [20].

Equation 2-3

$$S_V = \frac{4}{\bar{L}_3}$$

It was later claimed, however, that the requirement of convexity is unduly restrictive. Chalkley (1949) devised a method for obtaining the average surface-to-volume ratio of a system of particles, which involves both a point count and an intersection count on random section through the particles [21].

Equation 2-4

$$S_V = 4\frac{P}{pl}$$

Assuming that all the grains are the same size, Kaiser expressed S_V, the intergranular area per unit volume, in terms of N_V, the number of grains per unit volume [22], by

Equation 2-5

$$S_V = FN_V^{\frac{1}{3}}$$

Where F is a constant dependent on geometric shape. Values of F are 3 for cube, 2,866 for the hexagonal prism, 2.673 for the rhombic dodecahedron, and 2.659 for the truncated octahedron. For real grains, which were thought to approach the properties of rhombic dodecahedra most closely, Kaiser's equation is approximated as

Equation 2-6

$$S_V = \frac{8}{3}N_V^{\frac{1}{3}}$$

Guliver (1918) derived the following simple expression relating the number of grains in space and the planar grain area [23]

Equation 2-7

$$N_V = \frac{2}{3}\left(\bar{A}\right)^{-3/2}$$

Combining the above two equations gives the following expression

Equation 2-8

$$S_V = \frac{7}{3}\bar{N}_A^{\frac{1}{2}}$$

In an attempt to approximate the real structural shapes of polycrystalline aggregates more closely, some investigators abandoned the assumption of equal size and identical shape of all the constituent crystallites. Meijering (1939) determined analytically the parameters of the spatial structure of a metal polycrystal in which the crystal start to grow simultaneously and isotropically from nuclei distributed at random [24]. For the specific area, he derived the following relationship as a function of the number of grains per unit volume:

Equation 2-9

$$S_V = 2.91N_V^{\frac{1}{3}}$$

Approximate methods have been proposed for obtaining the specific surface area of discrete particles, provided that one can assume they have diameters of the same size. If the particles are spheres of diameter D, and the number of particles per unit volume is N_V, then their specific surface will be

Equation 2-10

$$S_V = \pi D^2 N_V$$

Volume fraction of the particles will be

Equation 2-11

$$V_V = \frac{\pi D^3 N_V}{6}$$

From the above two equations eliminating N_V yields

Equation 2-12

$$S_V = \frac{6V_V}{D}$$

S. Z. Bokshteyn developed the above equation by a different method, and then replaced D by the mean diameter of the particle cross sections $\bar{d}$ [25]. This gives the specific surface area of a monodispersed system,

Equation 2-13

$$S_V = \frac{6V_V}{\bar{d}}$$

with an error not more than 7 percent. Instead of making the approximate substitution, $\bar{d} \cong D$, one may use Fullman's statistically exact relation for uniformly sized spheres [26].

Equation 2-14

$$\bar{l} = \frac{2}{3}D$$

This substitution yields

Equation 2-15

$$S_V = \frac{4V_V}{\bar{l}}$$

In order to account for a distribution of sizes in the 3-D particles, Saltykov (1954) applied a correction term to the above relation.

Equation 2-16

$$S_V = \frac{6V_V}{\bar{d}}\left(\frac{\pi}{4}\frac{1}{1+\delta^2}\right)$$

Where δ is the ratio of $\sigma\{D\}$, the root-mean-square deviation of the diameter of the spatial particles to $\bar{D}$, their mean diameter, the coefficient of variance of the particle-size-distribution function. In order to calculate the surface area of spheroidal carbides, L. S. Moroz (1950) developed the expression [27]

Equation 2-17

$$S_V = 1.68\sqrt{C_K N_A}$$

Where C_K is the ratio of the volume fraction of the carbides to their weight percent of carbon (6.67). Cahn and Nutting (1959) investigated particle characteristics in thin films by electron transmission microscopy [28]. They derived the following expression for the surface area of these particles

Equation 2-18

$$S_V = \frac{4}{t}[A_A(proj) - V_V]$$

Where A_A (*proj*) is the projected area fraction of convex particles, and t is the thickness of the thin film. Their derivation utilized the following general expression for the surface area S of convex bodies, attributed to Cauchy [29] :

Equation 2-19

$$S = 4A(proj)$$

A familiar constituent of alloys is the lamellar structure. Perhaps the best-known example is pearlite in steels. The interface area of a lamellar structure depends on the magnitude of the spacing between lamellae. Gensamer, et al. (1942) proposed a method to calculate the mean intercept spacing $\bar{l}$ [30]. Many straight secants of definite length are drawn randomly across the microstructure, intersecting a great number of platelets at all possible angles. The total length of test secants divided by the total number of cementite platelets intersected is defined as the mean intercept spacing. Combining this definition and the basic equation for specific surface area they got the following expression

Equation 2-20

$$S_V = \frac{4}{\bar{l}}$$

In 1953, C. S. Smith and L. Guttman developed a new stereological method to find the length of lineal elements on a plane from a simple counting technique and derived the following expression [31].

Equation 2-21

$$L_A = \left(\frac{\pi}{2}\right) P_L$$

They also framed a stereological technique to find the total length of random lines in a given volume from a simple two-dimensional measurement. Mathematically their technique can be expressed as,

Equation 2-22

$$L_V = 2P_A$$

An equation for the ratio of perimeter length to area of isolated two-dimensional convex figures was given by Tomkeieff (1945), which he expressed in terms of the mean intercept length.

Equation 2-23

$$\frac{\bar{L}_p}{\bar{A}} = \frac{\pi}{\bar{L}_2}$$

It would be possible to observe true points in a volume only under unusual circumstances. The intersections of dislocations in planar arrays are observed frequently in thin metallic foils by means of electron transmission. The intersections actually represent a set of points in a three dimensional volume. Williams and Smith (1952) from their experiments established that if the grain edges of a polycrystalline aggregate were delineated, one could observe a three-dimensional network of lines (edges) terminating four at a grain corner (point) [32]. Hilliards (1962) developed a method to obtain no of points per unit volume in space [33]. In mathematical terms his method can be expressed as,

Equation 2-24

$$P_V = 2P_A P_L$$

Gurland (1958) derived an equation to find the contiguity C, which he defined as the fraction of the total interface area of a phase that is shared by particles of the same phase [34]. For a particulate structure with particles of α-phase in a homogeneous matrix of β-phase, he defined the contiguity as

Equation 2-25

$$C_{\alpha\alpha} = \frac{2(S_V)_{\alpha\alpha}}{2(S_V)_{\alpha\alpha} + (S_V)_{\alpha\beta}}$$

$$C_{\alpha\alpha} = \frac{4(P_L)_{\alpha\alpha}}{4(P_L)_{\alpha\alpha} + 2(P_L)_{\alpha\beta}}$$

Where $(P_L)_{\alpha\alpha}$ and $(P_L)_{\alpha\beta}$ are the number of intersections per unit length of test line with αα and αβ interface traces. Cahn and Hilliard (1959) proposed other parameters for describing quantitative aspects of particle contact [35]. One such parameter is $(L_V)_{\alpha\alpha\beta}$, the ααβ perimeter length per unit volume around contact areas between α-α particles; another parameter is $(L_V)_{\alpha\alpha\alpha}$, the ααα edge length per unit volume between

three contiguous α-particles. The total perimeter length per unit volume around αα-surfaces, $(L_V)_{\alpha\alpha}$, consists of contributions from both ααα- and ααβ-lines. Hence, the following equation is apparent from the above discussion:

Equation 2-26

$$(L_V)_{\alpha\alpha} = 6(P_A)_{\alpha\alpha\alpha} + 2(P_A)_{\alpha\alpha\beta}$$

Where the coefficient 6 includes a factor of three because each ααα-edge is shared by three αα-contacts. Each ααβ-edge, on the other hand, adjoins only one αα-contact. Cahn and Hilliard (1959) derived an expression for $(L_V)_{\alpha\alpha}$ in terms of the numbers of interface traces seen in a unit area on the section plane. Based on the above mentioned fact they obtained the following equation from which the final equation is obvious:

Equation 2-27

$$(N_A)_{\alpha\alpha} = \frac{3}{2}(P_A)_{\alpha\alpha\alpha} + \frac{1}{2}(P_A)_{\alpha\alpha\beta}$$
$$(L_V)_{\alpha\alpha} = 4(N_A)_{\alpha\alpha}$$

Thus the perimeter lengths $(L_V)_{\alpha\alpha}$ can be obtained either by counting contact traces or by counting "triple" points. The factor ½ in the first of the above two equations arises because each interface trace has two termini on the section plane. The above expressions dealing with contiguity are perfectly general, and can be evaluated by simple measurements on the section plane. Gurland (1958) has defined another quantity average number of contacts per grain $(N_C)_{\alpha\alpha}$ by incorporating the shape factor and the average and standard deviation of perimeter lengths as below:

Equation 2-28

$$(N_C)_{\alpha\alpha} = \frac{2(N_V)_{\alpha\alpha}}{(N_V)_{\alpha}}$$

Where the term in the numerator represents the number of α-grain contacts and the denominator is the total number of α-grains, both per unit volume. It is apparent that this expression can't be evaluated by measurements on a single section plane unless a particle shape is assumed. Forscher (1955) defined another attribute of particulate system, called the "continuity" of the particles, as the probability of the presence of infinitely long chains of connected particles [36]. Consideration of the probabilities of such chain formation fall under the theory of branching chains that is too far afield.

In 1967 J. W. Cahn and R. T. Dehoff independently developed a method for estimating the mean mean curvature of a spatial surface by a tangent count on plane sections [37-38]. Their formula is:

Equation 2-29

$$\bar{K} = \frac{\pi}{4}\bar{C} = \frac{\pi}{2}T_A / I_L$$

where I_L is the number of intersections per unit test line length, and T_A is the net tangent count per unit section area.

Oriented structures occur so frequently in metallic alloys that special procedures have been developed to determine their properties. Meteorites, twinned minerals or metals, banded rocks, dislocation arrays, nonmetallic "stringers" in extruded rods and the lamellar eutectic alloys are a few of the examples. The Stereological equations mentioned above are derived for random structures. For oriented systems analogous relations hold, but with changed coefficients.

The degree of orientation of a system of lines in a plane may be quantitatively defined as the ratio of the length of the oriented portions of the lines to the total length [39]. To estimate this property of a structure, it is necessary to determine separately the oriented portions of interest and compare their length to the total length of lines in the system. The oriented portion of the lines can be calculated separately from the isometric portion by measuring N_L at certain directions relative to the orientation axes. In a system with one orientation axis, two groups of secants would be used- one parallel to the orientation axis, the other perpendicular to it. This method has been called "directed secants on a plane" and is proposed by Saltykov. A partially oriented system of lines may be regarded as consisting of two superimposed systems. Then the numerical expression for the *degree of orientation* ω of a system of lines will be determined, in percent, by:

Equation 2-30

$$\omega = \frac{100(L_A)_{or}}{(L_A)_{or} + (L_A)_{is}}$$

where $(L_A)_{or}$ is the specific length of oriented portion of lines

$(L_A)_{is}$ is the specific length of isometric portion of lines

Saltykov proposed a special polar plot to summarize graphically the orientation of all line segments in the system of lines. Test lines are uniformly distributed over all

possible angels to the orientation axis, and then $P_L(\theta)$ is obtained for each angle. By using polar coordinates, the angles of the lines and the specific number of intersection can be represented readily by a curve, which he called as the "rose of the number of intersections" or simply "rose." Underwood derived a relation to find the length per unit area of a system of oriented (parallel) lines.

Equation 2-31

$$(L_A)_{or} = (P_L)_{\amalg}$$

But in real structures the lines in a microsection are usually either isometric or partially oriented. Only in rare cases, such as the Widmanstatten patterns in meteorites, do we find a completely oriented system of lines. In a partially oriented system of lines in a plane, part of the total length of lines is oriented in a definite direction (or directions). The remaining segments may have essentially a random orientation. Underwood derived another equation to find the L_A in such cases.

Equation 2-32

$$(L_A)_{is} = \frac{\pi}{2}(P_L)_{\parallel}$$
$$(L_A)_{or} = (P_L)_{\perp} - (P_L)_{\parallel}$$
$$L_A = (P_L)_{\perp} + 0.571(P_L)_{\parallel}$$

Now the degree of orientation of the lines in the system can be expressed as,

Equation 2-33

$$\omega = \frac{(P_L)_{\perp} - (P_L)_{\parallel}}{(P_L)_{\perp} + 0.571(P_L)_{\parallel}}$$

Completely oriented systems of lines in space with one orientation axis consist of straight lines that have equal or variable spacing, but are parallel to each other and to the orientation axis. Underwood derived an equation to find the length per unit volume of such oriented system of lines in space.

Equation 2-34

$$(L_V)_{or} = (P_A)_{\amalg}$$

The coefficient in the above equation is unity, whereas when the test planes are applied randomly to a system of lines in space, the coefficient is two. Schoeck (1962) investigated various planar arrays of dislocation lines in space and obtained coefficients with values between one and two, depending on the relative orientation of the section plane with respect to the dislocation arrays [40]. In case of partially oriented systems of

lines in space an equation analogous to the one described above for a partially oriented system of lines in plane is derived.

Equation 2-35

$$L_V = (P_A)_{\perp} + (P_A)_{\parallel}$$

He has derived the following equation to find the surface area per unit volume of the oriented system of plane surfaces.

Equation 2-36

$$(S_V)_{or} = (P_L)_{\amalg}$$

In case of partially oriented system of surfaces he obtained the following equation.

Equation 2-37

$$S_V = 1.571(P_L)_{\perp} + 0.429(P_L)_{\parallel}$$

The total surface S_V is equal, in general, to

Equation 2-38

$$S_V = (S_V)_{is} + (S_V)_{lin} + (S_V)_{pl}$$

Where, is, lin, pl refer to isometric, linear, and planar components of the systems of surfaces, respectively. The general equation for the degree of orientation of planes in space, in percent is

Equation 2-39

$$\omega_{or} = \frac{100(S_V)_{or}}{S_V}$$

Hilliards (1967) provided a new mathematical framework for the quantitative description of anisotropic microstructures [41]. He has developed a self-consistent and generalized mathematical treatment for both specifying and determining anisotropy. His approach is a completely general one. Two systems of lines are superimposed on one another and their probabilities of intersection are considered. One system of lines is arbitrarily designated as the test array, and the general equation is set up relating the line length of the other system of lines to the number of intersections with the test array. Methods are then indicated for obtaining the specific line length as a function of direction. Similar procedures are followed for systems of surfaces. The advantages of his analysis are that the functions are easy to interpret and provide for direct correlation of structural anisotropy with other properties; disadvantages lie in the number of angular measurement required and in the mathematical complexity of the solutions.

Spektor (1954) has also given an exact treatment for oriented systems of surfaces, but his method is restricted to symmetrical structures [42]. The equations derived by Hilliard for S_V, L_A, L_V are given below.

Equation 2-40

$$L_A = \pi L_A(\theta)$$
$$L_V = 2\pi L_V(\phi,\theta)$$
$$S_V = 2\pi S_V(\psi,\omega)$$
$$P_V = \frac{1}{2} S_V L_V$$

Fullman (1953) derived the following stereological relation to obtain a spatial parameter of great importance in particulate systems, the mean free distance, λ, between particles, say, of α-phase [26].

Equation 2-41

$$\lambda = \frac{1-(V_V)_\alpha}{N_L}$$

This equation is valid regardless of size, shape, or distribution of particles or other separated volume elements. Chandrasekhar (1943), Gurland (1961), Ashby (1966), Westmacott (1966) [43-45] defined some other distance and spacing parameters for expressing separation of particles. Depending on the desired application of the particular "spacing" the definitions are based on one, two, or more "nearest" -neighbor particles. Gurland used two precisely defined nearest-neighbor distances. These two distances are denoted by Δ_2 and Δ_3 and are defined as the average distance between nearest-neighbor pairs of point particles in a plane and in a volume, respectively.

Equation 2-42

$$\Delta_2 = 0.5 P_A^{-1/2}$$
$$\Delta_3 = 0.554 P_V^{-1/3}$$

Frequently the properties of a particulate or cellular structure can be represented satisfactorily by calculations based on a regular polyhedron or volume of revolution. Coexter (1963), Lyusternik (1963) have contributed to the geometrical analysis of regular polyhedrons [46-47]. Tomkeieff (1945), Hadwiger (1955), Kendall and Moran (1963) have dealt with general relationships for convex particles and figures of unspecified shape that are basic to a geometrical analysis. Smith and Guttmann (1953) presented general relationships for two-dimensional figures and three-dimensional objects, which assumes significance in the present context. Rutherford, Aborn, and

Bain (1937) made calculations on the truncated octahedron that form the basis for the ASM Metals Handbook tabulation of spatial and planar grain properties [48]. Kaiser (1938) tabulated properties of four basic space-filling regular polyhedrons with plane faces: i.e., the cube, hexagonal prism, rhombic dodecahedron, and the truncated octahedron. Hull and Houdk (1953) selected four regular polyhedrons for an analysis of intercept area distribution curves [49]. Saltykov (1958) reviewed his work in this field, and contributed some interesting analyses for spheres. The sphere has been substituted for particles or cells more than any other volume of simple shape. If it can properly be assumed that spheres approximate the real structure satisfactorily, one can readily obtain spatial parameters from simple planar measurements alone. The problem is still simpler if a constant sphere diameter can be assumed. Fullman (1953) showed the power of statistical-geometrical probability approach to the analysis of simple particles. He developed methods for the analysis of particle size measurements by area and lineal analysis when the particles are in the form of spheres, plates, or rods for both monodispersed and polydispersed systems of particles [26]. He derived quantitative relationships between various average quantities obtained from a polished cross section and the actual dimensions of the particles present. In case of spheres he has derived the following relations based on the fact that the probability of a plane intersecting a single sphere positioned at random within the unit cube is 2r. This fact is apparent since, of the various possible positions for the cross-sectional plane over the unit length from top to bottom of the cube, only those positions existing over the length 2r would lead to the plane intersecting the sphere.

Equation 2-43

$$\bar{A} = \frac{2}{3}\pi r^2$$

$$N_L = N_V \pi r^2$$

$$\bar{l} = \frac{4}{3} r$$

He derived similar relations for particles in the form of circular plates of uniform radius (radius r, thickness t, r>>t). He proved mathematically that the probability of a plate intersecting a singly randomly positioned and randomly oriented plate is equal to $\pi/2$ times the radius of the plate. Based on this relation he derived the following equations:

Equation 2-44

$$\bar{A} = 2rt$$

$$N_L = N_V \frac{\pi r^2}{2}$$

$$\bar{l} = 2t$$

He also dealt with the particles in the form of randomly oriented rods (radius r, length H, H>>r). He showed that the probability of a single randomly positioned and oriented rod cut by a plane is equal to half of the height of the rod. Based on this probability he derived the following equations for rod shaped particles:

Equation 2-45

$$\bar{A} = 2\pi r^2$$

$$N_L = N_V \frac{\pi r H}{2}$$

$$\bar{l} = 2r$$

It can be seen here that neither the average cross-sectional area nor the average lineal traverse of particles in the form of long thin rods depends on the length of the rods. This is due to the fact that for such particles there is negligible probability that a cross-sectioning plane will cut along the rod length. Later on his analysis is extended for many other shapes of the particles. Dehoff (1961) has treated ellipsoidal (prolate and oblate) particles in general [50], where as Myers (1963) treated simple particles with flat sides (regular polygons) [51]. All the equations given above are for monodispersed system of particles. Mean values of V,S,N_V and r for polydispersed systems of spheres and think circular disks are derived by Fullman. He divided the particles into class intervals, each of constant size, applied the equations described above to each class interval, then summed up all valued over the range of particle sizes. However, another measurement is required in order to express the average values in terms of measurable two-dimensional quantities. For a distribution of spheres, the required quantity is the mean value $\bar{m}$ of the reciprocals of the circle diameters on the test section. Some of the equations obtained by Fullman for spheres having a distribution of sizes are reproduced below:

Equation 2-46

$$\bar{V} = \pi V_V / 2\bar{m} N_A$$

$$\bar{S} = 2\pi N_L / \bar{m} N_A$$

$$N_V = 2\bar{m} N_A / \pi$$

$$\bar{r} = \pi / 4\bar{m}$$

Fullman also formulated the equations for polydispersed systems of thin disks. They are given below:

Equation 2-47

$$\bar{V} = \pi^2 V_V / 8\bar{E} N_A$$

$$\bar{S} = \pi^2 N_L / 2\bar{E} N_A$$

$$N_V = 8\bar{E} N_A / \pi^2$$

$$\bar{r} = \pi / 4\bar{E}$$

$$\bar{t} = \pi \bar{G} / 4\bar{E}$$

Where $\bar{E}$ is the mean value of the reciprocals of the disk lengths on the section plane and $\bar{G}$ is the mean value of the ratios of the width-to-length dimensions of disk sections.

The number of sections seen on a polished cross-section and the actual number of profiles in the volume are related by the following relation, which is treated as one of the basic stereological relations.

Equation 2-48

$$N_A = N_V \bar{H}'$$

Where $\bar{H}'$ is the mean of the projected heights of the system of randomly oriented particles. This relation is exact for convex particles of any shape. But $\bar{H}'$ can't be determined directly in many cases. For a monodispersed system of spheres, how ever, it is clear that the diameter D is equal to H' and in a polydispersed system of spheres, $\bar{D}$ is equal to $\bar{H}$. Thus, for spheres of equal size, the above equation becomes

Equation 2-49

$$N_V = N_A / \bar{D}$$

Weibel and Gomez (1962) found the following relationship between the numerical density of particles, N_V, the numerical profile density, N_A, and the volume fraction of particles, V_V as a measure of particle size [52]:

Equation 2-50

$$N_V = \frac{1}{\beta} \cdot \frac{N_A^{\frac{3}{2}}}{V_V^{\frac{1}{2}}}$$

Where, the coefficient β is solely dependent on the shape of the particles and not on their size, and is related to the volume v and average profile area of the particle $\bar{a}$ as

Equation 2-51

$$v = \beta . \bar{a}^{\frac{3}{2}}$$

Sterio(1984) proposed an unbiased estimator of number and size of aribitrary particles in 3D space, known as disector. By centering on the design of sampling strategies, the disector method first dropped all inherent assumptions about the particle shape in previous analysis methods, then the point-sampled intercept and some other methods followed. The disector comprised, for the first time, a complete rule for uniform sampling of 3-dimensional objects and other discrete events according to cardinality [53]. The disector comprises an integral test system and a counting rule: the number of structures sampled by the counting frame disappearing from one section plane to another, Q- is counted. The integral test system comprises the 2-dimensional counting frame with a certain area per test point, (a/p), and the number of times the test points hit the reference volume under study, P. The two parallel section planes are a known distance, h, apart and the numerical density of structures is estimated as:

Equation 2-52

$$N_V = \frac{Q^-}{(a/p).h.P}$$

Sampling with the disector is not restricted to isolated objects. Associate features of objects may also be sampled by the disector. Disector sampling has opened up for a whole range of local stereological estimators of size. However if the matter is opaque,

the physical dissector has to be used which is based on parallel sections a known distance apart. Then it is necessary to identify particles that are hit by both sections, which requires perfect registration of the relative position of the two images. Moreover a bias may be introduced because particles that are smaller than the distance between the two section planes cannot be detected. Often it is practically very difficult or even impossible to make parallel section, as of hard and brittle material. This is a reason why classical stereological methods using single sections are traditionally preferred by material scientists.

2.2 METHODS FOR ESTIMATION OF DISTRIBUTION FUNCTIONS

Estimation of the distribution of grain sizes in three dimensions in space is another similar problem that is of interest to metallurgists. Although the earliest work on quantitative microscopic analysis goes back to Délessé (1848), the estimation of particle size frequency functions dates only from Wicksell (1925) that is in connection with the biometric examination of corpuscles [54]. Through an integral equation, he related the size frequency function for spherical particles to that of circular intersections on a random plane of intersection. The fundamental treatise of Wicksell is one of the masterpieces of stereology.

Many different approaches have been used to solve Wicksell's problem or variants of it. The oldest technique for finding a solution is by discretizing the distribution of the sphere radii and the distribution of the planar circular profiles, the last discretization being estimated by a histogram of the observed data. The integral equation then becomes a system of linear equations, which is solved by numerical methods. This method and several of its variants are related to Saltykov's method (1967) [55]. The way the data are grouped (the choice of the histograms bin-widths) is critical for such methods and may give unreliable results for moderate samples.

One of the earliest analyses to be prompted by metallurgical problems is due to Scheil (1931) [56]. His method of unfolding sphere size distributions is rather inflexible and involves lengthy calculations. Scheil's solution of the integral equation that relates section distributions to sphere distribution, is based on a stepwise rather that on a smooth distribution function. The number of particles per unit volume is calculated for each size group, starting with the largest and proceeding down to the smallest size

group. The section diameters obtained from the plane of polish, with radii ranging from 0 to r_{max} (= R_{max}), are divided into 15 size groups. Particles of one size group are considered to be of only one size. From the geometrical relationships and the general integral equation relating the section-size and particle-size distributions of spheres he derived the following expression

Equation 2-53

$$(N_A)_{i,j} = (N_V)_j \Delta r \left[\sqrt{(2j)^2 - (2i-1)^2} - \sqrt{(2j)^2 - (2i+1)^2} \right]$$

Considering the term in the square bracket in the above equation as $X_{i,j}$ Scheil's basic equation can be written as

Equation 2-54

$$(N_V)_j = \frac{(N_A)_{i,j}}{\Delta r X_{i,j}} = \frac{(N_A)_i - (N_A)_{i,j+1} - (N_A)_{i,j+2} - \cdots - (N_A)_{15}}{\Delta r X_{i,j}}$$

where each term to be subtracted is evaluated by

Equation 2-55

$$(N_A)_{i,j+1} = (N_V)_{j+1} \Delta r X_{i,j+1}$$
$$(N_A)_{i,j+2} = (N_V)_{j+2} \Delta r X_{i,j+2}$$

etc., in sequence from largest to smallest sizes. The weakest part in the Scheil's treatment is in the estimation of $(N_V)_j$ for j<15, the calculated values are required, and not the measured values $(N_A)_i$.

Schwartz (1934) improved on Scheil's analysis in several respects [57]. The primary advantage of his method is that the number of particles in any size group can be calculated directly; i.e., there is no sequential dependence upon previous calculations of other particle sizes. Another improvement is that measured number of sections per unit area is used instead of the calculated values of number of particles per unit volume in the final equation. Schwartz didn't use the general integral equation relating the section-size and particle-size distributions of spheres. Rather, the coefficients required for the calculation are deduced from the probability of a random plane intersecting a sphere at a certain section size. A disadvantage of Schwartz's method is that the values of the coefficients change if a different number of intervals is selected. Hyam and

Nutting circumvented this problem by using a geometrical progression of size intervals [58].

Saltykov further developed Scheil's method as modified by Schwartz. Saltykov's method embodies the advantages of Schwartz's modification, but at the same time is free of its shortcomings. A direct calculation of the number of particles in any size group may be made regardless of whether the number of particles in any other group is known or not. This method is discussed in detail in the next chapter.

Saltykov's area analysis (1967) attempts to improve on older methods and succeeds in several regards [55]. It does not require sequential calculations or tables of coefficients. It has the advantages of simplicity of calculation and finer differentiation of the small sizes. It is applicable not only to polydispersed systems of spherical particles, but in principle, to convex particles as well. In this analysis, all particles must have the same shape. In order to specify the size of a section, Saltykov adopted the ratio A/A_{max} instead of the absolute area. Thus it is apparent that the correct value of A_{max} is very important. A large number of particles must be examined on the plane of polish, especially if the particles have a complicated shape. The scale factor used to determine the class intervals for A/A_{max} is based on a logarithmic scale of diameters with the factor $10^{-0.1}$. The advantage of using A/A_{max} to group the sections lies in the unique relationship of the particle shape to the N_A versus A/A_{max} frequency distribution. By intersecting a given particle with many random planes, one can obtain a distribution of sectional areas which is characteristic of that particular particle. For spherical particles, this distribution can be calculated readily and the values are tabulated by Saltykov. For particles of other shapes, the calculation of the (N_A) distribution versus A/A_{max} would be extremely difficult. The computations follow along the lines described previously. The procedure is similar, except that one successively subtracts those sections contributed by larger spheres. The spherical particles have diameters D_j corresponding to $(N_V)_j$. Saltykov derived the following general working formula which directly gives $(N_V)_j$ for any desired class interval.

Equation 2-56

$$(N_V)_j = \frac{1}{D_j}\begin{bmatrix} 1.6461(N_A)_i - 0.4561(N_A)_{i-1} - 0.1162(N_A)_{i-2} - 0.0415(N_A)_{i-3} \\ -0.0173(N_A)_{i-4} - 0.0079(N_A)_{i-5} - 0.0038(N_A)_{i-6} - 0.0018(N_A)_{i-7} \\ -0.0010(N_A)_{i-8} - 0.0003(N_A)_{i-9} - 0.0002(N_A)_{i-10} - 0.0002(N_A)_{i-11} \end{bmatrix}$$

Note that j can have any integer value up to and including 12. For example, to calculate the value of $(N_V)_4$, one would use just the first four terms in the brackets. It should be noted that for this particular derivation, the largest particle size corresponds to $j=1$ the $i=j$, with subscripts varying through $i-1, i-2, i-3, etc.$, down to 1.

The derivation by Spektor (1950) appears to be the first among the well-known analytical methods for determining particle-size distribution curves from chord-length distributions [59]. His method requires the shorter computational time, but measuring and recording individual chord lengths is slower than applying a circular template for the area method. The one extremely sensitive point in both analyses is the measurement of the smallest particles. His final working equation apply to either a continuous or a discontinuous size distribution and is expressed as follows

Equation 2-57

$$(N_V)_j = \frac{4}{\pi\Delta^2}\left[\frac{(n_L)_j}{2j-1} - \frac{(n_L)_{j+1}}{2j+1}\right]$$

where the $(N_V)_j$ and $(n_L)_j$ are the number of particles per unit volume and the number of chords per unit length of test line, respectively, for the indicated j-size. We can see form the above equation that no coefficients need be calculated for the $(n_L)_j$ terms. We merely select a convenient Δ value, then substitute it and the experimentally determined values of $(n_L)_j$ into the above equation.

Lord and Willis (1951) also did the same type of analysis as that proposed by Spektor, in an attempt to obtain the volume fraction and size distribution of spherical air bubbles in frost-resistant concrete [60]. But they pointed out that their method is applicable to any system containing "spherical dispersoids." In treating the relationship between a distribution of chord lengths and a distribution of sphere diameters, they gave both an analytical solution and a graphical procedure. Their analytical solution is analogous to the Spektor's analysis, but their graphical solution is unique. The main steps in their graphical solution may be listed as follows:

1) They show, for uniform spheres of diameter D_1, that the graph of the frequency distribution $n_L(l)$ of chord lengths l is a straight line from $l=0$, $n_L(l)=0$ to a maximum at $l=D_1$. Thus a monodispersed system of spheres is represented by

a triangle, the area of which equals the total number of chords per unit length of test line.

2) For two monodispersed systems of spheres, there will be two triangles; for three systems, three triangles; etc. These triangles can be recombined, preserving the individual triangle areas, in such a way that the resulting figure represents the total system.
3) A frequency distribution curve of chord lengths resulting from penetration of a polydispersed system by a test line is constructed in the same manner. The number of chords from each class interval contributes a triangular area, the dimensions of which are dependent on the diameter and number of spheres in the class interval.

For a polydispersed system of spheres a complete chord length distribution is plotted as described above. Figure 2-1 illustrates such a curve, where the number of chords per unit traverse length divided by the interval length is plotted against the medians of the corresponding intervals. The intercepted distances along the vertical line *AB* are related to the number of spheres per unit volume in each length interval. They have shown by simple mathematical analysis that

Equation 2-58

$$(N_V)_i = \frac{2}{\pi}\frac{(KN_V)_i}{OA}$$

When the distance *OA* is set off $2/\pi$ units on the *l* scale, the above equation reduces to

Equation 2-59

$$(N_V)_i = (KN_V)_i$$

Taylor (1982) was the first to use a kernel estimator for estimating, by a smooth function, the density of the planar circular profiles which is then substituted in the integral equation to obtain an estimate of the density of the sphere radii [61]. Taylor's method, which can be viewed as an operation smoother than the one produced by the histogram binning of Saltikov's method, relies also upon a good choice of the window width of the kernel smoother. Hall & Smith (1988) have shown that Taylor's method can be efficient only if the number N_A of observed planar circular sections is very large, which is rarely true in practical situations [62]. A kernel based approach for estimating the cumulative distribution of the squared three-dimensional radii has also been derived recently by Golubev & Levit (1998) [63]. Recently, Feuerverger & Hall (2000) studied

a thick-slice version of Wicksell's problem, and introduced an appropriate cross-validation criterion for selecting the kernel smoothing parameter [64]. Nychka et al. (1984) used a cross-validated spline regularization method to estimate the density of the sphere radii [65]. The solution is obtained by approximating the unknown density by a smooth combination of natural splines, in such a way that its integral transform stays close to a histogram of the data, with a number of classes much larger than the one that should be employed to estimate optimally the density of the planar sections. Antoniadis (2001) developed a method based on wavelet transforms for unfolding sphere size distribution. The method consists of first converting the wicksell's integral equation to a form suitable for application of thresholding wavelet methods and then deriving the asymptotic properties of their estimators [66].

The assumption of spherical grains is dubious for metal grains, which are known to be space filling. Scheil and Wurst (1936) determined the distribution of grain sizes based on actual grain shapes, rather than on grains having spherical or ellipsoidal shapes [67]. By successive sectioning of a sample of Armco iron, Scheil and Wurst obtained average section radii through 68 grains, from which they calculated a statistical grain shape. They provided a table of coefficients based on 14 class intervals for this particular statistical grain shape. The derivation of the spatial size distribution from the planar size distribution is similar to that described by Scheil for spherical particles. Paulaus (1963), who is interested in the magnetic and electrical properties of ferrites as influenced by their grain-size distributions, further improved the Scheil and Wrust analysis. On the basis of comparison of average characteristics of real grains and cells, Paulus selected the pentagonal dodecahedron as the prototype shape for ferrite grains. Using Hull and Houk's frequency distribution curve of diameters for the pentagonal dodecahedron, he calculated a table of coefficients in much the same way as Scheil and Wurst. Paulus offered both analytical and graphical methods [68]. The analytical method is based on Scheil's original analysis, except that class intervals are spaced according to a geometrical progression. With the help of the latter simplification, plus the assumption of lognormal distribution, Paulus prepared graphical solutions for several special cases. The limitations inherent in a Scheil-type analysis are circumvented to some extent in Paulus' graphical solution.

Cahn and Fullman (1956) analyzed the lamellar structures, which is the extension of their procedure for spheres [69]. The method applies to structures such as pearlite, in which hard lamellae are embedded regularly in soft matrix. Instead of a

calculated or analytical distribution function of lamellae spacing, this method is based on a measured lamellae spacing distribution curve. Cahn and Fullman considered two experimental parameters: true spacing σ_t and random intercept spacing σ_r, the true spacing is the perpendicular distance across two adjacent platelets, while the random spacing is the center-to center distance between hard lamellae along random test lines on the plane of polish. Using the geometrical probability principles and equivalence of volume fraction and lineal fraction, they derived the following expression for volume fraction distribution function of the true spacing of lamellae depending on lineal distribution function:

Equation 2-60

$$V_V(\sigma_t)_{\sigma_t=\sigma_r} = 2g(\sigma_r) + \frac{dg(\sigma_r)}{d\ln\sigma_r}$$

where $g(\sigma_r)$ is the lineal fraction distribution function of random spacings. Similarly depending on number distribution function of random spacings they derived the following expression for volume fraction distribution function of true spacings:

Equation 2-61

$$V_V(\sigma_t)_{\sigma_t=\sigma_r} = 3\sigma_r n_L(\sigma_r) + \sigma_r^2 \frac{dn_L(\sigma_r)}{d\sigma_r}$$

In 1926 in Wicksell dealt with the case of ellipsoidal particles [70]. Wicksell chose the geometric means of the diameters of triaxial ellipsoids and of their profiles as the characteristic measure or "diameter". He then found first that the frequency of profile "diameters" is related to the "diameter" of the central ellipse of the particle by the same fundamental Abel-type integral equation as he had found for spheres (1925). For prolate spheroids this was also the case if he chose the minor axis of both ellipsoids and section ellipses, or if for oblate spheroids he used the major axis. After rigorous mathematical analysis he concluded that exactly the same relations exist between the functions F (frequency of the central diameter of the ellipsoid) as in the case of spherical corpuscles. Hence applying the reductions deduced for the case of spherical corpuscles to the distribution of the minor diameters in section ellipses one can obtain the distribution of the minor diameters of the corpuscles, if they are all prolate ellipsoids of revolution. It is evident that the same result will hold if the corpuscles are all oblate ellipsoids of revolution, if we then apply the spherical reductions to the

distribution of the major diameters in the section ellipses. The result obtained will be the major diameters of the corpuscles.

Till 1962, no further attempts seem to have been made to re-derive Wicksell's solution for the size distribution of ellipsoidal particles. Dehoff (1962) modified the Schwartz-Saltykov analysis for spherical particles so as to obtain the size distribution of ellipsoidal particles of the same shape (axial ratio). This analysis is dealt in more detail in the next chapter.

The difficulty with Wicksell's and Dehoff's analyses of ellipsoidal particles is that it is not valid for a general population of ellipsoids because it was based on the rather strong assumption that size and shape were statistically independent. The general problem, which involves bivariate distributions of size and shape, has been solved by Cruz-Orive (1976) [71]. Spherical particles, or particles modeled by geometrical bodies of a constant shape (e.g. ellipsoids with constant axial ratios, cylinders with a constant height-to-diameter ratio, etc.), can be described by a single size parameter as proposed by Wicksell. The particulate phase is then described by a univariate size distribution, and the stereological problem consists simply in identifying this distribution from the univariate size distribution describing the set of profiles produced by a random plane section through the aggregate of particles. Particles exhibiting variation about a given type of shape as well as size variation, however, cannot be described by a single parameter. Such is the case of, ellipsoidal particles of variable size and eccentricities. Assuming that the spheroid centers are uniformly scattered within the specimen, the spheroids are isotropically and independently orientated about their centers and finally the size and shape of a randomly chosen spheroid are independent from its position within the specimen, Cruz-Orive solved the problem of estimating bivariate size-shape distribution of spheroids from the corresponding size-shape distribution of elliptical profile. This problem is explained in detail in the next section.

A. M. Gokhale (1996) derived a fairly general and flexible statistical relationship between the apparent bivariate distribution of size and orientation of micro crack traces observed in metallographic sections (which can be experimentally measured), and the true bivariate size and orientation distribution of micro cracks in three-dimensional microstructure, without assuming anything concerning anisotropy of micro cracks, their sizes, orientations, thickness, and any correlations between size and orientation [72]. Prior to his derivation Seaman et al (1978) developed a numerical analysis algorithm to calculate the histogram representation of true bivariate size and

orientation distribution of micro cracks from measurements performed on a metallographic section [73]. But they assumed that the true distribution is rotationally symmetric with respect to a reference axis, i.e. there is an axis of symmetry. They formulated the problem in a discretized format and this discrete (rather than closed form analytical) treatment does not permit development of more efficient numerical algorithms. Gokahle's formulation of the problem is not in discretized format. The apparent bivariate size and orientation distribution of micro cracks is related to the corresponding true bivariate distribution function through a double Abelian integral equation. This analytical treatment is convenient for calculation of the apparent bivariate size and orientation distribution of the micro crack traces for modeled true bivariate distributions of micro cracks. Actually the micro cracks are modeled as penny shaped cylindrical objects with flat circular ends (platelet like). Hence this method is applicable to any system of circular disc shaped particles. The mathematical treatment of this method is discussed in detail in next section.

The problem of unfolding bivariate distribution of unequiaxed particles modeled by triaxial ellipsoids of variable size and eccentricity parameters is indeterminate in its generality, because the elliptical profiles do not furnish sufficient information which permits a complete description of the ellipsoids [71]. Consider an α phase consisting of randomly oriented ellipsoids dilutely embedded in an opaque matrix. Let the principal semiaxes of an ellipsoid are denoted by a, b, c varying in the region $(0<c\leq b\leq B)$, $(b\leq a<\infty)$. Where, B is the largest value of b in the ensemble of ellipsoids. The two principal squared eccentricities are defined as $x_1^2=1-(b/a)^2$ and $x_2^2=1-(c/a)^2$, so that $0\leq x_1^2\leq x_2^2<1$. Let the ellipsoids are described by the three dimensional random variable (c, x_1^2, x_2^2), consisting of a size component plus two shape components. Their joint probability density function $g(c, x_1^2, x_2^2)$ is defined in the region $(0<c\leq B)$, $(0\leq x_1^2\leq x_2^2<1)$. The population of random, plane elliptical profiles is described by the bidimensional variable (m,y^2), with joint probability density function $f(m,y^2)$ defined in the region $(0<m\leq B)$, $(0\leq y^2<1)$. Where, m is the minor axis of the profile and y^2 its squared eccentricity parameter. The general version of Equation 3-29 can be expressed as,

Equation 2-62

$$f(m,y^2)=\int_0^{y^2}dx_1^2\int_{y^2}^{1}dx_2^2\int_{m\sqrt{(1-x_2^2)/(1-y^2)}}f^*g^*dc+\int_{y^2}^{1}dx_1^2\int_{x_1^2}^{1}dx_2^2\int_{m\sqrt{(1-x_2^2)/(1-x_1^2)}}f^*g^*dc$$

Where f^* denotes the conditional joint probability density function of (m,y^2) on the ellipses produced by a random plane T in a fixed ellipsoid K of parameter (c, x_1^2, x_2^2), whereas $g^*=g(c, x_1^2, x_2^2|T\cap K)$.

Let us suppose that all the ellipsoids in the α-phase are spheroids. Hence, the whole probability mass is concentrated in the two plane rectangular regions $\{(0<c\leq B), (0\leq x_1^2=x_2^2<1)\}$ and $\{(0<c\leq B), (0=x_1^2\leq x_2^2<1)\}$. In the former case, g takes the form $g_p(c, x^2, x^2)\equiv g_p(c, x^2)$, which describes the subpopulation of prolate spheroids. In the latter case g becomes, $g_o(c, 0, x^2)\equiv g_o(c, x^2)$, which describes the oblate subpopulation. Clearly, g_p and g_o must satisfy the identity

Equation 2-63

$$\int_0^1 dx^2\int_0^B(g_p+g_o)dc=1$$

For the mixture of spheroids as the one described above, the general expression Equation 2-62 reduces to

Equation 2-64

$$f(m,y^2)=\int_{y^2}^{1}dx^2\int_{m\sqrt{(1-x^2)/(1-y^2)}}f_o^*g_o^*dc+\int_{y^2}^{1}dx^2\int_{m}^{B}f_p^*g_p^*dc$$

$$=\int_{y^2}^{1}dx^2\int_{M}^{B}f_o^*g_o^*da+\int_{y^2}^{1}dx^2\int_{m}^{B}f_p^*g_p^*dc$$

Clearly, when $g_o=0$ (all spheroids are prolate), the equation reduces to the equation for prolate ellipsoids, and when $g_p=0$ (all the spheroids are oblate), the equation reduces to the equation for oblate spheroids. It is shown in Equation 3-27 and Equation 3-29, that these equations have unique solution. However, Equation 2-64does not admit unique solution for g_o and g_p. To check this let us put $f=qf+(1-q)f$, where q is a fixed but arbitrary number between 0 and 1 and consider the following equations,

Equation 2-65

$$qf = \int_{y^2}^{1} dx^2 \int_{M}^{B} f_o^{\bullet} g_o^{\bullet} da$$

$$(1-q)f = \int_{y^2}^{1} dx^2 \int_{m}^{B} f_p^{\bullet} g_p^{\bullet} dc$$

The above equations are of the form Equation 3-49 and g_o and g_p can be solved for unique solution as per Equation 3-51. It is evident that the two functions so obtained satisfy Equation 2-64, and hence they are solutions of it. However, one can obtain as many pairs (g_o, g_p) satisfying Equation 2-64 as one pleases, by simply choosing different values of q. It is clear from the above discussion that the problem of "mixture of spheroids" and hence the problem of "triaxial ellipsoids" is indeterminate.

Warren and Durand proposed a computer-modeled approach, which they named as "guess-and-compare process" to determine the 3-D particle size distribution in systems of uniform, identifiable particle shape. The methodology of this process is, guessing a 3-D size distribution and then, by computer modeling producing a 2-D result that can be compared with the experimental distribution. This process of guess and compare is repeated until satisfactory agreement is achieved.

In case of polyhedral shaped particles, the shape of the profiles will be triangle or any other polygon depending upon the order of the polyhedra of the particles. In case of cubes profiles will be anything between triangles and hexagons. So it does not make any sense to define any particular "diameter" in this case. The problem of estimation of the size distribution of cubical particles from the distribution of section profiles remained undetermined till J.Osher and M. Nippe (1997) proposed a method exploiting size and shape of the observed profiles [74]. They actually derived a methodology that is applicable to any homothetic particle system. As mentioned earlier the section profiles no longer form a system of homothetic figures, hence they carry additional information than can be expressed by one size parameter. They made two observations on planar sections: 1) measuring the maximum breadth of the profiles (caliper diameter) and 2) counting the number of vertices of the profiles. They also have shown that the size of a single cubic particle can be determined immediately from the shape of a given section profile if the number of vertices of that profile is greater than 3.

All the stereological unfolding procedures discussed above are model-based methods, i.e. the objects are assumed to have a particular size, shape, and orientation or

the objects are modeled (e.g., sphere, ellipsoid, cube, etc.). The data for all the above-mentioned unfolding methods comes from the 2-D measurements, which always contain sampling errors and bias. In almost all methods of deconvolution, calculation of the 3-D particle size distribution from 2-D profile distribution essentially involves a numerical solution to an Abelian integral equation. These numerical calculations still amplify the already present sampling errors and bias in the 2-D data and hence the final solution consists of more errors than in the raw data.

The other category of stereological methods, design based methods, are characterized by counting rules and sampling schemes that have been designed to eliminate considerations of the size, shape, and orientation of cells being counted. Design based techniques for counting requires not a priori knowledge about the size, shape or orientation of the objects being counted. Serial sectioning is one of the well known design based techniques. Conventional serial sectioning has been successfully used for quantitative characterization of microstructures, viz. to study the 3-D morphologies of the features that appear on microstructure, to estimate the number of particles per unit volume of space and to quantify the topological connectivity of microstructural features in 3-D. Conventional serial sectioning involves digitally recording a microstructural field of view, removing a small thickness of the specimen by controlled polishing, again recording the field of view exactly below the first one on the new section. This procedure is repeated to generate a stack of large number of aligned serial sections. The 3-D information of the microstructural features can be then obtained from this stack of serial sections. Since this technique involves serious edge effects and sampling bias, it has not been used for the estimation of 3-D particle size distribution. In order to get accurate measurements of particles sizes, microstructure has to be observed at sufficiently high magnification and the distance between consecutive serial sections has to be significantly less than the average size of the particles/grains under observation. At high magnification the field of view hardly contains 25-50 particles/grains. In practice at the most about 50-100 serial sections are generated. Therefore, the microstructural volume generated by conventional serial sectioning technique contains, at the most, a hundred particles or so. Such small statistical sample size is not sufficient for reliable estimation of the complete particle/grain size distribution. The edge effect also brings a lot of systematic bias into the raw data. This is because of the fact that larger particles are more likely to intersect the frame boundaries.

. A. Tewari and A. M. Gokhale (2000) developed a method by the application of montage-based efficient serial sectioning technique for estimation of particle size distribution, that overcome the shortcomings of conventional serial sectioning technique [75]. The basic idea behind this newly developed technique is that, first a small microstructural volume is reconstructed from a stack of conventional serial sections and then many contiguous small volumes are reconstructed surrounding the initial volume and finally all of them are pasted together after perfectly matching their boundaries to generate a large (about 25-100 times larger than the volume developed by conventional technique) three dimensional microstructural volume at high resolution from the same number (50-100) of serial sections as that in the conventional serial sectioning. The beauty of this new technique is with the same metallographic effort as in the case of conventional technique, one can generate a microstructural volume containing few thousands of particles. Such a large statistical sample is sufficient for reliable, unbiased, assumption-free and efficient estimation of 3-D particle size distribution.

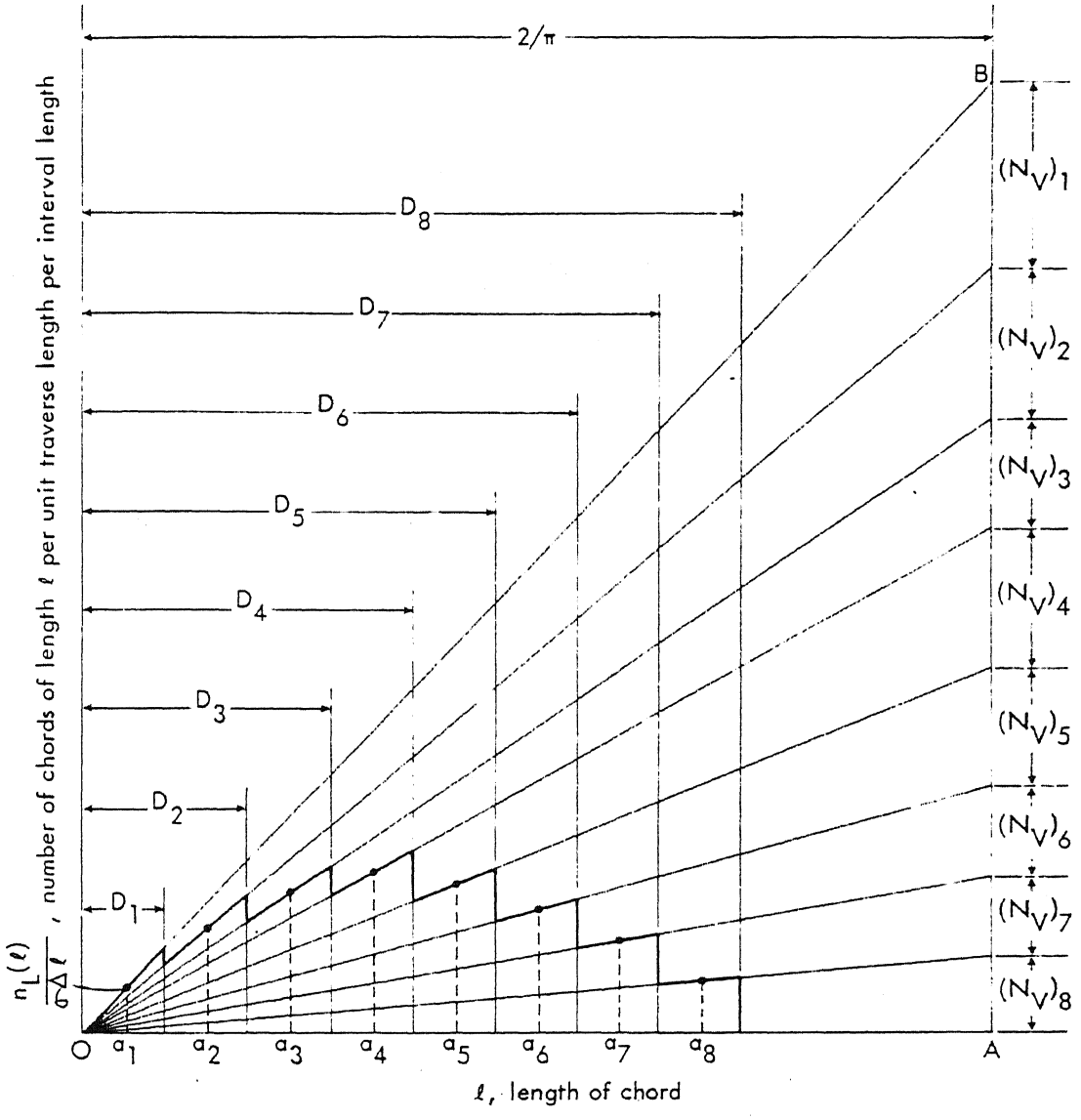

Figure 2-1 Distribution curve of chord lengths constructed by graphical method [18]

CHAPTER 3

COMPUTATIONAL BACKGROUND

3.1 SIZE DISTRIBUTION OF SPHERES

3.1.1 INTRODUCTION

Before going into detailed discussion about unfolding the size distribution of spheres from measured size distribution of circular profiles, a brief note is given here on how the profile sizes are distributed when a single sphere of radius *R* is randomly sectioned many times [76].

Consider a sphere of radius *R*, which is embedded in a cube of matrix material and is placed in x, y, z coordinate system with its center at the origin (See Figure 3-1). Now, a large number of equidistant section planes, which are parallel to x-y plane are placed into this cube of material. Only those sections, which lie between the upper and lower parallel tangent planes will cut the sphere inside the cube. It is evident that the number of section planes that cut the sphere is proportional to the diameter of the sphere, i.e. *2R* (in this case). Each of these section planes will produce a circular profile. The radii of the circular profiles thus produced are a function of the position of the section planes with respect to the z-axis, as shown below,

Equation 3-1

$$r(z) = \sqrt{\left(R^2 - z^2\right)}$$

The size distribution of profiles is characterized by determining the probability density with which a profile radius r_i falls into the range

Equation 3-2

$$r > r_i > (r - dr)$$

Since the sectioning planes are parallel to x-y plane, the probability measure must be related to the distance along the z-axis between the plane that will produce a profile of radius *r* and that, which produces a profile of radius (*r-dr*). Let us denote this distance by dz. From the rules of geometric probability, the probability of sectioning any object with a plane is the ratio of the tangent diameter of the object to the tangent diameter of the containing space. Hence, the probability of having r_i in the class {*r*, (*r-dr*)} is given by,

Equation 3-3

$$\Pr\{r > r_i > (r-dr)\} = \begin{Bmatrix} dz/R & for & r \le R \\ 0 & for & r > R \end{Bmatrix}$$

It should be noted that the slice thickness dz is not constant, but is a function of r as shown in Figure 3-2. From the definition of dz one can write,

Equation 3-4

$$dz = z(r-dr) - z(r)$$

From the equation of the circle we can derive,

Equation 3-5

$$z(r) = \sqrt{(R^2 - r^2)} \text{ and}$$

Equation 3-6

$$z(r-dr) = \sqrt{(R^2 - (r-dr)^2)}$$

Inserting Equation 3-5 and Equation 3-6 in Equation 3-4, we get,

Equation 3-7

$$dz = \sqrt{(R^2 - (r-dr)^2)} - \sqrt{(R^2 - r^2)}$$

Differentiating Equation 3-7 with respect to r, we get,

Equation 3-8

$$\frac{dz}{dr} = \frac{-r}{\sqrt{(R^2 - r^2)}}$$

Inserting Equation 3-7 in Equation 3-3 the probability density becomes,

Equation 3-9

$$\Pr\{r > r_i > (r-dr) \mid R\} = \frac{1}{R}\left[\sqrt{(R^2 - (r-dr)^2)} - \sqrt{(R^2 - r^2)}\right]$$

Inserting Equation 3-8 in Equation 3-3 the probability density becomes,

Equation 3-10

$$\phi(r \mid R)dr = \frac{r}{R\sqrt{(R^2 - r^2)}}dr$$

In the above equation the sign of the right hand side term is changed to give positive probabilities. In Equation 3-9 and Equation 3-10 the argument of the left hand side function is extended to note that it depends on both the sphere size and the profile size. It should be noted that Equation 3-10 is continuous version of Equation 3-9 and it becomes Equation 3-9 if $\phi(r \mid R)$ is integrated between the class limits *{r, r-dr}*.

Equation 3-11

$$\Pr\{r, r-dr\} = \int_{r-dr}^{r} \phi(r \mid R)dr = \Pr\{r \mid R\}$$

The form of the curve $\phi(r \mid R)$ is shown in fig (6.3a). Since $\phi(r)$ is a probability density function, if Equation 3-10 is integrated over the range 0 to R, the result must be unity. A more realistic representation of this function is perhaps a histogram as shown is fig (6.3b) whereby dr may be chosen as fine as desired ($dr \rightarrow 0$ at the limit). The values $Pr\{r|R\}$ of the histogram columns is obtained by Equation 3-9.

From the above analysis we find that, although all profiles are equally likely to occur, the probability density of profile radii varies with profile size, i.e. larger profiles are more likely to be found on section than smaller ones. This is not paradoxical. Because, in defining the probability of obtaining a certain profile we proceed at sectioning the sphere at equal intervals along the z-axis normal to the sectioning plane. The increments $dr(z)$ in profile radius will then become smaller as the section plane moves down as shown in Figure 3-3. In defining the probability density of measuring a certain profile radius we assume equal increments of r by dr. This produces larger intervals $dz(r)$ between the slice boundaries as r becomes larger as shown in Figure 3-4. In the above analysis we have assumed that one sphere was sectioned many times. This assumption is similar to assuming a monodispersed system of spheres being randomly embedded in a large block and this block being sectioned once, or a few times at great distances.

3.1.2 METHODOLOGY

3.1.2.1 DISCRETE MODEL

Consider a polydispersed system of spheres, i.e. a system of spherical particles of varying size, such as the one shown in Figure 3-5. If this population of spheres is randomly sectioned with a plane, one gets a distribution of circular profiles. There are basically three factors that may influence in some way or another the number of profiles contributed to each profile class. They are,

(a) The numerical density of spheres occurring in each class of the sphere size distribution;

(b) The probability of hitting a sphere of a certain size with a random sectioning plane, which is related to its (mean tangent) diameter;

(c) The frequency distribution of profiles derived from each class of spheres.

Let us assume that the sphere and profile size classes have the same interval, i.e. $\Delta R = \Delta r$. Hence, the sphere and profile radii can be expressed as integer multiples of ΔR or Δr, as follows,

Equation 3-12

$$R_j = j.\Delta R = j.\Delta r$$
$$r_i = i.\Delta R = i.\Delta r$$

Let the number of spheres of size R_j per unit volume of the system be $(N_V)_j$ and the number of section profiles that fall in the size class i be $(N_A)_i$. Let the radius of the largest sphere is R_k. From the basic stereological principle regarding particle size distributions Equation 2-48 we can write,

Equation 3-13

$$(N_V)_j = \sum_i (N_A)_{i,j} \Big/ 2R_j$$

Where the subscript j refers to the sphere size and the subscript i refers to the section size. The term $\sum_i (N_A)_{i,j}$ expresses the number of sections of all sizes per unit area obtained from particles of a fixed size j. The contribution of spheres of class j to profiles of size class i can be determined by the profile size frequency given in Equation 3-9, as follows,

Equation 3-14

$$\begin{aligned}(N_A)_{i,j} &= \sum_i (N_A)_{i,j} \Pr\{r_i \mid R_j\} \\ &= (N_V)_j.2R_j \left\{ \frac{1}{R_j} \left[\sqrt{\left(R_j^2 - (r_i - \Delta r)^2\right)} - \sqrt{\left(R_j^2 - r_i^2\right)} \right] \right\} \\ &= (N_V)_j.2.\left[\sqrt{\left(R_j^2 - (r_i - \Delta r)^2\right)} - \sqrt{\left(R_j^2 - r_i^2\right)} \right]\end{aligned}$$

It should be noted that not all sphere classes may contribute to $(N_A)_i$. It is evident that spheres whose radius $R_j < r_i$ cannot give rise to any profiles of size class i. Keeping this in mind it can be written as,

Equation 3-15

$$(N_A)_i = \sum_{j=i}^{k} (N_A)_{i,j}$$

Inserting Equation 3-14 for $(N_A)_{i,j}$ in Equation 3-15 we get,

Equation 3-16

$$(N_A)_i = \sum_{j=i}^{k} (N_V)_j .2\left[\sqrt{\left(R_j^2 - (r_i - \Delta r)^2\right)} - \sqrt{\left(R_j^2 - r_i^2\right)}\right]$$

Dividing the above equation with N_A on both sides,

Equation 3-17

$$\frac{(N_A)_i}{N_A} = \frac{1}{N_A}\sum_{j=i}^{k} (N_V)_j .2\left[\sqrt{\left(R_j^2 - (r_i - \Delta r)^2\right)} - \sqrt{\left(R_j^2 - r_i^2\right)}\right]$$

$$\Rightarrow f(r_i) = \frac{1}{N_A}\sum_{j=i}^{k} (N_V)_j .2\left[\sqrt{\left(R_j^2 - (r_i - \Delta r)^2\right)} - \sqrt{\left(R_j^2 - r_i^2\right)}\right]$$

Where $f(r_i)$ is the frequency of observed profiles in size class i.

Now considering the basic stereological relation according to Equation 2-48

Equation 3-18

$$N_A = N_V .2\overline{R}$$

Where $\overline{R}$ is the mean radius of all spheres, which is given by

Equation 3-19

$$\overline{R} = \frac{1}{N_V}\left[(N_V)_1 R_1 + (N_V)_2 R_2 + \cdots + (N_V)_j R_j + \cdots + (N_V)_k R_k\right]$$

$$= \frac{1}{N_V}\sum (N_V)_j R_j$$

Inserting Equation 3-18 for N_A in Equation 3-17 we get

Equation 3-20

$$f(r_i) = \frac{1}{N_V .2\overline{R}}\sum_{j=i}^{k} (N_V)_j .2\left[\sqrt{\left(R_j^2 - (r_i - \Delta r)^2\right)} - \sqrt{\left(R_j^2 - r_i^2\right)}\right]$$

$$= \frac{1}{\overline{R}}\sum_{j=i}^{k} \frac{(N_V)_j}{N_V}\left[\sqrt{\left(R_j^2 - (r_i - \Delta r)^2\right)} - \sqrt{\left(R_j^2 - r_i^2\right)}\right]$$

$$= \frac{1}{\overline{R}}\sum_{j=i}^{k} F(R_j)\left[\sqrt{\left(R_j^2 - (r_i - \Delta r)^2\right)} - \sqrt{\left(R_j^2 - r_i^2\right)}\right]$$

Where $F(R_j)$ is the frequency of spheres of size class R_j. Inserting Equation 3-12 for R_j and r_i in Equation 3-20 we arrive at the following equation relating the frequency distribution of profile sizes in 2D and the frequency distribution of corresponding sphere sizes in 3D.

Equation 3-21

$$f(i) = \frac{1}{j}.\sum_{j=1}^{k} F(j)\left[\sqrt{\left(j^2 - (i-1)^2\right)} - \sqrt{\left(j^2 - i^2\right)}\right]$$

Now, the problem is to work back from the above equation, i.e. to estimate the frequency distribution of sphere sizes in 3D from the measured frequency distribution of profile sizes on 2D section plane.

It should be noted from Figure 3-6, that the circular sections have a distribution of sizes, even though they are all obtained from the spheres of uniform diameter. This is due to the fact that the sectioning plane intersects each of these spheres at different distances from their centers, giving rise to sections of different sizes. Another important fact is that in a polydispersed system of spheres, the spheres of different size will contribute sections of same size. In order to find the distribution of three-dimensional spheres from the distribution of two-dimensional sections, the source of each of the sections must be determined. From Equation 3-14 we can write the following general expression

Equation 3-22

$$(N_V)_j = \frac{\sum_j (N_A)_{i,j}}{\Pr\{r_i \mid R_j\}} \frac{1}{D_j}$$

from which $(N_V)_j$ may be determined.

Let us assume that the polydispersed system of spheres under consideration is separated into k class intervals. The number of spheres per unit volume in each class interval is

$$(N_V)_1, (N_V)_2, \cdots\cdots, (N_V)_k$$

and their corresponding radii are

$$r_1, r_2 \cdots\cdots, r_k$$

The section profiles observed on the plane of polish are also separated into the same number of (k) of class intervals. The number of circular sections per unit area in each class interval is

$$(N_A)_1, (N_A)_2, \cdots\cdots, (N_A)_k$$

where the section radii vary from

$$0 \text{ to } r_1, r_1 \text{ to } r_2, \cdots\cdots, r_{k-1} \text{ to } r_k$$

respectively. Figure 3-7 illustrates the possibilities arising from a random plane intersecting a polydispersed system of spheres with k=5. It can be clearly seen from Figure 3-7 that spheres of size r_j yield sections of radii $r_1 \cdots r_j$. Keeping this fact in mind we can write

Equation 3-23

$$(N_A)_i = \sum_{j=i}^{k} (N_A)_{i,j}$$

In order to use Equation 3-22 to calculate the number of spheres per unit volume in a specific size class, we have to determine the number of sections having the same radius as their spheres, i.e. $(N_A)_{1,1}, (N_A)_{2,2}, \cdots\cdots, (N_A)_{k,k}$. Since the sections in the last class interval are contributed only by the spheres of largest size we start with the largest particles and their sections and proceed to the smallest size. . From the above discussion and from Figure 3-7 we can easily write the following equations.

Equation 3-24

$$\begin{aligned}
(N_A)_{k,k} &= (N_A)_k \\
(N_A)_{k-1,k-1} &= (N_A)_{k-1} - (N_A)_{k-1,k} \\
(N_A)_{k-2,k-2} &= (N_A)_{k-2} - (N_A)_{k-2,k} - (N_A)_{k-2,k-1} \\
&\vdots \\
&\vdots \\
&\vdots \\
(N_A)_{1,1} &= (N_A)_1 - (N_A)_{1,k} - (N_A)_{1,k-1} - \cdots\cdots - (N_A)_{1,3} - (N_A)_{1,2}
\end{aligned}$$

In the above set of equations, the first term on the right hand side of each equation is a measured quantity. Since $(N_A)_k$ is a measured quantity, $(N_A)_{k,k}$ is known. We can calculate $\Pr\{r_k \mid R_k\}$ from Equation 3-9. Substituting this probability value, $(N_A)_{k,k}$ and the measured D_k in Equation 3-22, we can calculate $(N_V)_k$, i.e. the number of three-dimensional spheres per unit volume of the largest class interval. Having the value of $(N_V)_k$ in hand one can now proceed to calculate $(N_V)_{k-1}$. The probability of hitting a size-k sphere to get a size- (k-1) section $P_{k-1,k}$ can be calculated using Equation 3-9. Using this value in Equation 3-22, the value of $(N_A)_{k-1,k}$ can be calculated, which when subtracted from the measured value $(N_A)_{k-1}$, yields $(N_A)_{k-1,k-1}$ (as shown in Equation 3-24). The probability for hitting a size- (k-1) sphere to get a size- (k-1) section $(P_{k-1,k-1})$ can be calculated using the Equation 3-9. Using this probability and knowing $(N_A)_{k-1,k-1}$, $(N_V)_{k-1}$ can be easily calculated from Equation 3-22.

By an extension of this procedure, step by step, until all class intervals are exhausted, we can calculate the number of spheres per unit volume in all the size classes. Now the frequencies of sphere size distribution can be easily calculated from,

Equation 3-25

$$F(j)=\frac{(N_V)_j}{\sum_{l=1}^{k}(N_V)_l}$$

It can be clearly seen that in the calculation of $(N_V)_j$ each subtracted term depends on the previously calculated values of $(N_V)_k,(N_V)_{k-1},(N_V)_{k-2}$, etc. This leads to the accumulation of errors towards the smallest particle size and the calculated number of smallest particles may be inaccurate, especially if the number of size classes is more.

3.1.2.2 CONTINUOUS MODEL

In the above model the population of spheres is considered to be made of discrete size classes and the profiles are sorted into likewise discrete profile size classes. For analytical purposes it is convenient to allow both the sphere size distribution *F(R)* and the profile size distribution f(r) to be continuous by letting both *dR* and *dr* become infinitesimally small, i.e. $dR \to 0, dr \to 0$ at the limit. From Equation 3-10 and Equation 3-11 we can write,

Equation 3-26

$$\sqrt{\left(R^2-(r-dr)^2\right)}-\sqrt{\left(R^2-r^2\right)}=\frac{r.dr}{\sqrt{\left(R^2-r^2\right)}}$$

If we now replace the summation in Equation 3-21 with an integral and considering Equation 3-26 we obtain the following continuous distribution,

Equation 3-27

$$f(r)dr=\frac{1}{R}\int_{r}^{R_{max}}F(R)\frac{r.dr}{\sqrt{\left(R^2-r^2\right)}}.dR$$

Dividing the above equation on both sides with *dr* we obtain the following fundamental probability density function for profile size, relating the distribution of spheres, and that of profiles.

Equation 3-28

$$f(r)=\frac{r}{R}\int_{r}^{R_{max}}F(R)\frac{dR}{\sqrt{\left(R^2-r^2\right)}}$$

Allowing for continuous distribution of sphere sizes, the above equation can be rewritten in its final form as

$$f(r) = \int F(R)\phi(r \mid R)dR$$

It should be noted that the upper limit of integration is changed to $\propto$ instead of R_{max} to allow for continuous distribution of sphere size.

3.2 SIZE SHAPE DISTRIBUTION OF VARIABLE SPHEROIDS

3.2.1 INTRODUCTION

The constraints of the surroundings often impose a particular shape on cells and their constituents, especially during their growth stage. Thus cells, which are basically spherical in shape, become polyhedral when they are densely packed, and the nuclei simulate the shape of the cell, becoming flattened or oblate ellipsoids in flattened cells, or prolate ellipsoids in columnar or elongated cells. There is a certain error introduced if one substitutes, a "volume-equivalent" sphere for non-spherical particles, but this error is predictable. In case of higher order polyhedra, as one can expect, this error is rather small, but for shapes such as cubes, octahedra or cylinders it is appreciable. With ellipsoids the error obviously increases as their eccentricity (or axial ratio) deviates from 1.

Particles of spherical shape or those modeled by geometrical bodies of a constant shape (e.g. ellipsoids with constant axial ratios, cylinders with a constant height-to-diameter ratio, etc.), can be described by a single size parameter. The particulate phase is then described by a univariate size distribution. In this case the stereological unfolding problem consists simply in estimating the univariate size distribution of particles from the univariate size distribution of profiles produced by a random plane section through the aggregate of particles. Very often, this assumption is unrealistic, and complete information relative to the joint variation of size and shape is called for. In many cases particles exhibit a variation about a given type of shape as well as size. Such a system of particles can't be described by a single parameter. Such is the case of ellipsoidal particles of variable size and eccentricities. If one allows the size and the shape of the ellipsoidal particles to vary, one will have to establish a relationship between a particle size and shape distribution and the corresponding profile size and shape distribution resulting from random sectioning. This matter is not a simple straightforward one. This is because of the fact that even if all the particles are of same shape, the profiles resulting from random sectioning will not have the same shape. For example, consider a prolate ellipsoid of axial ratio 2:1. When this particle is randomly cut with a plane, the resulting profiles will have axial ratios ranging from 1:1 (circles) to 2:1 (ellipses), depending on the spatial orientation between the particle and the section plane as shown in Figure 3-8.

The problem of unfolding a bivariate distribution describing a phase of variable ellipsoids of revolution (spheroids) from the corresponding bivariate profile distribution is determinate provided the spheroids are all of the same type, namely, either all prolate or all oblate (See Figure 3-9). This is because of the fact that the random, elliptical profiles can furnish complete information only if the ellipsoids are spheroids of the same family. Prolate ellipsoids are generated by ellipses revolving around their major principal axis, whereas oblate ellipsoids are generated by ellipses revolving around their minor principal axis. If the particulate phase consists of a mixture of prolate and oblate ellipsoids, then the relative proportion of each type of spheroids in the mixture introduces an extra parameter, making the problem indeterminate. Modeling a phase of particles of variable size and shape by variable spheroids of the same type cut by a sectioning plane seems appropriate for three main reasons. (1) Often, the model will be much more realistic than a sphere's model, or a model consisting of spheroids of identical shape. (2) The profiles are always of the same type, namely ellipses, thus making the problem manageable in theory and practice. (3) The stereological problem is determinate (If one uses line probes instead of plane probes, the problem becomes indeterminate, because intercept length distributions are essentially univariate.) A few assumptions are made in setting up the model. (1) The spheroid centers are uniformly scattered in the specimen. (2) The spheroids are isotropically and independently orientated about their centers (3) The size and shape of a randomly chosen spheroid are independent from its position within the specimen. All the foregoing assumptions will be fulfilled only approximately, because the spheroids cannot overlap.

3.2.2 METHODOLOGY

3.2.2.1 CONTINUOUS MODEL

Any spheroid (either oblate or prolate) is fully determined by giving its major and minor principal semi axes a and b respectively. Here in this model both a and b are variable [71]. For both types of spheroids the eccentricity parameter x^2 is defined as $1-\left(\frac{b}{a}\right)^2$, so that $0 \le x^2 < 1$. To make the manipulations simpler a prolate spheroid is described via the bidimensional random variable (b, x^2) and an oblate spheroid via (a, x^2). Clearly, a or b is a size variable, whereas x^2 (which is the square eccentricity parameter) is a genuine shape variable. The respective joint probability density

functions $g(b,x^2)$ and $g(a,x^2)$, exist and are defined in the rectangles $\{0<a<B, 0<x^2<1\}$ and $\{0<b<B, 0<x^2<1\}$ respectively. Random plane probes (random with respect to the particles, but not necessarily with respect to the specimen) determine elliptical profiles in the transected spheroids. The elliptical profiles are described by the variable (m,y^2), with joint probability density function $f(m,y^2)$ defined in a rectangle $\{0<m\le B, 0\le y^2<1\}$ if the parent spheroid is prolate, and by the variable (M,y^2) with joint probability density function $f(M,y^2)$ defined in a rectangle $\{0<M\le B, 0\le y^2<1\}$ if the parent spheroid is oblate. Where M and m represent the major and minor principal semi axes of the elliptical profile and $y^2=1-\left(\frac{m}{M}\right)^2$ is its square eccentricity parameter.

From the conditional probability calculus, for prolate spheroids one can write the following expression,

Equation 3-29

$$f(m,y^2)=\int_m^B db\int_{y^2}^1 f(m,y^2\mid b,x^2,T\uparrow K)g(b,x^2\mid T\uparrow K)dx^2$$

In the above integrand the first function represents the conditional probability density function of (m,y^2) on the set of ellipses produced (i.e. probability of getting an ellipse of size and shape (m,y^2)) when a prolate spheroid K of fixed size b and shape x^2 is transected by a plane T. The event of plane T transecting the spheroid K is denoted by $T\uparrow K$. The second function in the above integrand represents the conditional probability density function of (b,x^2) on the population of transected spheroids (i.e. probability of T hitting the spheroid K of size and shape (b,x^2)). In case of oblate spheroids Equation 3-29 becomes,

Equation 3-30

$$f(M,y^2)=\int_M^B db\int_{y^2}^1 f(M,y^2\mid a,x^2,T\uparrow K)g(a,x^2\mid T\uparrow K)dx^2$$

The functions in the above integrand have the similar meaning as explained above in case of prolate spheroids.

Consider a fixed spheroid K, with its center at the origin of coordinates, and its rotatory axis along the Z-axis. When a plane T, defined by the spherical polar

coordinates (p,ϕ,θ) (of the foot of the perpendicular drawn from origin to T) intersects K, the size and shape of the resulting elliptical profile have the following expressions:

If K is a prolate spheroid,

Equation 3-31

$$m=\left[b^2-\frac{(1-x^2)p^2}{1-x^2\sin^2\theta}\right]^{\frac{1}{2}}, \quad y^2=x^2\sin^2\theta$$

If K is an oblate spheroid,

Equation 3-32

$$M=\left[a^2-\frac{p^2}{1-x^2\cos^2\theta}\right]^{\frac{1}{2}}, \quad y^2=\frac{x^2\sin^2\theta}{1-x^2\cos^2\theta}$$

Since the element of invariant measure for random planes in three dimensions equals $\sin\theta\, dp\, d\phi\, d\theta$ [1], the joint probability density function of (p,θ) conditional on the event that the random plane T hits K, is proportional to $sin\theta$. For prolate K it becomes,

Equation 3-33

$$t(p,\theta\mid b,x^2,T\uparrow K)=\{2E_\theta[H(\theta)]\}^{-1}\sin\theta\ ,$$

For oblate K,

Equation 3-34

$$t(p,\theta\mid a,x^2,T\uparrow K)=\{2E_\theta[H(\theta)]\}^{-1}\sin\theta\ ,$$

for $p\in[-H(\theta),H(\theta)], \theta\in[0,\pi/2]$, *and* $t(p,\theta\mid b,x^2,T\uparrow K)=0$ *otherwise.* In Equation 3-33 and Equation 3-34 the function $H(\theta)$, represents half the caliper diameter of the spheroid in the direction θ, and $E_\theta[H(\theta)]$ is its mean value over all the directions. For prolate spheroid half the caliper diameter is given by,

Equation 3-35

$$H(\theta)=b(1-x^2)^{-1/2}(1-x^2\sin^2\theta)^{1/2}$$

For oblate spheroid it is given by,

Equation 3-36

$$H(\theta)=a(1-x^2\cos^2\theta)^{1/2}$$

The mean caliper diameter of a spheroid is given by,

Equation 3-37

$$E_\theta[H(\theta)] = \int_0^{\pi/2} H(\theta)\sin\theta\, d\theta$$

After making the change of variable Equation 3-31 in Equation 3-33, the first probability density function in the integrand of Equation 3-29 becomes:

Equation 3-38

$$f(m, y^2 \mid b, x^2, T \uparrow K) = [2E_\theta(H)]^{-1}\left[\frac{m}{\sqrt{b^2 - m^2}}\right]\left[\frac{1}{x\sqrt{1-x^2}}\sqrt{\frac{1-y^2}{x^2-y^2}}\right],$$

for $m \in (0, b]$, $y^2 \in [0, x^2]$ and $f \equiv 0$ otherwise. For oblate spheroids making the change of variable Equation 3-32 in Equation 3-33 the first probability density function in the integrand of Equation 3-30 becomes:

Equation 3-39

$$f(M, y^2 \mid a, x^2, T \uparrow K) = [2E_\theta(H)]^{-1}\left[\frac{M}{\sqrt{a^2 - M^2}}\right]\left[\frac{(1-x^2)^{3/2}}{x(1-y^2)^2\sqrt{x^2-y^2}}\right],$$

for $M \in (0, a]$, $y^2 \in [0, x^2]$ and $f \equiv 0$ otherwise. One can notice from Equation 3-38 and Equation 3-39 that these two functions factorize as product of two independent functions as $f_1(m, or\, M) \cdot f_2(y^2)$. It can also be noticed that the bounds of *m*, (or *M*), do not involve y^2, and *vice versa*. This indicates that for a fixed spheroid, the size (*m*, or *M*) and shape (y^2) of an elliptical profile are independently distributed, whatever the type, size and shape of the parent spheroid.

Considering the probability that the plane probe *T* hits the spheroid *K* is proportional to half the mean caliper diameter of the spheroid, the second probability density function in the integrand of Equation 3-29 can be expressed as:

Equation 3-40

$$g(b, x^2 \mid T \uparrow K) = [E_g E_\theta(H)]^{-1}[E_\theta(H)]g(b, x^2),$$

for $b \in (0, B]$, $x^2 \in [0, 1)$ and $g \equiv 0$, otherwise. For oblate spheroid the second probability density function in the integrand of Equation 3-30 becomes:

Equation 3-41

$$g(a, x^2 \mid T \uparrow K) = [E_g E_\theta(H)]^{-1}[E_\theta(H)]g(a, x^2),$$

for $a \in (0,B], x^2 \in [0,1)$ and $g \equiv 0$, otherwise. In Equation 3-40 and Equation 3-41 the function $E_g E_\theta(H) = (\overline{H})$ denotes half the mean of mean caliper lengths in the population of spheroids. It is used as normalizing constant in the above two equations.

Inserting Equation 3-38 and Equation 3-40 in Equation 3-29 and Equation 3-39 and Equation 3-41 in Equation 3-30 the integral equations expressing the profile densities in terms of particle densities become as follows:

For prolate spheroids,

Equation 3-42

$$f(m,y^2) = \frac{m\sqrt{1-y^2}}{2\overline{H}} \int_m^B \frac{db}{\sqrt{b^2-m^2}} \int_{y^2}^1 \frac{g(b,x^2)}{x\sqrt{1-x^2}\sqrt{x^2-y^2}} dx^2,$$

for $m \in (0,B], y^2 \in [0,1)$, and $f \equiv 0$ otherwise.

For oblate spheroids,

Equation 3-43

$$f(M,y^2) = \frac{M}{2\overline{H}(1-y^2)^2} \int_M^B \frac{da}{\sqrt{a^2-M^2}} \int_{y^2}^1 \frac{(1-x^2)^{3/2} g(a,x^2)}{x\sqrt{x^2-y^2}} dx^2,$$

for $M \in (0,B], y^2 \in [0,1)$, and $f \equiv 0$ otherwise. It can be noted from both Equation 3-41 and Equation 3-42 that the first integral depends exclusively on particle and profile size, whereas the second integral contains both the bivariate size-shape distribution and the shape parameters.

In order to unfold the three-dimensional particle size and shape distributions from two-dimensional profile size and shape distributions one needs the inverse relations of Equation 3-41 and Equation 3-42. Both of these equations are double integral equations of Abel-type. In order to transform these two equations into a single one of a standard type, the following substitutions are made:

For prolate spheroids,

Equation 3-44

$$(1-y^2)^{-1/2} f(m,y^2) \equiv \phi(m,y), \text{ and } (1-x^2)^{-1/2} g(b,x^2) \equiv \gamma(b,x)$$

For oblate spheroids,

Equation 3-45

$$(1-y^2)^2 f(M,y^2) \equiv \phi(M,y), \text{ and } (1-x^2)^{3/2} g(a,x^2) \equiv \gamma(a,x).$$

After making the above substitutions in Equation 3-41 and Equation 3-42, the final integral equation whose solution is sought becomes,

Equation 3-46

$$\phi(u,v)=\frac{u}{H}\int_{u}^{B}\frac{ds}{\sqrt{s^2-u^2}}\int_{v}^{1}\frac{\gamma(s,t)}{\sqrt{t^2-v^2}}dt,$$

which can be regarded as a double integral equation of Abel type. To solve this equation put the second integral as,

Equation 3-47

$$\int_{v}^{1}\frac{\gamma(s,t)}{\sqrt{t^2-v^2}}dt=\psi(s,v)$$

Equation 3-47 is an ordinary Abelian integral equation. Sneddon in 1966 [77] has solved this equation and the solution is

Equation 3-48

$$\gamma(s,t)=-\frac{2}{\pi}\frac{\partial}{\partial t}\int_{t}^{1}\frac{v\psi(s,v)}{\sqrt{v^2-t^2}}dv$$

On the other hand, Equation 3-46 after inserting Equation 3-47 in it becomes,

Equation 3-49

$$\phi(u,v)=\frac{u}{H}\int_{u}^{B}\frac{\psi(s,v)}{\sqrt{s^2-u^2}}ds$$

Equation 3-49 is in the same form as Equation 3-47, hence its solution is

Equation 3-50

$$\psi(s,v)=-\frac{2\overline{H}}{\pi}\frac{\partial}{\partial s}\int_{s}^{B}\frac{\phi(u,v)}{\sqrt{u^2-s^2}}du$$

Inserting Equation 3-50 for the function $\psi(s,v)$, in Equation 3-48, we obtain the following unique solution of Equation 3-46

Equation 3-51

$$\gamma(s,t)=\frac{4\overline{H}}{\pi^2}\frac{\partial}{\partial t}\left\{\int_{t}^{1}\frac{v}{\sqrt{v^2-t^2}}\left[\frac{\partial}{\partial s}\int_{s}^{B}\frac{\phi(u,v)}{\sqrt{u^2-s^2}}du\right]dv\right\}$$

By using the following mathematical relation

$$\frac{d}{ds}\int_{s}^{B}F(u,s)ds=\int_{s}^{B}\frac{\partial}{\partial s}F(u,s)du-F(s,s),$$

repeatedly, the right hand side of Equation 3-51 can be expanded in a form suitable for our purposes as,

Equation 3-52

$$\gamma(s,t)=\frac{4Hst}{\pi^2}\left\{\begin{array}{l}\dfrac{\phi(B,1)}{B\sqrt{B^2-s^2}\sqrt{1-t^2}}-\dfrac{1}{B\sqrt{B^2-s^2}}\displaystyle\int_t^1\frac{\dfrac{\partial}{\partial v}\phi(B,v)}{\sqrt{v^2-t^2}}dv \\ -\dfrac{1}{\sqrt{1-t^2}}\displaystyle\int_s^B\frac{\dfrac{\partial}{\partial u}\left[\dfrac{1}{u}\phi(u,1)\right]}{\sqrt{u^2-s^2}}du+\int_t^1\frac{dv}{\sqrt{v^2-t^2}}\int_s^B\frac{\dfrac{\partial^2}{\partial u\partial v}\left[\dfrac{1}{u}\phi(u,v)\right]}{\sqrt{u^2-s^2}}du\end{array}\right\}$$

If the function ϕ satisfies the following conditions

$$\phi(B,v)\equiv 0 \text{ and } \phi(u,1)\equiv 0 \text{ for all } u,v$$

Equation 3-52 reduces to

Equation 3-53

$$\gamma(s,t)=\frac{4Hst}{\pi^2}\left\{\int_t^1\frac{dv}{\sqrt{v^2-t^2}}\int_s^B\frac{\dfrac{\partial^2}{\partial u\partial v}\left[\dfrac{1}{u}\phi(u,v)\right]}{\sqrt{u^2-s^2}}du\right\}$$

Taking Equation 3-44 into account the above mentioned conditions are equivalent to

Equation 3-54

$$f(B,y^2)\equiv 0 \text{ and } \lim_{y^2\to 1}\left[(1-y^2)^{-1/2}f(m,y^2)\right]\equiv 0,$$

respectively. The equalities in Equation 3-54 imply that the population hardly contains big (size = B), very unequiaxed ($y^2\to 1$) profiles. This assumption is a realistic one. Under the above mentioned conditions from Equation 3-44 and Equation 3-53, the solution of Equation 3-42, for the system of prolate spheroids becomes

Equation 3-55

$$g(b,x^2)=\frac{4}{\pi^2}\overline{H}bx\sqrt{(1-x^2)}\int_b^B\frac{dm}{\sqrt{m^2-b^2}}\int_{x^2}^1\frac{1}{\sqrt{y^2-x^2}}\frac{\partial^2}{\partial m\partial y^2}\left[\frac{f(m,y^2)}{m\sqrt{(1-y^2)}}\right]dy^2$$

for $b\in(0,B]$, $x^2\in[0,1)$, and $g\equiv 0$ otherwise.

In case of oblate spheroids, if the joint size-shape probability density function of elliptical profiles satisfies the following expression,

Equation 3-56

$$f(B,y^2)\equiv 0, \text{and } \lim_{y^2\to 1}\left|(1-y^2)^2 f(M,y^2)\right|=0$$

then from Equation 3-45 and Equation 3-53 the solution of Equation 3-43 is given by, Equation 3-57

$$g(a,x^2)=\frac{4H}{\pi^2}ax(1-x^2)^{3/2}\int_a^B\frac{dM}{\sqrt{M^2-a^2}}\int_{x^2}^1\frac{\frac{\partial^2}{\partial M\partial y^2}\left[\frac{f(m,y^2)}{m\sqrt{1-y^2}}\right]}{\sqrt{y^2-x^2}}dy^2$$

for $a\in(0,B]$, $x^2\in[0,1)$, and $g\equiv 0$ otherwise.

3.2.2.2 DISCRETE MODEL

In practice, the profile size and shape distributions are obtained by distributing the measurements into size and shape classes. The resulting distributions are discrete (See Figure 3-10) in nature. A similar procedure as that described in case of spherical particles can be derived for unfolding discrete size-shape distribution of spheroids.

The size variable b or a, of prolate or oblate spheroid is assumed to vary in the range *(0, B)*, where B is a constant bigger than, or equal to the largest value of b (or of a). This range is divided into s classes of equal width $\Delta = B/s$, $(s>1)$. The shape component x^2 varies in the range (0 ,1), which is divided into k classes of equal width 1/k. Thus the rectangular domain of variation of (b,x^2) or (a,x^2) is divided into a grid comprising of $s\times k$ classes, each class being represented by a rectangle of sides Δ and *1/k* (See Figure 3-10b). It should be noted that each of the spheroids in the particulate system under consideration belongs to exactly one of such classes. Any spheroid that satisfies the inequalities $(i-1)\Delta < b(or\ a)\le i\Delta$ and $(j-1)/k < x^2 \le j/k$, where i = 1, 2, ..., s and j = 1, 2, ... , k, belongs to *ij* th class and is called an *ij*-spheroid. The number of *ij*-spheroids per unit volume of specimen is denoted by $N_V(i,j)$, so that $\sum_{i=1}^{s}\sum_{j=1}^{k}N_V(i,j)=N_V$, which is the overall numerical density of spheroids. The elliptical profiles are also classified by means of the same size-shape grid used for the spheroids (See Figure 3-10a). Thus any elliptical profile that satisfies the inequalities $(\alpha-1)\Delta < m(or\ M)\le\alpha\Delta$ and $(\beta-1)/k < y^2 \le \beta/k$, where $\alpha=1, 2, ..., s$, and $\beta=1, 2$, ... , k, belongs to $\alpha\beta$ th class and is called $\alpha\beta$-ellipse. The number of $\alpha\beta$-ellipses observed on random section per unit area of section is denoted by $N_A(\alpha,\beta)$, so that

$\sum_{\alpha=1}^{s}\sum_{\beta=1}^{k} N_A(\alpha,\beta) = N_A$ which is the total number of elliptical profiles per unit area of section. From basic stereological relationships and from geometrical probability theory the ellipse number densities are related to the spheroid number densities as follows:

Equation 3-58

$$N_A(\alpha,\beta) = \Delta\sum_{i=\alpha}^{s}\sum_{j=\beta}^{k} p_{\alpha i} N_V(i,j) q_{j\beta}$$

for each $\alpha = 1, 2, \ldots, s$; $\beta = 1, 2, \ldots, k$. Clearly this relationship is the discrete form of the continuous equations Equation 3-55 and Equation 3-57. It can be seen that this equation is analogous to Equation 3-22 for spheres. Here in the above equation the coefficients $p_{\alpha i}$ are size-correctors and they are independent from Δ- as in the case of spheres- and also from the spheroid type. They can be calculated from the following expressions [78]:

Equation 3-59

$$p_{\alpha i} = \begin{cases} \sqrt{\left(\left(i-\frac{1}{2}\right)^2 - (\alpha-1)^2\right)} - \sqrt{\left(\left(i-\frac{1}{2}\right)^2 - \alpha^2\right)}, & for\ \alpha < i \\ \sqrt{\left(i-\frac{3}{4}\right)}, & for\ \alpha = i \\ 0, & for\ \alpha > i \end{cases}$$

It can be noted that this equation is similar to the one given for spheres Equation 3-9. In Equation 3-58 the coefficients $q_{j\beta}$ are shape correctors, and as one can expect they obviously depend on number of shape classes 'k' and also on spheroid type. These coefficients can be calculated from the following expressions:

For prolate spheroids,

Equation 3-3

$$q_{j\beta} = \begin{cases} \sqrt{(t_1^2 - 1)}\{f(t_\beta) - f(t_{\beta+1})\} & for\ \beta < j \\ \sqrt{(t_1^2 - 1)} f(t_1), & for\ \beta = j \\ 0, & for\ \beta > j \end{cases}$$

where $f(t) = t/(t^2 - 1) + arc\tanh t$, $t_\beta = \left\{(2k - 2\beta + 2)/(2j - 2\beta + 1)\right\}^{\frac{1}{2}}$.

For oblate spheroids,

Equation 3-4

$$q_{j\beta} = \begin{cases} \sqrt{(1 + t_1^{-2})}\{f(t_\beta) - f(t_{\beta+1})\}, & for\ \beta < j \\ \sqrt{(1 + t_1^{-2})} f(t_j), & for\ \beta = j \\ 0, & for\ \beta > j \end{cases}$$

In order to estimate the size shape distribution of spheroids from the measured size shape distributions of elliptical profiles one has to reverse Equation 3-1. The reverse relation reads as follows:

Equation 3-5

$$N_V(i, j) = \Delta^{-1} \sum_{\alpha=i}^{s} \sum_{\beta=j}^{k} p^{i\alpha} N_A(\alpha, \beta) q^{\beta j}$$

for all i = 1, 2, ..., s; j = 1, 2, ..., k. In the above equation the coefficient $p^{i\alpha}$ is the $i\alpha$ th element of the inverse of a matrix whose αi th element is just $p_{\alpha i}$; likewise, the coefficient $q^{\beta j}$ is the βj th element of a matrix having $q_{j\beta}$ as the $j\beta$ th element. It should be noted that the density of spheroids in any class can be directly obtained using Equation 3-5, without any need to calculate the density of spheroids in the preceding classes. The main drawback of this approach is that it might require very large profile samples.

3.3 SIZE AND ORIENTATION DISTRIBUTION OF CIRCULAR DISKS

3.3.1 INTRODUCTION

In all the above analyses it was assumed that the particles have random orientations (in other words the structures are isotropic), or the measurements represent an average over metallographic planes of different random angular orientations and the size and orientations are not correlated. In the later case the information concerning particle orientations is lost in the averaging process. Metallurgists often come across microstructures having particles, whose spatial orientations are anisotropic. The size and orientations of these particles effect many of the properties of the materials. Thus it is of interest to characterize the ensemble of these particles in three-dimensional microstructures to understand their effect on the behavior of materials. In a number of cases, there is a strong correlation between the spatial orientation and size of the particles. The particles in certain orientations are larger than those in the other orientations. For example, in a mechanically worked material, particles that are parallel to the compression axis are larger than the particles that are inclined to this direction. In such microstructures, the estimation of the joint size and orientation distribution of particles provides useful insight into the growth of particles as a function of their size and orientation. The sizes and orientations of the observed two-dimensional profiles do not necessarily represent the true size and orientations of the corresponding particles [72]. Thus, it is of interest to develop a statistical relationship between true bivariate particle size and orientation distribution function and the corresponding apparent bivariate particle size and orientation distribution function measured on a metallographic plane.

3.3.2 THE MODEL

In this particular analysis particles are modeled as penny shaped cylindrical objects with flat circular ends as shown in Figure 3-11 embedded in a matrix of material. When such a system of particles is sectioned with a random plane, the intersections of penny shaped particles almost always yield profiles that are chords generated by intersections of the flat circular ends with the sectioning plane as shown in Figure 3-12. Let the variable R represents the radius of the circular flat ends of the particles. Let R_m be the radius of the largest particle. The thickness of any particle is expected to be much less than its radius R. It should be noted that this assumption is not

necessary for this analysis and the analysis is also applicable to the particles of zero thickness. Let the *Z*-axis of the *XYZ* coordinate system be the reference axis (or vertical axis). Although any direction in the three-dimensional space can be chosen as the vertical axis, in practice the direction of applied stress or similar physically meaningful direction is chosen as the vertical axis. Any sectioning plane that contains the vertical axis is called a vertical sectioning plane (see Figure 3-13). Orientation of a vertical sectioning plane is given by the angle $\phi_p \left(0 \le \phi_p \le 2\pi\right)$. The spatial orientation of the particle is given by the angles θ and ϕ pertaining to the vector normal to its flat faces, as shown in Figure 3-11, where $0 \le \theta \le \pi/2$ and $0 \le \phi \le 2\pi$. Let $F(R, \theta, \phi)$ be the joint size and orientation frequency distribution of the particles in three dimensions. From the basic principle of geometric probability, $F(R, \theta, \phi)\, sin\theta\, d\theta\, d\phi dR$ is equal to the fraction of the particles having the size in the range of R to $(R+dR)$, and the orientation in the range of θ to $(\theta+d\theta)$ and ϕ to $(\phi+d\phi)$. Clearly, $F(R, \theta, \phi)$ depends on the orientation angles θ and ϕ. But, it is the orientation of the particle with respect to the vertical axis (i.e. angle θ) that is of primary interest rather than the amount of rotation around this direction as specified by the angle ϕ. This is obvious from the way vertical axis is chosen. The bivariate distribution $F(R, \theta)$ is given as follows,

Equation 3-63

$$F(R,\theta) = \int_0^{2\pi} F(R,\theta,\phi)\, d\phi$$

Consider a vertical sectioning plane of some arbitrarily chosen orientation, say ϕ_p. As mentioned earlier, the intersection of the penny shaped particles with the vertical sectioning plane yields traces that are chords as shown in Figure 3-12. Let the variable r represent the size (half the length) of these chords. Particles of different radii R yield chords of different sizes r ranging from 0 to R_m. The angular orientation of a chord is given by the angle α between the chord and the vertical axis as shown in Figure 3-12. Let $f(r, \alpha, \phi_p)$ be the joint bivariate size and orientation frequency distribution of the observed chords on the vertical sectioning plane of orientation ϕ_p, in such a way that $f(r, \alpha, \phi_p) dr\, d\alpha$ is equal to the fraction of the chords having the size in the range r to (r+dr) and the orientation in the range α to $(\alpha+d\alpha)$. The function $f(r, \alpha, \phi_p)$ can be estimated from the experimental measurements of r and α. Let $f_0(r, \alpha)$ be the joint

bivariate size and orientation frequency distribution of chords, obtained by averaging $f(r, \alpha, \phi_p)$ over all the vertical plane orientations (i.e. $\phi_p=0$ to 2π) as shown below,

Equation 3-64

$$f_0(r,\alpha)=\frac{1}{2\pi}\int_0^{2\pi} f(r,\alpha,\phi_p)\,d\phi_p$$

In actual practice, $f_0(r, \alpha)$ can be estimated by measuring $f(r, \alpha, \phi_p)$ on a few vertical sectioning planes of different independent orientations ϕ_p, keeping the vertical axis orientation constant and taking an average of these measurements.

From Equation 3-63, $F(R, \theta) \sin\theta\, dR\, d\theta$ is equal to the fraction of particles having the size in the range R to $(R+dR)$ and the angle with the vertical axis in the range θ to $(\theta+d\theta)$; the angle ϕ may be anywhere in the range 0 to 2π. Now the objective of this analysis is to develop a relation between the true bivariate size and orientation frequency distribution of particles $F(R, \theta)$ and the experimentally estimated apparent size and orientation frequency distribution of the chords $f_0(r, \alpha)$.

The geometry of intersection of a particle with a vertical sectioning plane is shown in Figure 3-14. The orientation angle α of a chord in the vertical section of orientation ϕ_p, and the orientation angles θ and ϕ of the corresponding particle in 3D are related as follows,

Equation 3-65

$$\sin(\phi_p-\phi)=\cot\alpha\,\cot\theta$$

From the geometry shown in (Fig6) the distance between the center of the circular flat end of the particle and the vertical plane, d can be expressed in terms of the particle radius R, its orientation angle θ, the size of the particle profile observed in the vertical plane, r, and the orientation angle of the profile, α, as follows,

Equation 3-66

$$d=\frac{\cos\theta\left[R^2-r^2\right]^{1/2}}{\sin\alpha}$$

It should be noted from the above equation that the distance d is independent of the orientation angle ϕ of the particle and the orientation angle ϕ_p of the vertical plane. From Figure 3-14 it is evident that for a particle of size R $(\geq r)$ and the orientation (θ,ϕ), as the distance between the particle center and the vertical plane decreases from the value d given by Equation 3-66 the profile size increases, but the orientation angle of

the profile α doesn't change as is evident from Equation 3-65. Hence, all the particles of size R and orientation (θ,ϕ), whose center is at a distance less than d from the vertical plane, generates chords of size larger than r. Let N_V be the total number of particles per unit volume. Let $C(r, \alpha, R, \theta)$ be a function such that $C(r, \alpha, R, \theta, \phi_p)dR\ d\theta\ d\alpha$ is equal to the average number of profiles per unit area of vertical plane ϕ_p, having orientation in the range α to $(\alpha+d\alpha)$ and size larger than r, originating only from the particles in the size range R to $(R+dR)$ having the orientation in the range θ to $(\theta+d\theta)$ and ϕ to $(\phi+d\phi)$. This quantity is equal to the expected number of particles, whose centers lie in a box of unit cross sectional area and thickness $2d$ (d on either side of the vertical plane) as shown in Figure 3-15. Now we can write,

Equation 3-67

$$C(r,\alpha,R,\theta,\phi_p)dR\ d\alpha\ d\theta = 2d\,N_V\,F(R,\theta,\phi)\sin\theta\,dR\,d\theta\,d\phi$$

Inserting Equation 3-66 for d in Equation 3-67 we get,

Equation 3-68

$$C(r,\alpha,R,\theta,\phi_p)dR\ d\alpha\ d\theta = 2\frac{\cos\theta\left[R^2-r^2\right]^{1/2}}{\sin\alpha}N_V\,F(R,\theta,\phi)\sin\theta\,dR\,d\theta\,d\phi$$

From Equation 3-65 it is evident that for given values of ϕ_p and θ, α and ϕ can't be varied independently. Hence, in Equation 3-68 $d\phi$ and $d\alpha$ are not independent. Differentiating Equation 3-65, keeping ϕ_p and θ constant we obtain,

Equation 3-69

$$d\phi\cos(\phi_p-\phi)=\cot\theta\frac{d\alpha}{\sin^2\alpha}$$

Inserting from Equation 3-65 for $\cos(\phi_p-\phi)$ in Equation 3-69 we get,

Equation 3-70

$$d\phi=\cot\theta\frac{d\alpha}{\sin^2\alpha}\frac{1}{\sqrt{1-\cot^2\alpha\cot^2\theta}}$$

Inserting Equation 3-70 for $d\phi$ in Equation 3-68 yields,

Equation 3-71

$$C(r,\alpha,R,\theta,\phi_p)dR\ d\alpha\ d\theta = 2\frac{\cos\theta\left[R^2-r^2\right]^{1/2}}{\sin\alpha}N_V\,F(R,\theta,\phi)\sin\theta\,dR\,d\theta\cot\theta\,\frac{d\alpha}{\sin^2\alpha}\frac{1}{\sqrt{1-\cot^2\alpha\cot^2\theta}}$$

$$\Rightarrow\ C(r,\alpha,R,\theta,\phi_p)dR\ d\theta\ = g(\alpha,\theta)\left[R^2-r^2\right]^{1/2}N_V\,F(R,\theta,\phi)dR\,d\theta$$

Where

Equation 3-72

$$g(\alpha,\theta)=\frac{2\cos^2\theta\sin\theta}{\sin^2\alpha\left[\sin^2\alpha-\cos^2\theta\right]^{1/2}}$$

Let $C_0(r,\ \alpha,\ R,\ \theta)$ be the value of $C(r,\ \alpha,\ R,\ \theta,\ \phi_p)$ averaged over all the vertical plane orientations, keeping $r,\ \alpha,\ R,\ \theta$ constant. Then we can write,

Equation 3-73

$$C_0(r,\alpha,R,\theta)=\frac{1}{2\pi}\int_0^{2\pi}C(r,\alpha,R,\theta,\phi_p)d\phi_p$$

To calculate this average, integrating Equation 3-71 over ϕ_p gives,

Equation 3-74

$$\int_0^{2\pi}C(r,\alpha,R,\theta,\phi_p)d\phi_p dR\ d\theta\ = g(\alpha,\theta)\left[R^2-r^2\right]^{1/2}N_V\int_0^{2\pi}F(R,\theta,\phi)d\phi_p dR\,d\theta$$

In the above integration, as mentioned earlier $r,\ \alpha,\ R,\ \theta$ are to be kept constant. Thus, only the orientation angle ϕ of the particle may vary as the vertical plane orientation ϕ_p changes. It should be noted at this point that the $d\phi$ expressed by Equation 3-70 is at constant ϕ_p and θ, whereas the $d\phi$ we are considering at this context is at constant $\alpha,\ \theta$. At constant $\alpha,\ \theta$, Equation 3-65 dictates that $d\phi$ must be precisely equal to $d\phi_p$. Thus, we can integrate $F(R,\ \theta,\ \phi)$ in Equation 3-74 over ϕ, instead of ϕ_p. Now, Equation 3-74 can be rewritten as

Equation 3-75

$$\int_0^{2\pi}C(r,\alpha,R,\theta,\phi_p)d\phi_p dR\,d\theta\ = g(\alpha,\theta)\left[R^2-r^2\right]^{1/2}N_V\int_0^{2\pi}F(R,\theta,\phi)d\phi dR\,d\theta$$

Inserting Equation 3-63 and Equation 3-73 in Equation 3-75 yields,

Equation 3-79

$$f_0(r,\alpha)=\frac{4rN_V}{\pi N_A \sin^2\alpha}\int_{r}^{R_m}\int_{(\pi/2-\alpha)}^{\pi/2}\frac{\cos^2\theta\sin\theta F(R,\theta)d\theta dR}{\left[R^2-r^2\right]^{1/2}\left[\sin^2\alpha-\cos^2\theta\right]^{1/2}}$$

The above double integral equation can be changed into the form of standard double Abelian integral equation and can be solved in the same manner as described in section 3.2.2.1 to give the following general solution,

Equation 3-80

$$N_V F(R,\theta)=\frac{N_A}{\pi\left[\cos^2\theta\sin\theta\right]}\frac{\partial^2}{\partial R\partial\theta}\int_{R}^{R_m}\int_{\theta}^{(\pi/2)-\theta}\frac{\sin^3\alpha\cos\alpha f_0(r,\alpha)d\alpha dr}{\left[\cos^2\alpha-\sin^2\theta\right]^{1/2}\left[r^2-R^2\right]^{1/2}}$$

The quantity on the left hand side of the above equation is the three dimensional counter part of $n_A(r, \alpha)$ and is denoted by $n_V(R, \theta)$. Thus the quantity $n_V(R, \theta)\ \sin\theta\ dR\ d\theta$ is equal to the number of particles per unit volume of the three-dimensional microstructure having size in the range R to $(R+dR)$ and the orientation in the range θ to $(\theta+d\theta)$. Now the above equation can be rewritten to give the final form of the expression for estimation of the true bivariate particle size and orientation distribution from the corresponding measured average apparent bivariate distribution on the vertical sections as,

Equation 3-81

$$n_V(R,\theta)=\frac{1}{\pi\left[\cos^2\theta\sin\theta\right]}\frac{\partial^2}{\partial R\partial\theta}\int_{R}^{R_m}\int_{\theta}^{(\pi/2)-\theta}\frac{\sin^3\alpha\cos\alpha n_A(r,\alpha)d\alpha dr}{\left[\cos^2\alpha-\sin^2\theta\right]^{1/2}\left[r^2-R^2\right]^{1/2}}$$

It should be noted that none of the above equations contains the particle thickness term and hence all of the above equations are applicable for any thickness value of the particles, including zero.

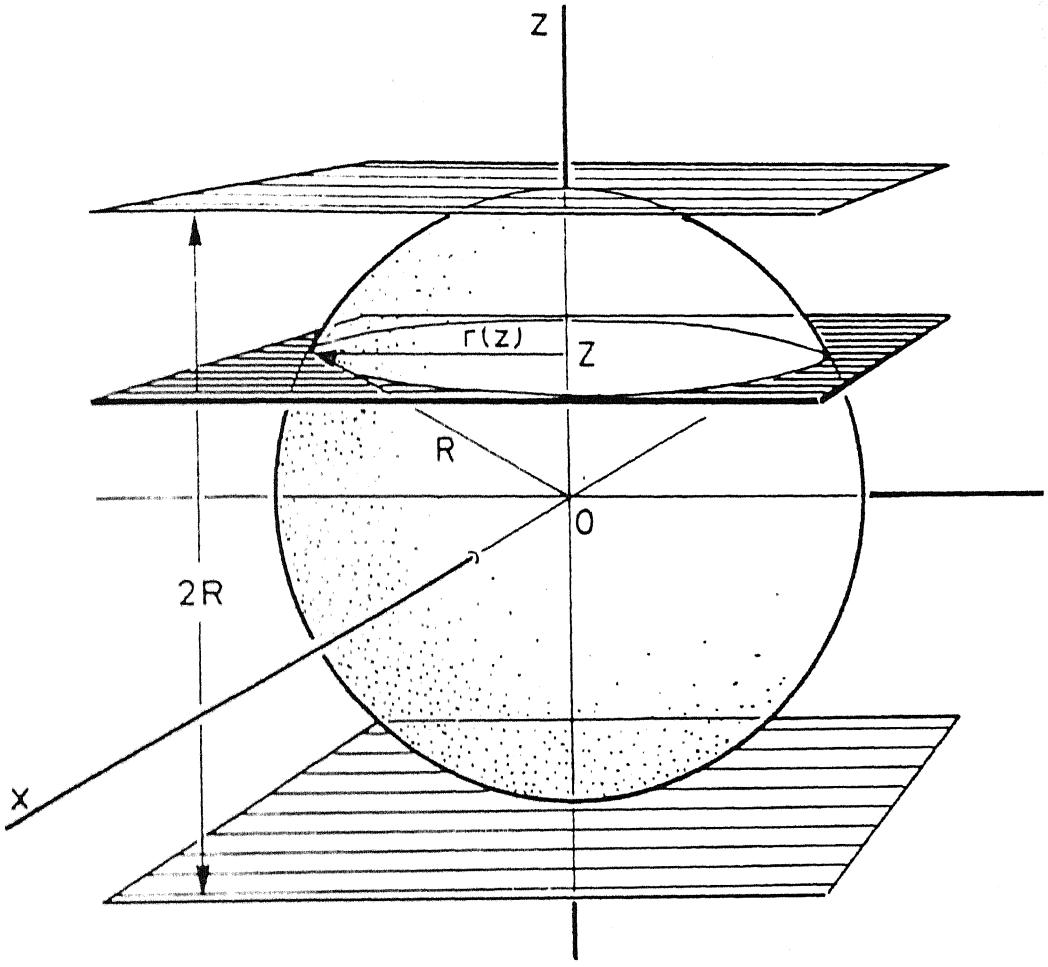

Figure 3-1 Sectioning sphere of radius R yields profile of radius r(z) depending on distance z of section from sphere center.

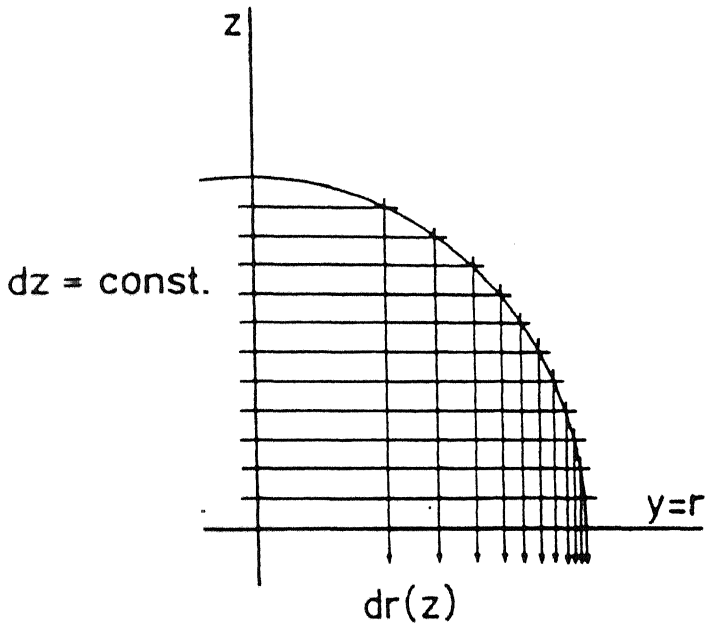

Figure 3-3 Variation of dr(z) keeping dz constant

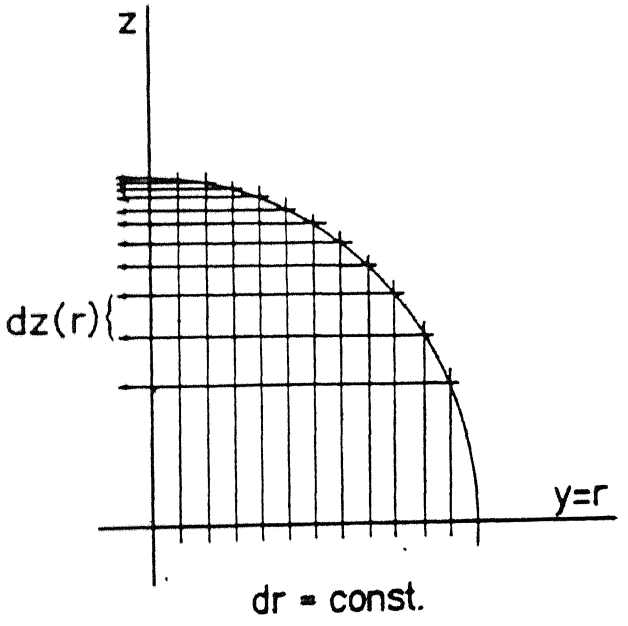

Figure 3-4 Variation of dz(r) keeping dr constant

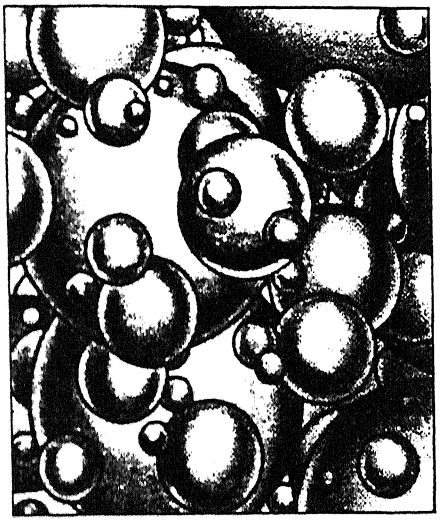

Figure 3-5 Polydispersed system of spheres

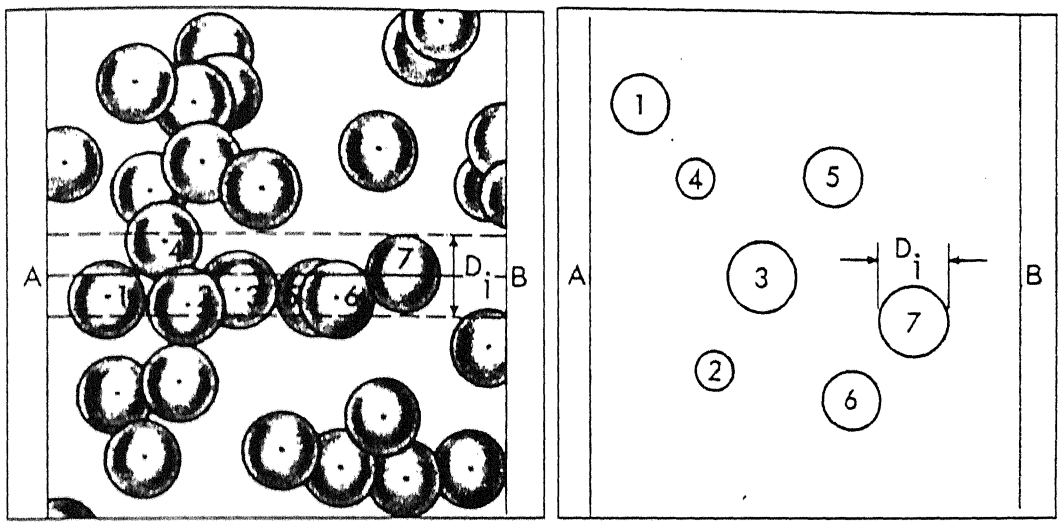

(a) (b)

Figure 3-6 (a) Monodispersed system of spheres of diameter D_j

(b) Circular sections resulting from a plane intersecting the monodisperesed system through AB

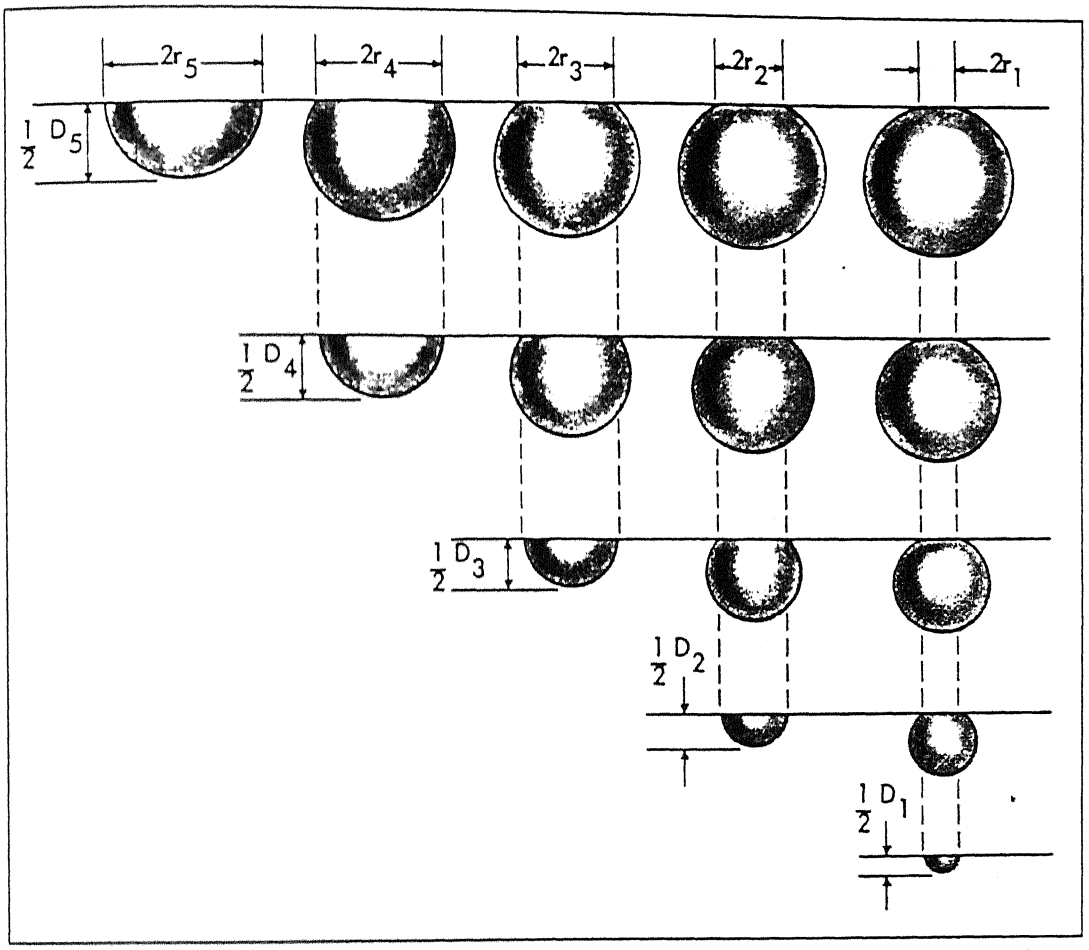

Figure 3-7 Schematic illustration of the sectioning of spheres of diameters D_1 to D_5 to give circular section of diameters $2r_1$ to $2r_5$

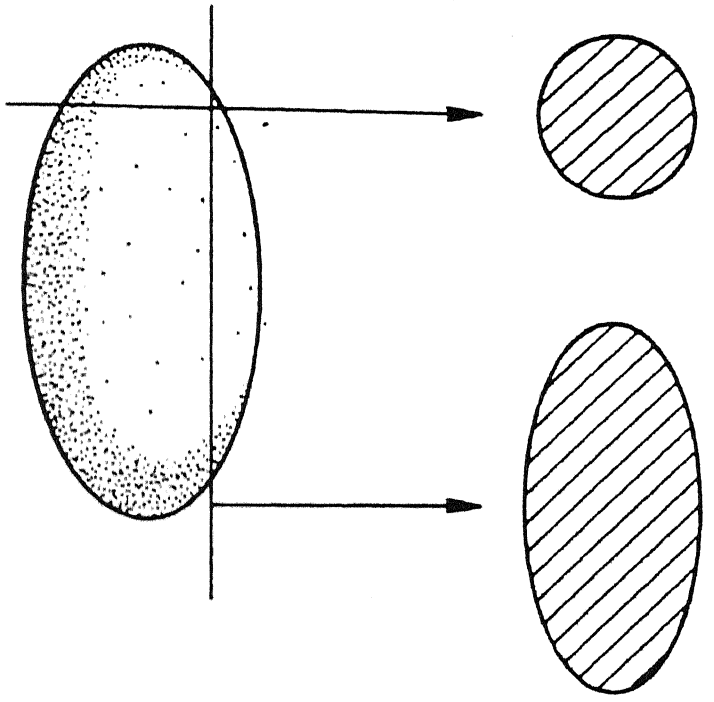

Figure 3-8 Transverse and longitudinal section of spheroid. Axial ratio of spheroid is reflected in axial ratio of longitudinal section.

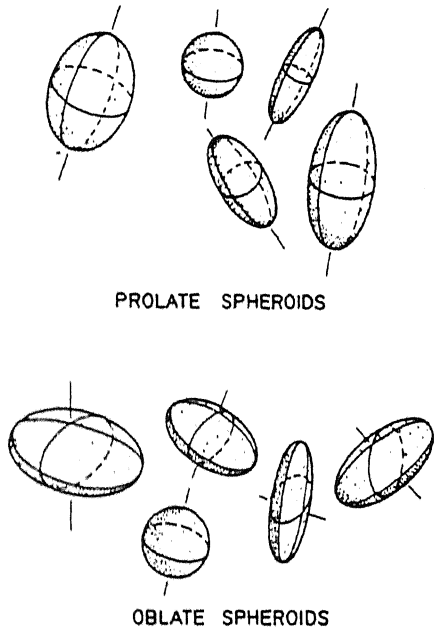

Figure 3-9 Shape variation by variation of axial ratio within the types of spheroids (prolate or oblate)

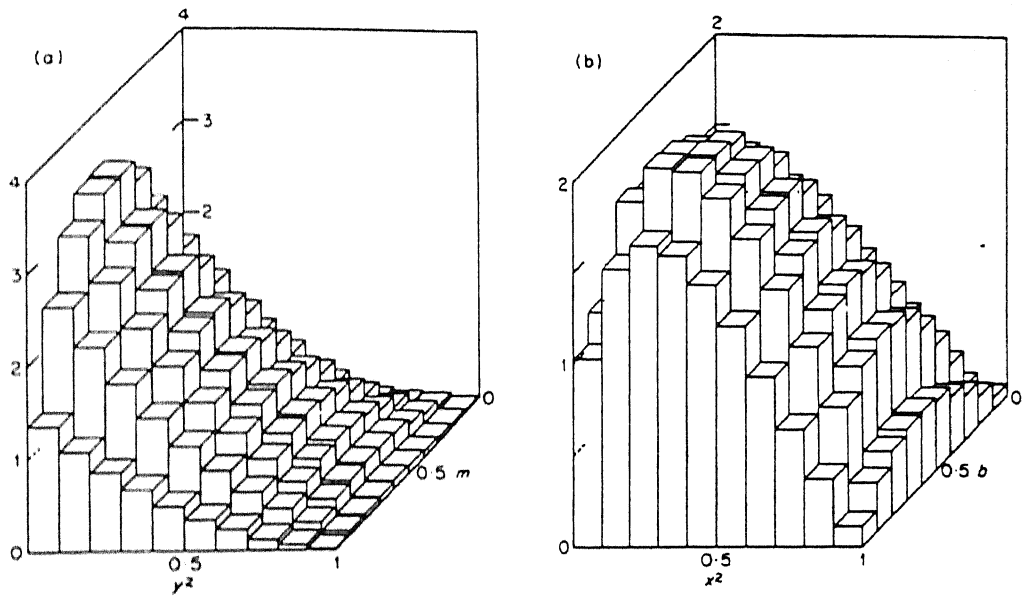

Figure 3-10 Discrete size-shape distribution of prolate spheroids (b) and their sections (a)

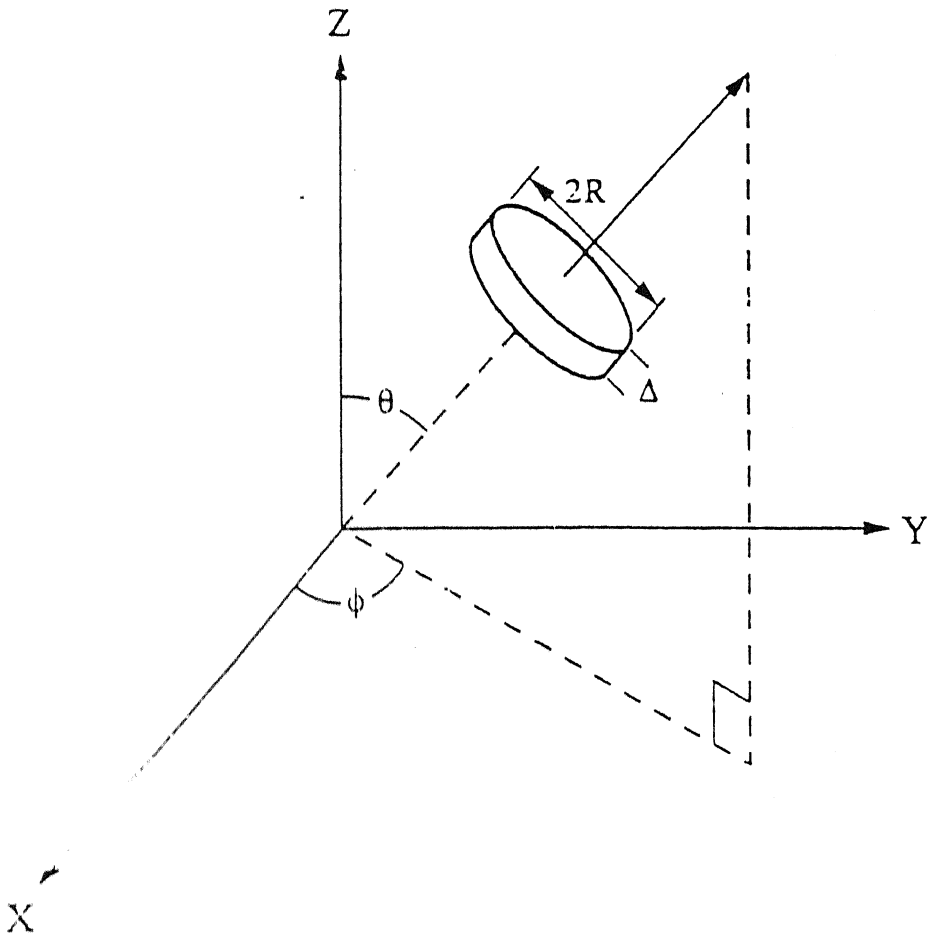

Figure 3-11 Model shape for microcracks, and specification of microcrack orientation.

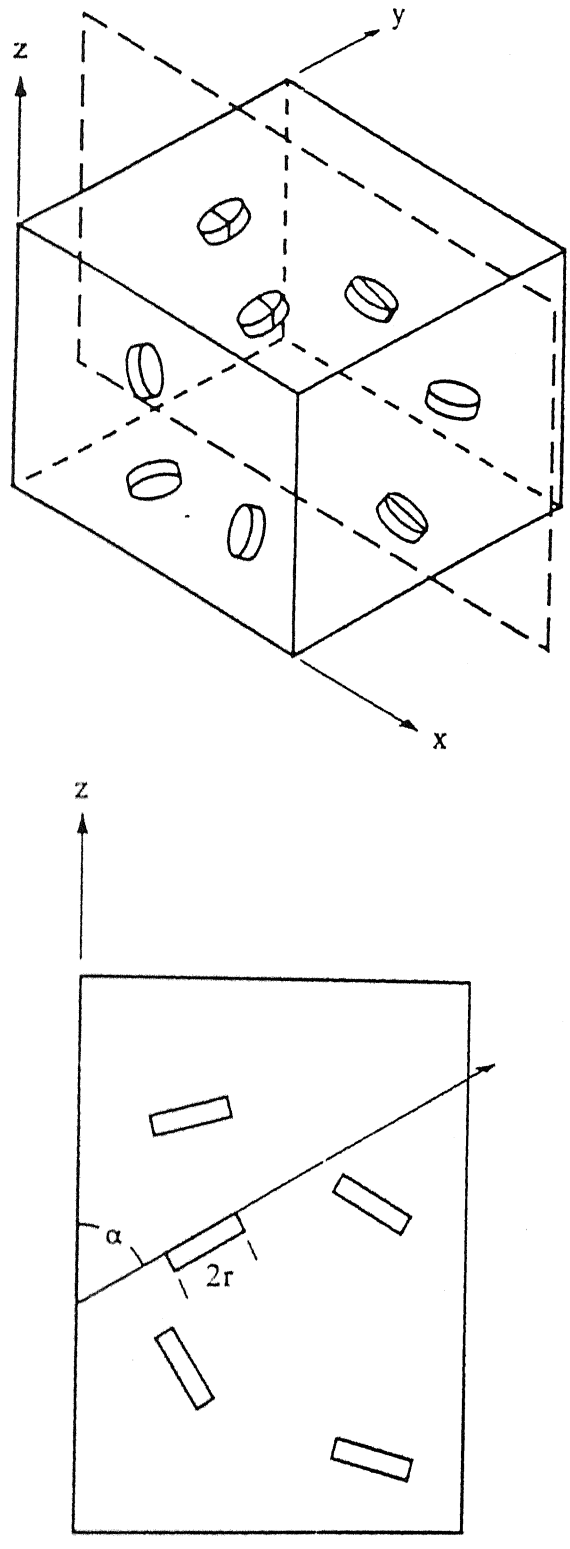

Figure 3-12 Specification of size and orientation of microcrack traces in a vertical plane. Note that the vertical axis is contained in all the vertical planes, and hence it can be identified in each vertical plane.

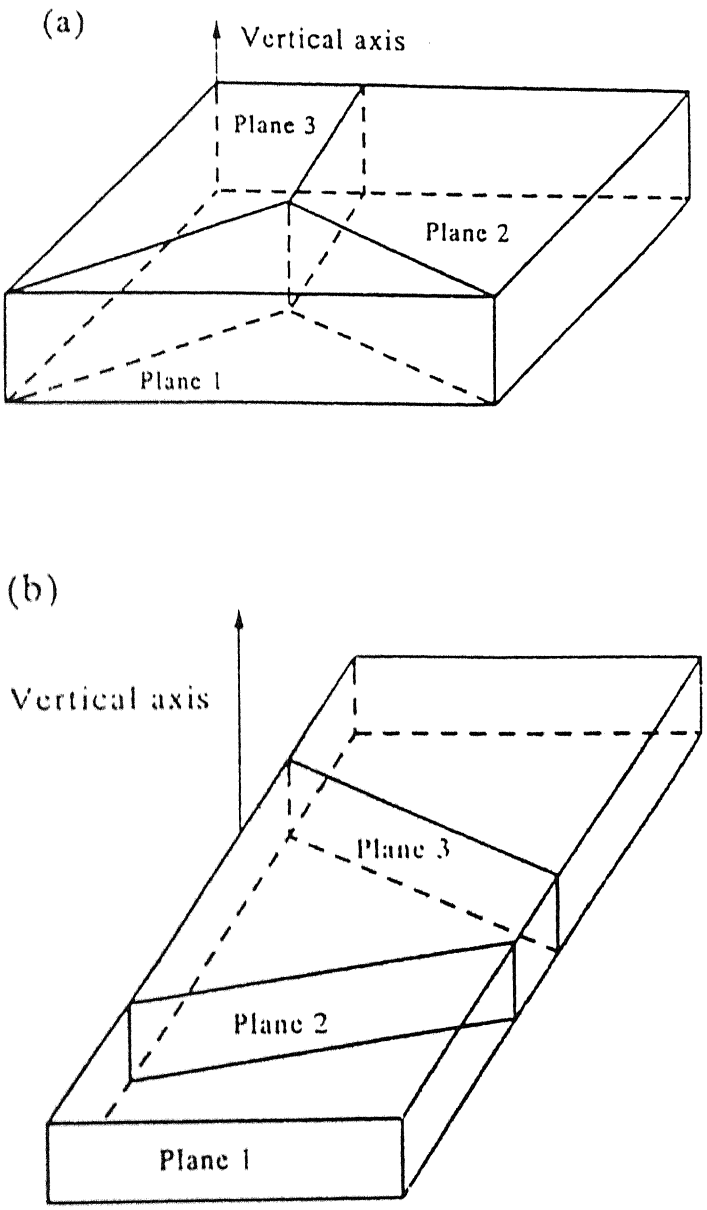

Figure 3-13 (a)Vertical planes of different angular orientations (b) Vertical planes at different locations in the specimen and with different orientations.

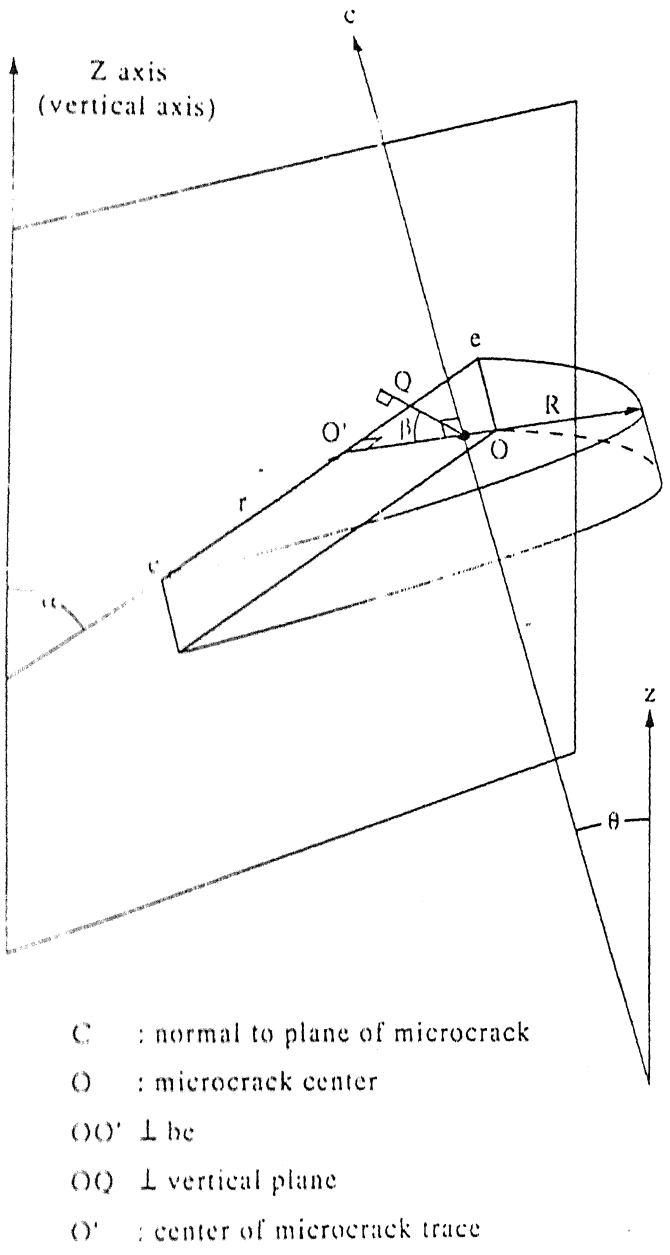

Figure 3-14 Geometry involved in the intersection of a penny shaped microcrack and a vertical plane. A decrease in the distance d brings the microcrack closer to the vertical plane and increases the size r of the microcrack trace.

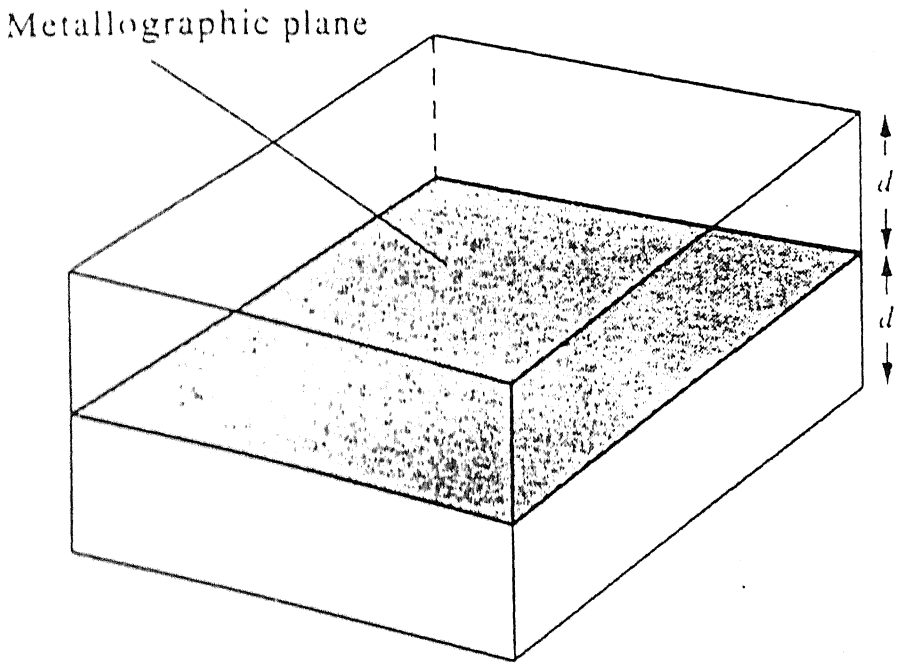

Figure 3-15 All the microcracks of a given size and orientation, whose centers are inside the box, yield traces of larger size than r.

CHAPTER 4

RESULTS AND DISCUSSION

4.1 ANALYSIS OF NUMERICAL METHODS

4.1.1 COMPARISON WITH EXACT SOLUTIONS

The numerical procedures developed are validated for their exactness by using raw data, for which exact solutions are known before hand. Basically computer programs are written to solve the problem of numerical de-convolution of 2D data to obtain the 3D distribution for the following three categories of particles:

a) Monodispersed and polydispersed systems of spheres

b) Prolate and oblate spheroids of varying size and shape

c) Platelets having varying size and orientation.

In each case raw data is developed from a known 2D distribution function, for which exact 3D solution is known.

4.1.1.1 SPHERES

In case of spherical particles, the 3D probability density function ,F(R) is assumed to be a normal distribution function with a mean value of 10 and a standard deviation of 3. The corresponding probability density function for expected circular profile sizes f(r) is obtained by solving this function analytically. The probability densities of both of these functions are shown in Figure 4-1. A universe of 5000 profiles is generated using f(r).

The generated 2D data is then fed into the computer program developed to estimate back the 3D particle size distribution and 3D mean particle size, and the results obtained are presented in and Figure 4-3. 3D particle size distributions are obtained using 8, 15 and 25 number of size classes. As can be seen from, although the sample size is large enough (5000) the estimated 3D distribution is not perfectly matching with the exact 3D distribution when the particle sizes are descretised into 8 classes. The error is not because of small sample size (since 5000 is a large enough sample size) but because of using inappropriate descretisation of particle sizes. This is evident from figures showing estimated 3D size distribution using 15 and 25 size classes ((b),(c)), where the estimated 3D size distribution matches well with the exact 3D size distribution.

From the estimated 3D particle size distribution, mean 3D particle size is calculated in all the three cases and also in cases of 10 and 20 size classes and the results obtained are presented in Figure 4-3. It is evident that the estimated mean size approaches the exact value on increasing the number of bins. This is because on increasing the number of bins the class interval decreases providing more detailed description of the distribution. Although this is only applicable if we have a large sample size. It should also be noted that the mean profile size (2D) is less than the real 3D mean particle size in this particular case. In general, the mean profile size can be either less, more or equal to the real 3D mean particle size (e.g. bimodal distribution of 3D particle sizes). Hence using the mean profile size as a representative of real mean 3D particle size may lead to erroneous results.

4.1.1.2 VARIABLE SPHEROIDS

Applicability of the numerical solution developed for the estimation of 3D bivariate size-shape distribution of variable spheroids is tested. This involved de-convolution of 2D bivariate size-shape distribution of corresponding elliptical profiles, generated on 2D sectioning plane by spheroids. A hypothetical population of variable prolate spheroids, whose size and shape are governed by the following joint probability density function, [71] is considered.

Equation 4-1

$$g(b,x^2) = C'bx\sqrt{1-x^2}\left[\left(1-b^2\right)+\left(1-x^2\right)\right]$$

The three-dimensional representation of the above equation can be seen in Figure 4-4(a). The joint probability density function of the corresponding elliptical profiles is obtained from Equation 3-14and is given by

Equation 4-2

$$f(m,y^2) = \frac{2C'}{3H}m\sqrt{1-m^2}\left(1-y^2\right)\left[\left(1-m^2\right)+\left(1-y^2\right)\right]$$

This is graphically represented in Figure 4-4(b). Using this 2D bivariate size-shape probability density function a universe of 5000 elliptical profiles is generated, with the size of minor principal axis varying from 0.01 to 1.0 and the square eccentricity parameter varying from 0 to 1.

The generated 2D elliptical profile data is then fed into the computer program developed to estimate the 3D bivariate size-shape distribution of variable spheroids and the results obtained are presented in Figure 4-5 and Figure 4-6. Two cases are

considered for this analysis. In the first case the particle sizes and shapes are descretised into a grid of 10 X 10 size. Whereas in the second case a size-shape grid of 25 X 25 is used. Similar to the sphere size distribution problem, the effect of class interval on the estimated 3D distribution can be seen from Figure 4-5(a-b). In the first case the estimated 3D bivariate size-shape distribution of variable prolate spheroids is significantly different from the exact 3D bivariate distribution, although the sample size is quite large (5000). Whereas, in the second case the estimated and exact 3D bivariate size-shape distributions are almost similar. The histogram representation of the exact and the estimated 3D size-shape distributions are represented in Figure 4-6.

4.1.1.3 PLATELETS HAVING VARYING SIZE AND ORIENTATION

A computer simulated population is generated to validate the suitability of the numerical procedure developed for the estimation of 3D size and orientation distribution of disk shaped particles (platelets). The population consists of rectangular traces generated from hypothetical joint probability density of size and orientation governed by the following expression [72]

Equation 4-1

$$n_A(r,\alpha) = \left[12\times10^{22}/\pi\right] r\left[(r_m)^2-(r)^2\right]^2$$

The underlying assumption in solving the size orientation problem leads to a fact that a randomly oriented (in this context) disk is not actually randomly oriented with respect to the solid angle distribution. The joint probability density function for corresponding disks in 3D can be obtained from Equation 3-19and is given by

Equation 4-2

$$n_V(R,\theta) = 64\times10^{22} R\left[(R_m)^2-(R)^2\right]^{3/2}/\pi^2$$

Both the above exact joint probability density functions (Equation 4-1 for 3D disks and Equation 4-2 for corresponding 2D profiles) for 3D discs and are graphically represented in Figure 4-7. A universe of 5000 2D rectangular profiles is generated using Equation 4-1, with the size of the traces varying from 0.00005 to 0.001 and the orientation from 0 to 90 degrees.

Estimation of 3D bivariate size-orientation distribution of disk shaped particles is generated by numerical de-convolution of the above 2D data. The results obtained are presented in Figure 4-8 and Figure 4-9. The size and orientations of the particles are descretised into 25 classes each. It can be clearly seen from Figure 4-8 and Figure 4-9 that the estimated true bivariate size and orientation distribution of disks almost follows

the corresponding exact bivariate distribution, except for a negligible discrepancy in the frequency values.

4.1.2 ANALYSIS OF APPROXIMATION METHODS

The objective of this analysis is to study the appropriateness of assuming spherical shapes for non-spherical particles to de-convolute 3D particle size distribution. For this analysis the same universe of five thousand elliptical profiles as in 4.1.1.2 is considered. The numerical procedure developed for 2D to 3D conversion of spherical particles is applied to estimate the size distribution and mean particle size of this non-spherical system. This analysis basically consists of two parts.

a) Arithmetic approximation

b) Geometric approximation.

In arithmetic approximation, an elliptical profile is approximated as a circle of radius 'r' equal to the arithmetic mean of the principal semi axes of the elliptical profile. Thus an elliptical profile of minor principal semi axis 'm' and square eccentricity parameter 'y' is approximated as a circle of radius 'r' where,

Equation 4-5

$$r = \left[m + m \Big/ \sqrt{1-y} \right]$$

In case of geometric approximation, an elliptical profile is approximated as a circle of equivalent area. Thus an elliptical profile of minor principal semi axis 'm' and square eccentricity parameter 'y' is approximated as a circle of radius 'r' where,

Equation 4-6

$$r = \sqrt{m \cdot m \Big/ \sqrt{1-y}}$$

Essentially Equation 4-5 and Equation 4-6 assume that the radius of circular profile is an arithmetic mean and a geometric mean of the two elliptical radii respectively.

The generated universe of 2D elliptical profiles is converted into 1) universe of equivalent circular profiles using arithmetic approximation 2) universe of equivalent area circular profiles using geometric approximation. Then the corresponding 3D size distribution of particles is estimated for both these universes by using the numerical routine deployed in 4.1.1.1. Since the estimates provide size distributions of spheres, whereas the true 3D distribution is for bivariate spheroids, we need to convert the true 3D distribution to an equivalent spherical distribution. This is again done using arithmetic and geometric approximation by taking equivalent sphere radius as

arithmetic mean and geometric mean of radii of spheroids. The results obtained are presented in Figure 4-10, Figure 4-11 and Figure 4-12. The error involved in approximating the non-spherical particles as spherical particles in estimating the true particle size distribution is evident from Figure 4-10. It is observed that the geometric approximation gives better results than arithmetic approximation. In Figure 4-10 we can clearly see that the curve representing the estimated true particle size distribution in case of geometric approximation follows almost the same trend as the curve representing the exact true particle size distribution, except for some significant discrepancy in the frequencies, whereas the curve representing the estimated true particle size distribution in case of arithmetic approximation is more off from the exact true particle size distribution. However, in both the cases, it is observed that the approximation method always results in overestimation of the number of small particles and underestimation of large particles. Figure 4-11 shows the same graphs shown in Figure 4-10 but are widely spread near the large particle size range. It can be seen in Figure 4-11 that the approximation of non-spherical particles as spheres also leads to prediction of some large particles, which are actually not present in the true population of variable spheroids.

The mean true particle size of the non-spherical system under consideration is also estimated from the size distribution obtained by approximation methods. The results obtained are depicted in Figure 4-12. In this figure three average sizes are shown for each case of approximation. The exact mean size corresponds to the mean of equivalent spherical radius of the true population of variable spheroids. The bivariate mean size is similar to the exact mean size except that the bivariate spheroid distribution is not true distribution but has been generated by de-convoluting 2D bivariate distribution as outlined in 4.1.1.2. The approximate mean size corresponds to the mean size of the distribution of spheres which is generated from 2D ellipses assuming them as circles. It can be seen from Figure 4-12 that the geometrical approximation method gives better result than the arithmetic approximation method. In fact in this particular case the geometrical approximation method gives almost the same result as obtained by the bivariate estimation method. It is interesting to note that although the approximation methods overestimate the smaller size particles and underestimate the large size particles, they give a mean particle size that is more than the exact mean particle size. It may be because of the fact that the approximation methods estimate some non-existing very large size particles.

4.2 SAMPLING REQUIREMENTS AND ASSOCIATED ERRORS

The objective of this analysis is to emphasize the importance of sample size in the estimation of 3D particle size distribution and 3D mean particle size by numerical de-convolution of apparent 2D profile size distribution. For this analysis the same 3D probability distribution function of spheres deployed in 4.1.1.1 is used to generate a universe of 10000, 2D circular profiles. From this universe 5 samples each of sizes 100, 200, 500, 1000 and 2000 are taken at random. These samples are used to generate estimations of 3D distribution and are stored as a data set.

The numerical procedure developed for de-convolution of 2D data to approximate the true sphere size distribution is run with all these randomly generated datasets. In all these cases the particle sizes are descretised into 8 classes. The results obtained are presented in Figure 4-15. It is seen from Figure 4-15 that the estimated particle size distribution approaches the exact particle size distribution with increase in the sample size. This is due to decrease in sampling error with increasing sample size. It may be noted that this seems similar to the predictions of central limit theorem[underwood], though the theorem is not exactly applicable since this not a sampled random variate. It is also noticeable from Figure 4-15 that the precision obtained in the estimation of particle size distribution is not a linear function of the sample size. The estimated particle size distributions are significantly different from the exact particle size distribution in case of samples with sizes of 100 and 200. Whereas, samples of sizes 500, 1000 and 2000 are all very close to the exact distribution with only minor improvements in estimation with increasing sample size. This implies that increase in sample size don't yield corresponding betterment of estimates beyond a certain sample size.

The effect of sample size on the estimation of mean 3D particle size is also analyzed and the results obtained are presented in Figure 4-13 and Figure 4-14. The estimated mean values show a lot of scatter around the true mean, which decreases with increase in sample size. This decrease in scatter with increasing sample size is obvious, since it decreases sampling error as stated in previous paragraph. Further, it is noted that the scatter is not uniformly distributed about the true mean and is predominantly an over estimate rather than random, for all the sample sizes. This is a very peculiar observation, indicating a bias in the process of de-convolution, since the sampling was randomly done without any bias. It was realized that the mathematics of de-convolution

was exact and thus the only source of bias could be due to the numerical method. This meant that either the bias was due to descretisation or floating point operations. Since the bias was appreciable it was concluded that it couldn't be due to 8-bit floating point operations. Hence by process of elimination it was assumed that descretisation was the most probable reason for the bias. On revisiting the numerical method for descretisation it was realized that the size class is being indicated by the arithmetic mean of the interval. Since the bias was an over estimation and it is a well known fact that arithmetic mean is greater than geometric mean and harmonic mean, it was anticipated that representation of mean bin size by geometric mean and harmonic mean would result in lowering the mean probably removing/decreasing the bias. The results of application of geometric mean and harmonic mean are shown in Figure 4-14. As expected the estimates of mean size are lower than that of arithmetic mean. Although these seem to be also biased with an under estimate. Hence it was realized that a more appropriate function should be used to represent the size class in the process of descretisation. As a test function root mean square value of the interval was taken as mean size of the bin. The calculations based on this are shown in Figure 4-14. It is interesting to note that use of root mean square value for mean bin size results in an evenly distributed scatter around the exact mean, indicating absence of any bias. It is also seen that the spread in the scatter significantly decreases on using the root mean square value. Hence, root mean square value should be the function of choice in representing the mean bin size in solving the de-convolution problem for spheres.

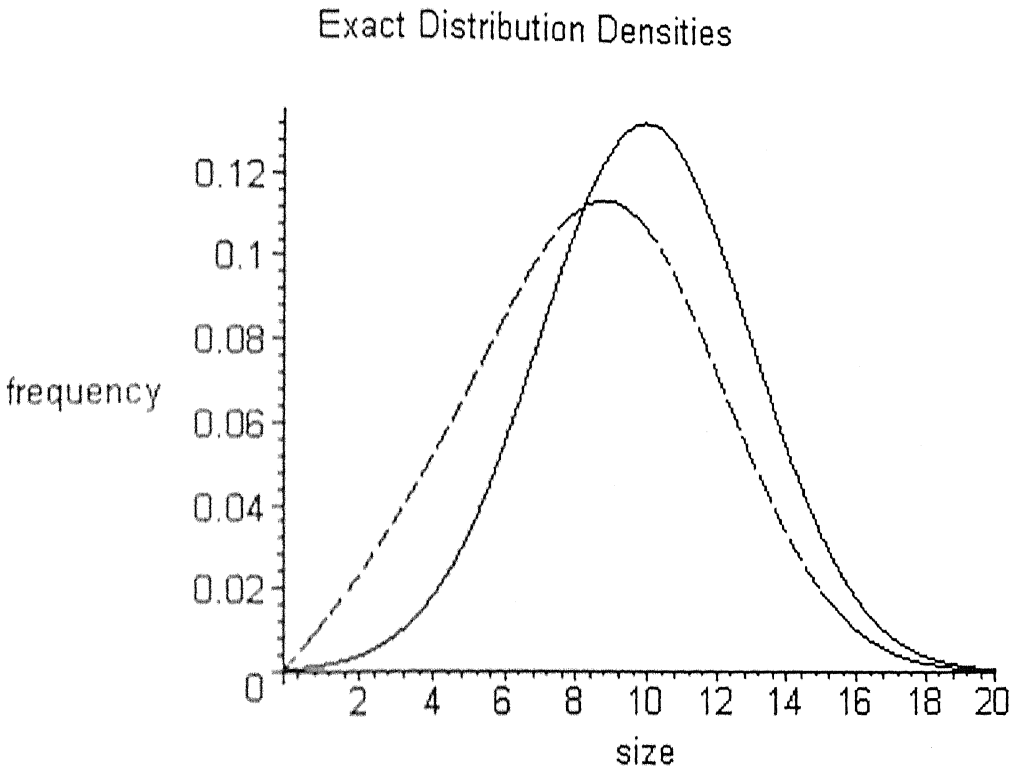

Figure 4-1 A sphere size distribution and the corresponding profile size distribution. Solid line corresponds to the sphere size distribution density , whereas the dotted line represents the probability density of corresponding circular profile sizes.

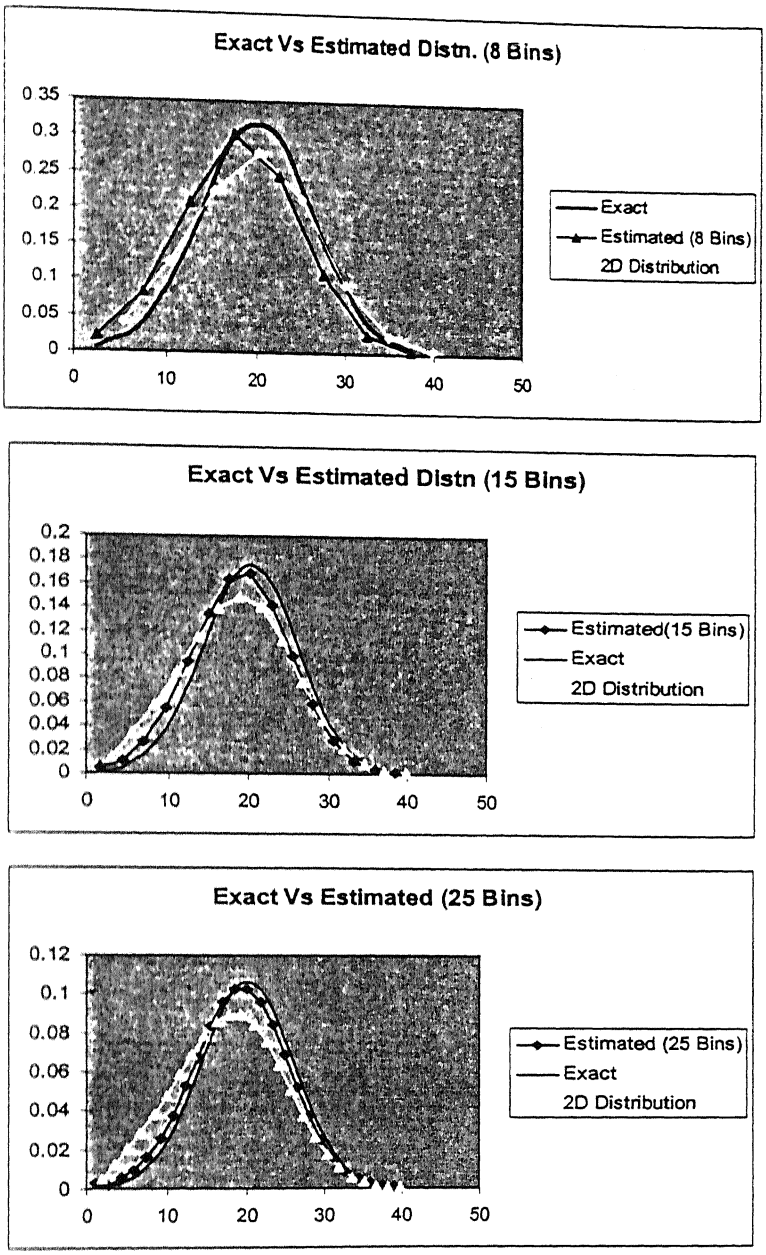

Figure 4-2 Comparison of the estimated 3D sphere size distribution with the exact 3D sphere size distribution. The apparent 2D circular profile size distribution is also shown. In a) Particle sizes are descretised into 8 classes, in b) Particle sizes are descretised into 15 classes and in c) Particle sizes are descretised into 25 classes. Same 2D profile data is used in all the three cases.

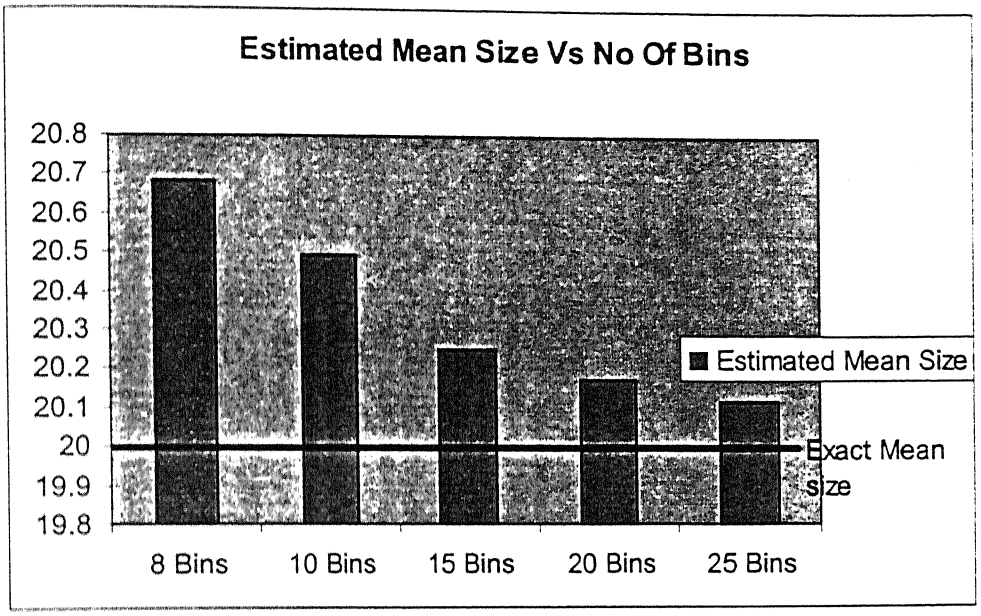

Figure 4-3 Illustration of variation of estimated 3D mean size of the spheres with change in number of size classes. Notice that the estimated mean size moves closer to the exact 3D mean size with decreasing class interval.

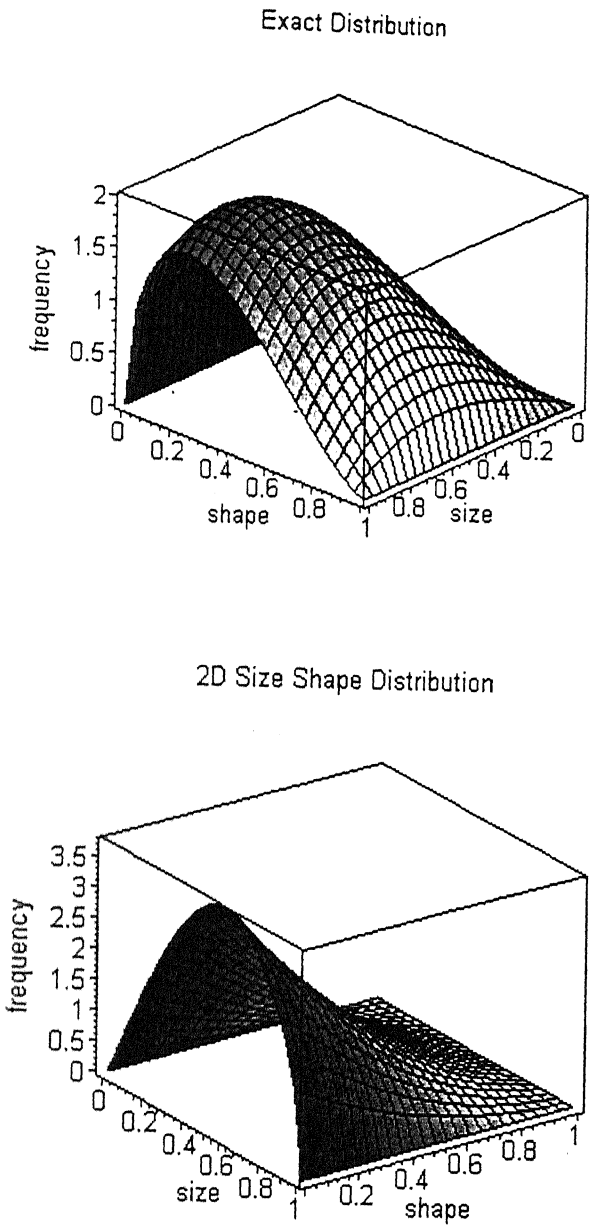

Figure 4-4 3D representation of size-shape probability density function. The surface in (a) describes a hypothetical population of variable, prolate spheroids. The surface in (b) corresponds to the variable elliptical profiles determined in the spheroids by random sectioning.

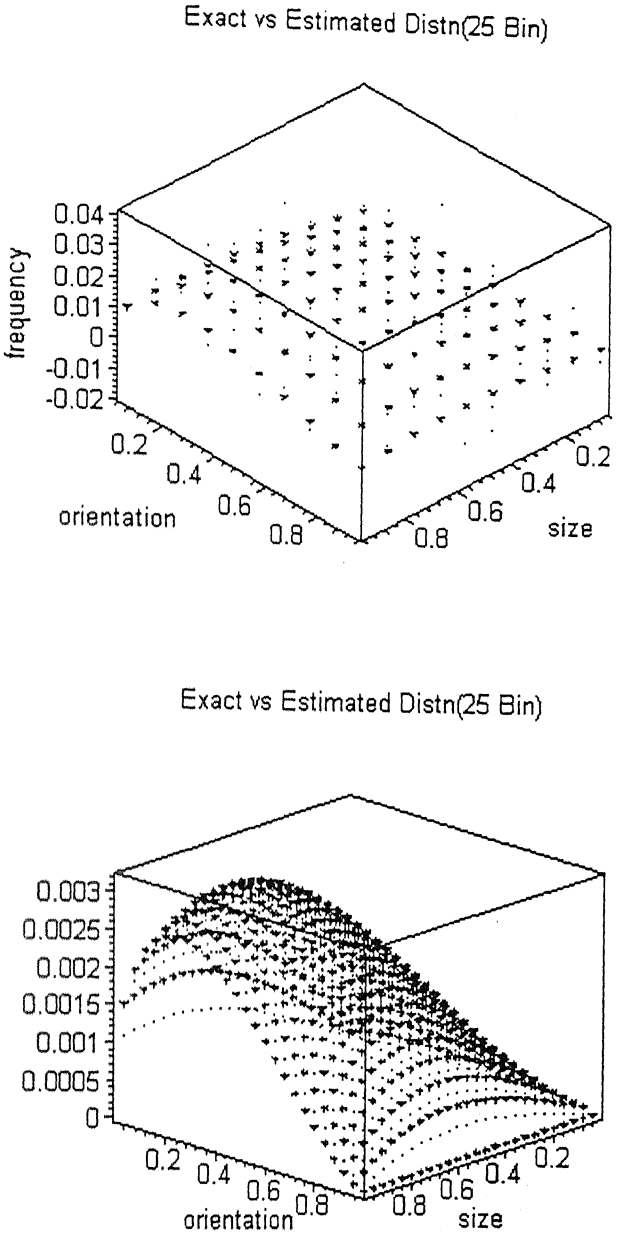

Figure 4-5 Comparison of the estimated 3D size-shape probability density of variable spheroids (represented by Figure 4-4(a)) obtained by numerical de-convolution from 2D data with the exact 3D size-shape probability density. In (a) Particles are distributed into 10 size classes and 10 shape classes and in (b) Particles are distributed into 25 size classes and 25 shape classes.

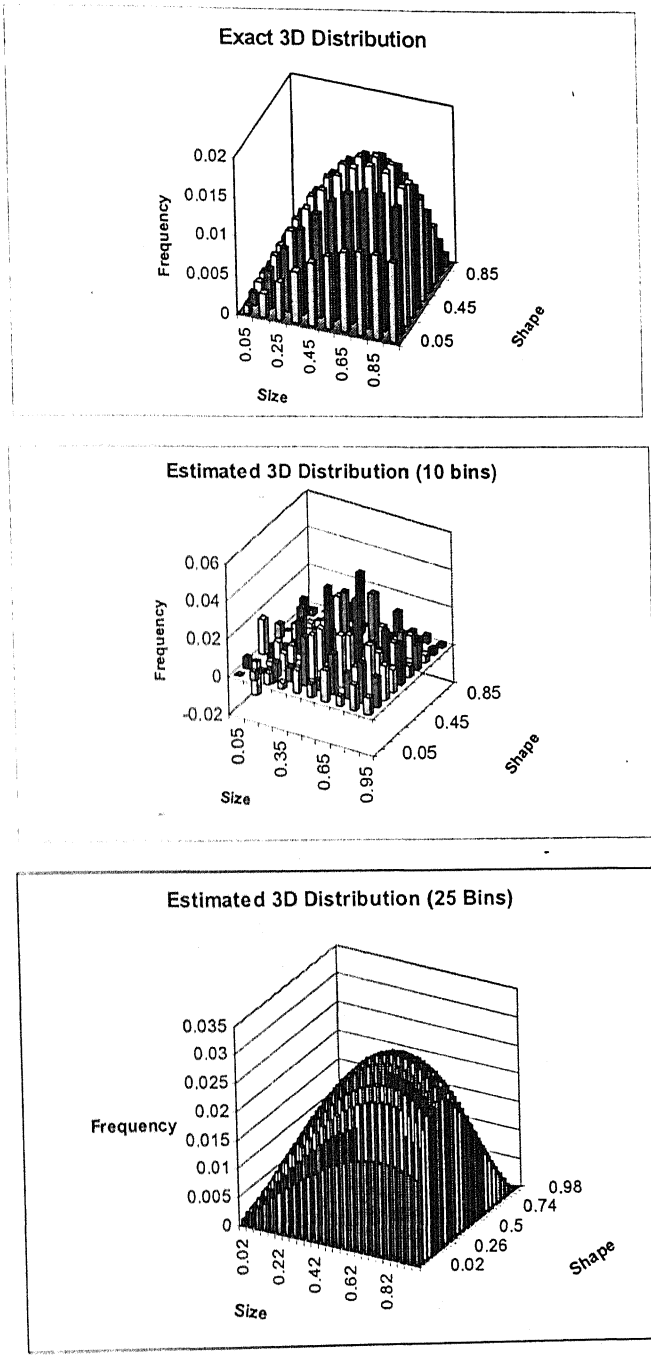

Figure 4-6 Histogram representation of 3D size-shape distribution of (a) Population of variable spheroids shown in Figure 4-3(a), (b) Population estimated by numerical de-convolution with a 10 by 10, size-shape grid and (c) Estimated population with a 25 by 25 size-shape grid.

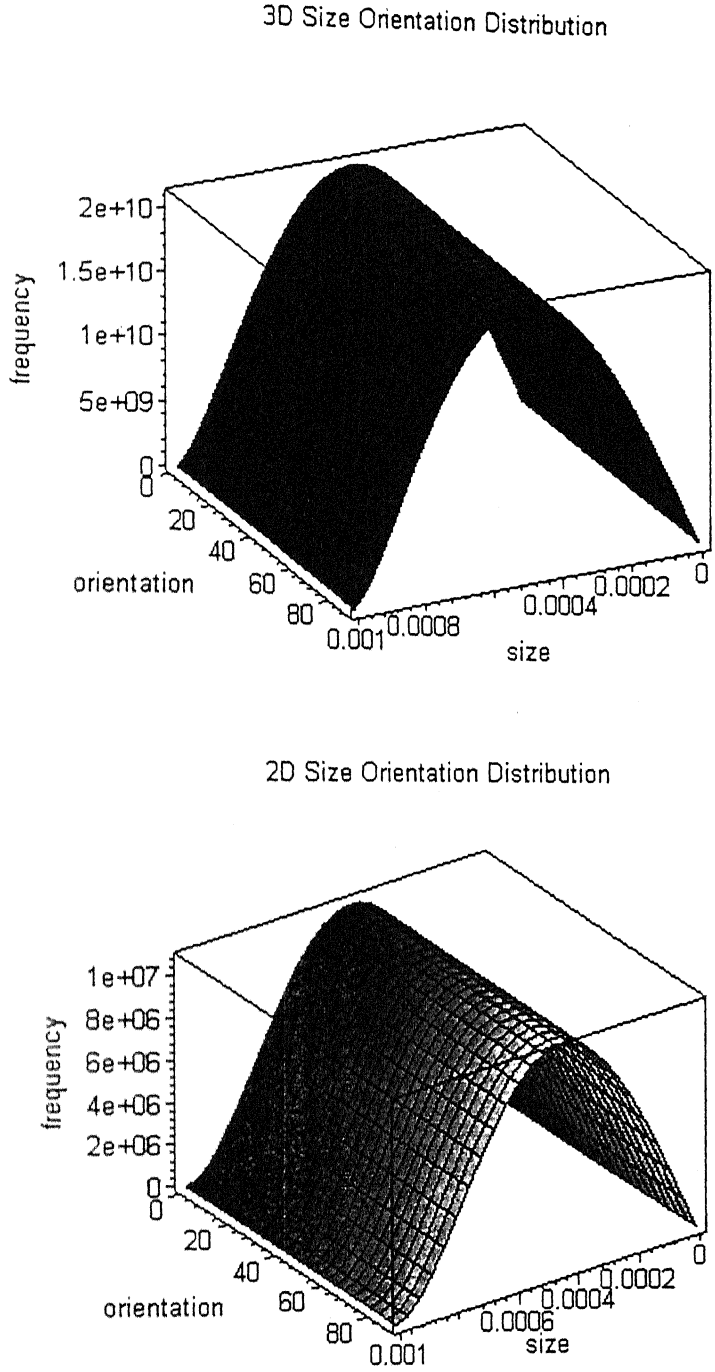

Figure 4-7 3D representation of size-orientation distribution function. The surface (a) describes a hypothetical population of randomly oriented disks. The surface in (b) corresponds to the apparent disk trace distribution in vertical planes.

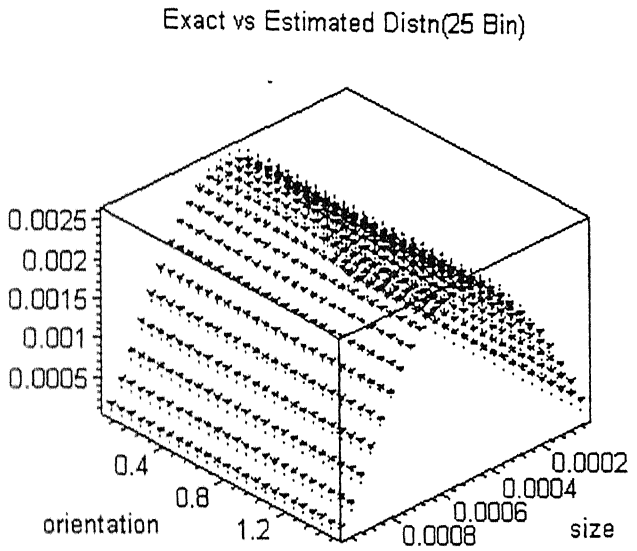

Figure 4-8 Comparison of calculated true bivariate size and orientation distribution obtained by numerical de-convolution of apparent bivariate size and orientation distribution of microcrack traces (represented by Figure 4-6(b)) with the exact size and orientation distribution of microcracks. Particle sizes are descretised into 25 classes and orientations too are descretised into 25 classes.

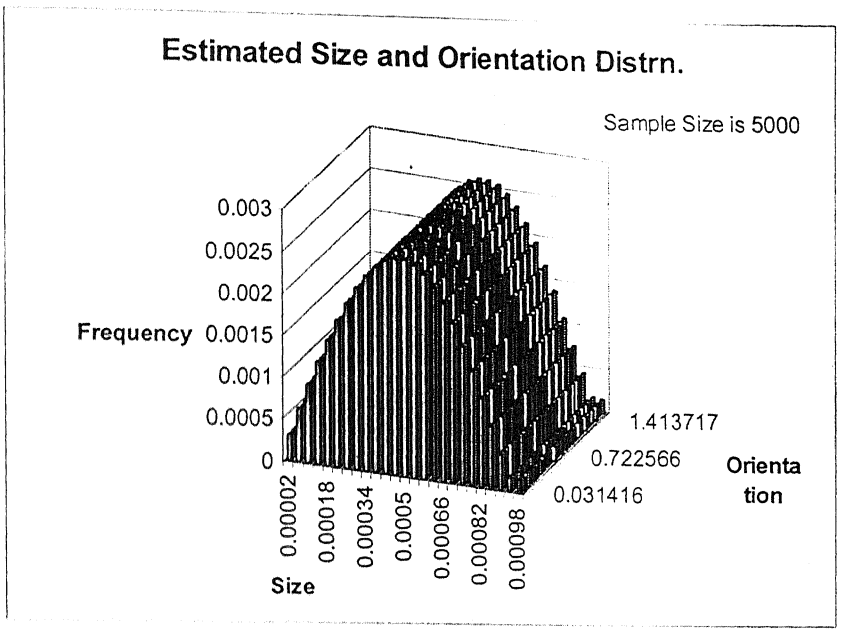

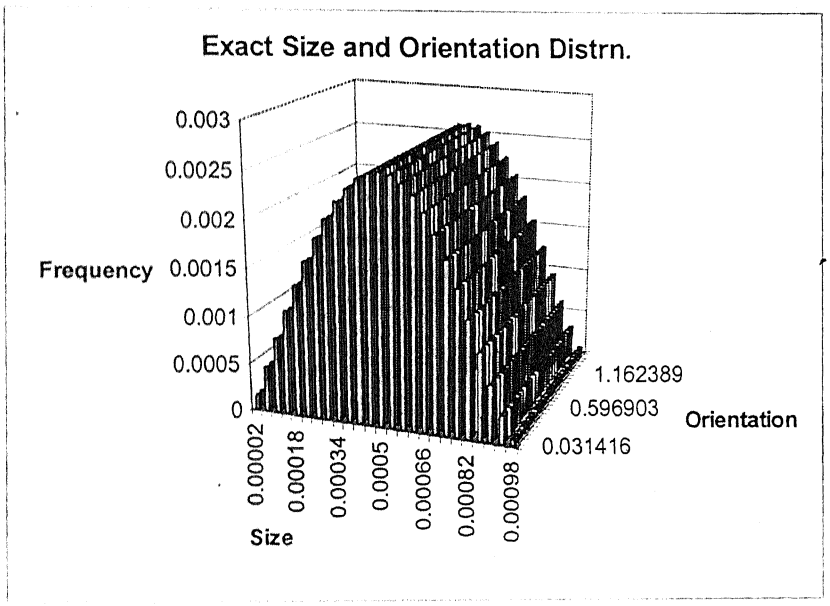

Figure 4-9 Histogram representation of 3D size-orientation distribution of (a) Hypothetical population of randomly oriented microcracks (b) Population estimated by numerical de-convolution.

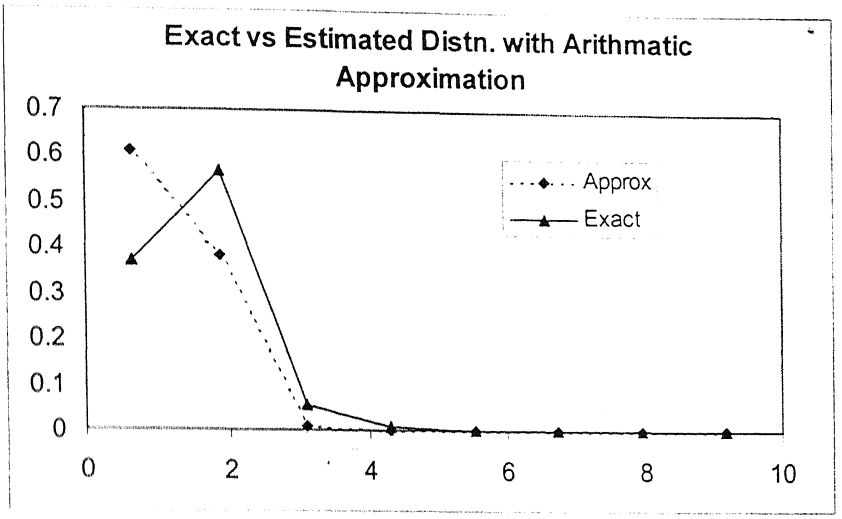

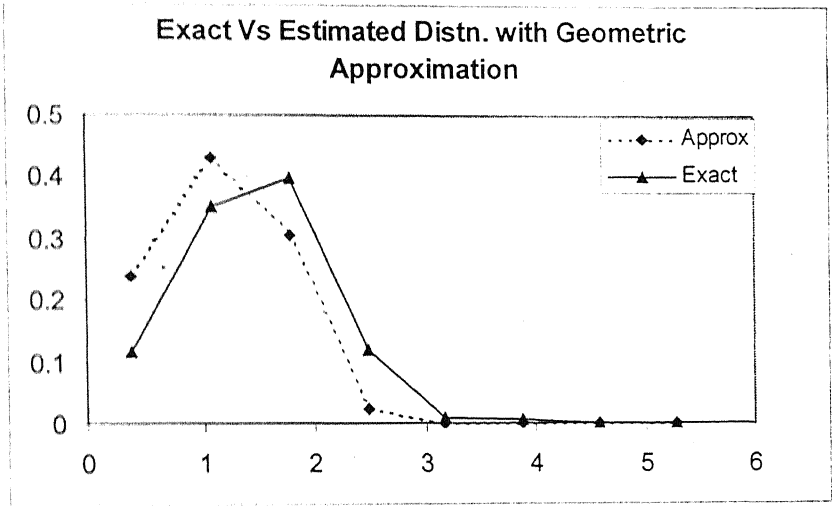

Figure 4-10 Spurious distribution curves resulting from application of spherical conversion coefficients to non-spherical particles (prolate spheroids, in this case). Solid lines are the exact 3D size distributions. In (a) the elliptical profiles are approximated as circles of radius equal to the arithmetic mean of their major and minor principal semi axes. In (b) the elliptical profiles are approximated as circles of equal area, i.e circles of radius equal to the geometric mean of their major and minor principal semi axes.

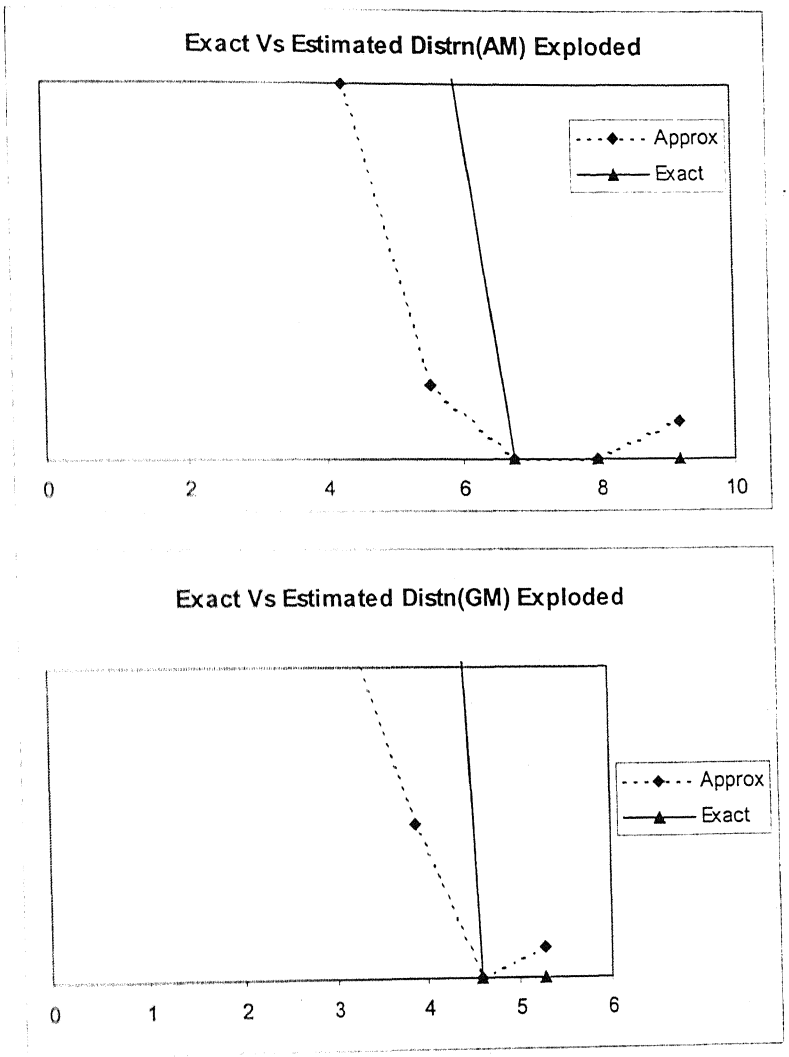

Figure 4-11 The same distribution curves as shown in Figure 4-10 are exploded to show the difference between the estimated and exact distribution curves in the larger particle size region.

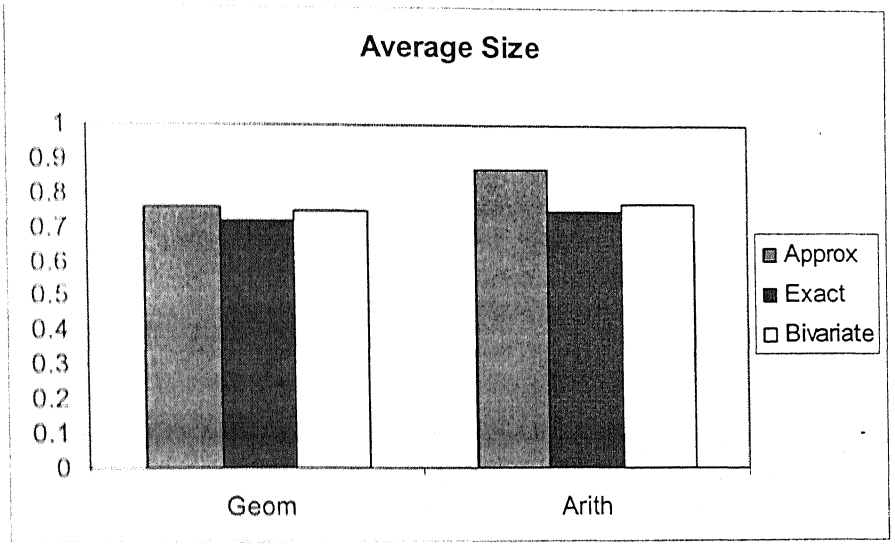

Figure 4-12 Comparison of mean particle size obtained by approximating the non-spherical particles as spheres (both arithmetic and geometric approximation) with the exact mean particle size. Mean particle size obtained by using the actual non-spherical conversion coefficients is also shown.

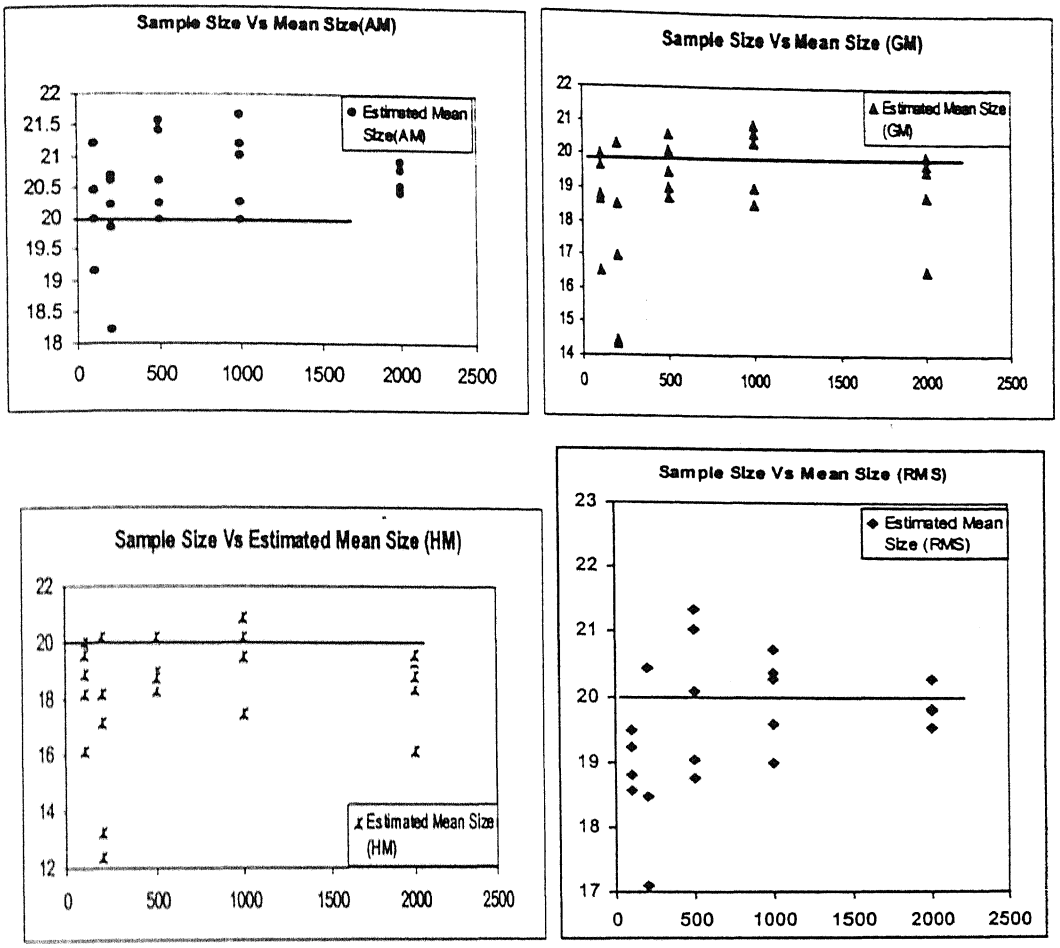

Figure 4-13 Illustration of variation of estimated mean particle size with the sample size (100, 200, 500, 1000, 2000). In (a) size of the particles in a particular bin is taken as the arithmetic mean of the sizes corresponding to the ends of the bin. In (b) Geometric mean is taken as the particle size. In (c) Harmonic mean is considered as the particle size and in (d) root mean square value is taken as the particle size.

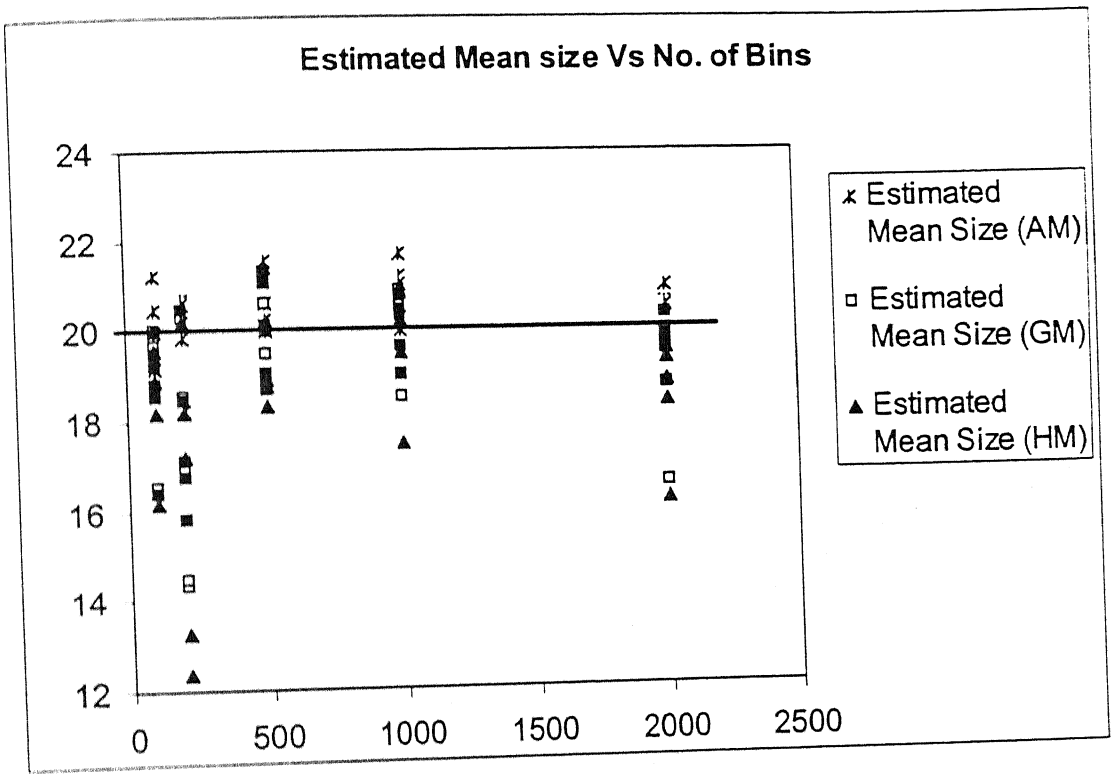

Figure 4-14 Illustration of bias involved in considering the particle size as arithmetic mean size, geometric mean size, harmonic mean size and root mean square size in estimating the 3D mean particle size by numerical de-convolution of 2D data.

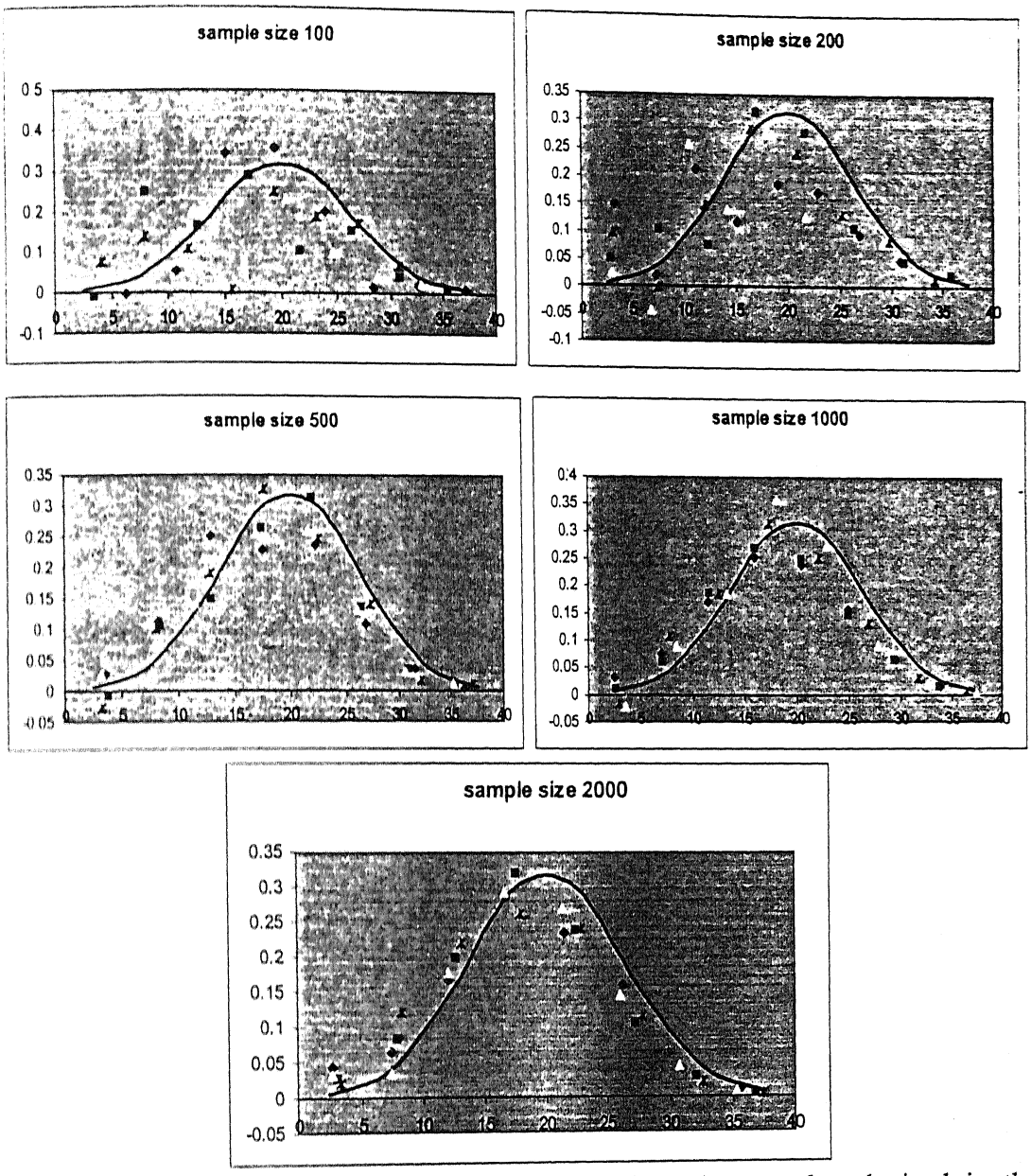

Figure 4-15 Effect of sample size on the precision, that can be obtained in the estimation of 3D particle size distribution by numerical de-convolution of 2D data. 5 samples each of sizes 100, 200, 500, 1000, 2000 are considered for this analysis.

CHAPTER 5

CONCLUSIONS

This study of 2D to 3D de-convolution problem led to the following conclusions.

1. Numerical methods are developed for de-convolution of observed 2D profiles of spheres, variable size-shape spheroids and variable size-orientation disks were successfully developed.
2. The numerical methods for solving the do-convolution problem for all the three (spheres, variable spheroids, variable disks) yield very precise 3D distributions (provided enough sampling is done).
3. For large sample size fine descretisation is required to achieve better estimations.
4. Use of profiles of spheroids as equivalent area circles to de-convolute 3D size distribution is not a bad approximation.
5. Approximation of spheroids as spheres led to prediction of unrealistic large particles and also increase frequency of lower size class particles. Though the two factors negated each other in the estimation of mean.
6. The error in estimation can be decreased by increasing sample size. Though the increase in sample size don't yield corresponding betterment of estimates beyond a certain sample size. This sample size was seems to be about 500.
7. In de-convolution of spheres the descretisation process laeads to a bias in the estimate. It is a positive bias when the mean bin size is represented by arithmetic mean of interval and a negative bias when it is represented by geometric mean and harmonic mean of the interval.
8. Use of root mean square value (in de-convolution of spheres) to represent mean bin size provides the most bias free estimate with least spread about the exact mean.

GUIDELINES FOR FUTURE WORK

1) The numerical methods developed in this thesis can be further analyzed for their applicability with other kinds of distributions like lognormal distribution, bimodal distribution etc.
2) Effect of standard deviation of the exact distribution on the accuracy of estimated distribution can be studied.
3) Numerical method for unfolding trivariate size, shape and orientation distribution of spheroids will be a more helpful microstructure characterization tool, since spheroidal particles often have a trivariate distribution.

REFERENCES

1. M. G. Kendall and P. A. P. Moran, "Geometrical probability" Griffin, London (1963).
2. L. A. Santalo, "Integral Geometry and Geometric Probability". Vol. 1 of Encyclopedia of Mathematics and its Applications, Addison Wesley, Mass (1967).
3. D. L. Sahagian, A. A. Proussevitch, "3D Particle Size Distributions from 2D Observations: Stereology for Natuaral Applications", *J. Volcanology and Geothermal Research*, 1998, 173-196.
4. W. L. Nicholson, "Estimaion of Linear Properties of Particle Size Distributions", *Biometrika*, 1970, 57(2), 273.A. Delesse, Procede mechanique pour determiner la composition des roches, ann. Mines, 1848, 4, 13-379.
5. A. Delesse, "Procede Mechanique Pour Determiner La Composition Des Roches", *Ann. Mines*, 1848, 13, 379.
6. H. C. Sorby, On Slaty cleavage, as Exhibited in the Devonian Limestones of Devonshire, Phil. Mag., 1856, 4, 11-20.
7. W. J Sollas, "Contributions to the Knowledge of the Leinster Granites", *Trans. Roy. Irish Acad.*, 1887-92, 29, 471.
8. A. A. Junlien, Genesis of the Amphibole Schilsts and Serpentines of Manhattan Island, New York. *Bull. Geol. Soc. Amer.*, 1993, 14, 466.
9. A. Rosiwal, Ueber Geometrische Gesteinsanalysen. Ein Einfacher Weg zur Ziffermaessigen Feststellung des Quantitaetsverhaeltnisses der Mineralbestandteile, 1898, 5-6, 143.
10. J. Joly, "The Petrological Examination of Paving Sets", *Proc. Roy. Dublin Soc.*, 1903-05, 10, 62.
11. A. Johannsen, "A Planimetric Method for the Determination of the Percentage Compositions of Rocks", *J. Geology*, 1919, 27, 276.
12. E. Thomson, "Quantitative Microscopic Analysis", *J. Geology*, 1930, 38, 193.
13. M. W. Lightner and C. H. Herty, "The tranverse Impact Strength of Plain Carbon, Normalized Steels", *Cooperative Bulletin*, 1932, 59.

14. F. S. Gardner, M. Cohen, and D. P. Antia, "Quantitative Determination of Austenite by X-Rays", *Trans. AIME*, 1943, 154, 306.

15. H. S. Rawdon, "Determination of structural Composition of Alloys by a Metallographic Planimeter", *Trans. AIME*, 1925, 71, 669.

16. E. Polushkin, "Determination of structural Composition of Alloys by a Metallographic Planimeter", *Trans. AIME*, 1925, 71, 669.

17. T. Ericsson, "Computers in Materials Technology", Pergamon, Oxford, U.K.,1981.

18. Ervin E. Underwood, "Quantitative Stereology", Addison-Wesley, London,1970.

19. S. A. Saltykov, "Stereometric Metallography", Metallurgizdat, Moscow, 1958.

20. S. I. Tomkeieff, "Linear Intercepts, Areas and Volumes", *Nature*, 1945, 155 (24), 107.

21. H. W. Chalkley, J. Cornfield, and H. Park, "A Method for Estimating Volume-Surface Ratios", *Science*, 1949, 110, 295.

22. H. F. Kaiser, "The Estimation of Inter-Granular Surfaces and Volumes", *Metals and Alloys*, 1938, 9-23.

23. G. H. Gulliver, "Note on Grain Size", *J. Inst. Metals*, 1918,1,19-145.

24. J. L. Meijering, "Interface Area, Edge Length, ad Number of Vertices in Crystal Aggregates with Random Nucleation", *Philips res. Rept.*, 1953, 8-270.

25. S. Z. Bokshteyn, Zh. Tekhn. Fiz., 1947, 12.

26. R. L. Fullman, "Measurement of Particle Sizes in Opaque Bodies", *Trans. AIME*, 1953, 447-452.

27. L. S. Moroz, "Collection, Dedicated to the 70-Aniversary of Academician A. F. Joffe", *Izvestiya akademii Nauk SSSR*, Moscow, 1950.

28. J. W. Cahn and J. Nutting, "Transmission Quantitative Metallography", *Trans. AIME*, 1959, 215-526.

29. V. Vouk, "Projected Area of Convex Bodies", *Nature*, 1948, 162-330.

30. M. Gensamer, E. B. Pearsall, W. S. Pellini, and J. R. Low, "The Tensile Properties of Pearlite, Bainite, and Spheroidite", *Trans. ASTM*, 1942, 30-983.

31. C. S. Smith, and L. Guttman, "Measurement of Internal Boundaries in Three Dimensional Structures by Random Sectioning", *Trans. AIME*, 1953, 197, 81.

32. W. M. Williams and C. S. Smith, "A Study of Grain Shape in an Aluminium Alloy and other Applications of Stereomicroradiagraphy", *Trans. AIME*, 1952, 194, 755.

33. J. E. Hilliard, "The Counting and Sizing of Particles in Transmission Microscopy", *Trans. AIME*, 1962, 224, 906-917.

34. J. Gurland, "The Measurement of Grain Contiguity in Two-Phase Alloys", *Trans. Met. Soc. AIME*, 1958, 212, 452.

35. J. W. Cahn and J. E. Hilliard, "The Measurement of Grain Contiguity in Opaque Samples", *Trans. Met. Soc. AIME*, 1959, 215, 759.

36. F. Forscher, "Analysis of Continuity of One Phase in a Powder Mixture of Two Phases", *J. Franklin Inst.*, 1955, 259, 107.

37. R. T. Dehoff, *Trans. Met. Soc. AIME*, 1967, 239, 617.

38. J. W. Cahn, *Trans. Met. Soc. AIME*, 1967, 239, 611.

39. R. T. Dehoff and F. N. Rhines, "Quantitative Microscopy", Mc-Graw Hill, New York.

40. G. Schoeck, "Correlation Between Dislocation Length and Density", *J. Appl. Phys.*,1962, 33, 1745.

41. J. E. Hilliard, "Determination of Structural Anisotropy", Stereology, edited by H. Elias, *Proc. Second Int. Cong. For Stereology*, New York: Springer-Verlag, 1967, 219.

42. A. G. Spektor, 1954, 5, 20.

43. S. Chandrasekhar, "Stochastic Problems in Physics and Astronomy", *Rev. Mod. Phys.*, 1943, 15, 86.

44. J. Gurlad, "The Measrement of Distribution, Spacing, Contact and Continuity of Particles in a Matrix", *Powder Metallurgy in the Nuclear Age, Plansee Proceedings* , edited by F. Benesovsky, 1961, 507.

45. M. F. Ashby and R. Ebeling, "On the Determination of the Number, Size, Spacing and Volume Fraction of Spherical Second-Phase Particles from Extraction Replicas" *Trans. AIME*, 1966, 14, 1628.

46. H. S. M. Coxeter, "Regular Polytopes", Macmillan, New York,1963.

47. L. A. Lyusternik, "Convex Figures and Polyhedra", Dover, New York, 1963.

48. J. J. B. Rutherford, R. H. Aborn, and E. C. Bain, "The Relation between the Grain Areas on a Plane section and the Grain size of a Metal", *Metals and Alloys*, 1937, 8, 345.

49. F. C. Hull and W. J. Houk, "Statistical Grain Structure Studies: Plane Distribution Curves of Regular Polyhedrons", *Trans. AIME*, 1953, 197, 565.

50. R.T. Dehoff, "The Determination of the Size Distribution of Ellipsoidal Particles from Measurements Made on Random Plane Sections", *Trans. Met. Soc. AIME*, 1962, 224, 474-477.

51. E. J. Myers, "Sectioning of Polyhedrons", Proc. First Int. Congress for Stereology, Vienna Medical Academy, Vienna, 1963.

52. E. R. Weibel, and D. M. Gomez, "A principle for counting tissue structures on random sections", *Appl. Physiol.*, 1962, 17, 343.

53. D. C. Sterio, "The Unbiased Estimation of Number and sizes of Arbitrary Particles Using Disector", *J. Miscroscopy*, 1984, 134, 127-136.

54. D. D. Wicksell, The corpuscle problem I.,*Biometrika*, 1925, 17, 84.

55. S. A. Saltykov, The determination of the size distribution of panicles in an opaque material from a measurement of the size distributions of their sections. In "Stereology". *Proc. the Second International Congress for Stereology*, Springer Verlag, New York: 1967, p.163.

56. E. Scheil, Die Berechnung der Anzahl der Grossenverteilung kugelformiger Kristalle in undurchsichtigen Korpern mit Hilfe der durch einenebenen Schnitt erhaltenen Schnittkreise. Z. Anorg. Allg. Chem., 1931, 27, 201.

57. H. A. Schwartz, "The metallographic determination of the size distribution of temper carbon nodules", *Metals and Alloys*, 1934, 5, 139.

58. E. D. Hyam and J. Nutting, "The Tempering of Plain Carbon Steel", *J. Iron Steel Inst.*,1956, 184,148.

59. A. G. Spektor, "Analysis of Distribution of Spherical Particles in Non Transparent Structures", *Zav. Lab*, 1950, 16, 173.

60. G. W. Lord and T. F. Wills, "Calculation of Air Bubble Size Distribution From Results of a Rosiwal Traverse of Aerated Concrete", *A.S.T.M. Bull.*,1951, 56,177.

61. C. C. Taylor, "A New Method for Unfolding Sphere Size Distributions", *J. Microscopy*, 132, 57-66.

62. G. K. Golubev and B. Y. Levit , "Asymptotically efficient estimation in the Wicksell problem", *The annals of Statistics*, 1988, 26, 2407-2419.

63. P. Hall and R. L. Smith "The kernel method for unfolding sphere size distributions", J. *computational physics*, 1988, 74, 409-421.

64. D. Nychka, G. Wahba, S. Goldfarb and T. Pugh , "Cross-validated spline methods for the estimation of three-dimensional tumor size distribution from observations

on two-dimensional cross section", *J. American statistical association*, 1984, 79, 832-846

65. A. Feuerverger and P. Hall ,"Methods for density estimation in thick-slice versions of wicksell's problem', *J. American statistical association*, 2000, 95, 535-546.
66. A. Antoniadis, J. Fan and I. Gijbels, "A Wavelet Method for Unfolding Sphere Size Distributions", *The Canadian Journal of Statistics*, 2001, 29(7).
67. E. Shceil and H. Wurst, "Statistische Gefugeuntersuchungen 2", *Z. Metallk.*, 1936, 28, 340-343.
68. M. Paulus, "Methode Detude De La Structure Granulaire.", Metaus, *Corrosion-Industries*, 1962, 37, 448.
69. J. W. Cahn. R. L. Fullman, " On the Use of Lineal Analysis for Obtaining Particle Size Distribution Functions in Opaque Samples", *Trans AIME*, 1956, 206, 610.
70. S. D. Wicksell, "The corpuscle Problem II", *Biometrika*, 1926, 18, 152.
71. L. M. Cruz Orive, "Particle Size-Shape Distributions: The general Spheroid Problem", *J. of Microscopy*, 1976, 107, 235-253.
72. A. M. Gokhale, "Estimation of Bivariate Size and Orientation Distribution of Microcracks", *Acta Materiallia*, 1996, 475-485.
73. L. Seaman, D. R. Curran and R. C. Crewdson, "Transformation of Observed Crack Traces on a Section to True Crack Density for Fracture Calculations", J. Applied Physics, 1978, 49(10), 5221-5229.
74. J. Osher and M. Nippe, "Stereology of Cubic Particles: Various Estimators for the Size Distribution", J. of Microscopy, 1997, 187, 22-30.
75. A. Tewari and A. M. Gokhale, "Estimation of Three-Dimensional Grain Size Distribution from Microstructural Serial Sections", Materials Characterization, 2001, 46, 329-335.
76. E. R. Weibel, "Stereological Methods 2", Academic Press, London, 1980.
77. I. N. Sneddon, "Mixed Boundary Value Problems in Potential Theory", North-Holland, Amsterdam, Holland, 1966.
78. L. M. Cruz-Orive, "Particle Size-Shape Distributions: The General Spheroid Problem. II. Stochastic Model and Practical Guide", *J. Microscopy*, 1978, 112, 153.